Cargese (23 April 2013)

Exploring Earth's deep interior with ambient noise and earthquake signals

Rob van der Hilst
Massachusetts Institute of Technology

Acknowledgments:

Scott Burdick (MIT), Huang Hui (MIT), Xuefeng Shang (MIT), Yao Huajian (now at USTC), Maarten de Hoop (Purdue University), Liu Qiyuan (Institute of Geology, China Earthquake Administration)

Overview of lecture:

1. Introduction/background
2. Ambient noise and surface wave tomography
3. Reverse time migration of converted waves
4. Interferometry of teleseismic (coda) waves

Frequency	**Mhz-kHz**	**10000-100Hz**	**100-10Hz**	**10Hz-1Hz**	**1-0.01Hz**
Domain	Laboratory acoustics	Underwater acoustics	Shallow seismic imaging	Seismic imaging	Seismology-large scale
Applications	NDT Monitoring	Tomography Source detection	Structure of shallow layers Geotechnical applications, land slides Monitoring	Natural resources Natural hazards Monitoring	Structure of the Earth, Earthquake risk zonation, Monitoring
Wave type	elastic waves, also sound in water	Acoustic waves	Elastic waves	Elastic waves	Elastic waves
Propagation	Reverberant, andMultiple-Scattering	Weak scattering	Strong attenuation	Weak (crust) to strong (volcanoes) scattering	Weak scattering

Frequency	**Mhz-kHz**	**10000-100Hz**	**100-10Hz**	**10Hz-1Hz**	**1-0.01Hz**
Domain	Laboratory acoustics	Underwater acoustics	Shallow seismic imaging	Seismic imaging	Seismology-large scale
Applications	NDT Monitoring	Tomography Source detection	Structure of shallow layers Geotechnical applications, land slides Monitoring	Natural resources Natural hazards Monitoring	Structure of the Earth, Earthquake risk zonation, Monitoring
Wave type	elastic waves, also sound in water	Acoustic waves	Elastic waves	Elastic waves	Elastic waves
Propagation	Reverberant, andMultiple-Scattering	Weak scattering	Strong attenuation	Weak (crust) to strong (volcanoes) scattering	Weak scattering

Figure 2.7-1: Seismograms recorded at a distance of 110°, showing surface waves.

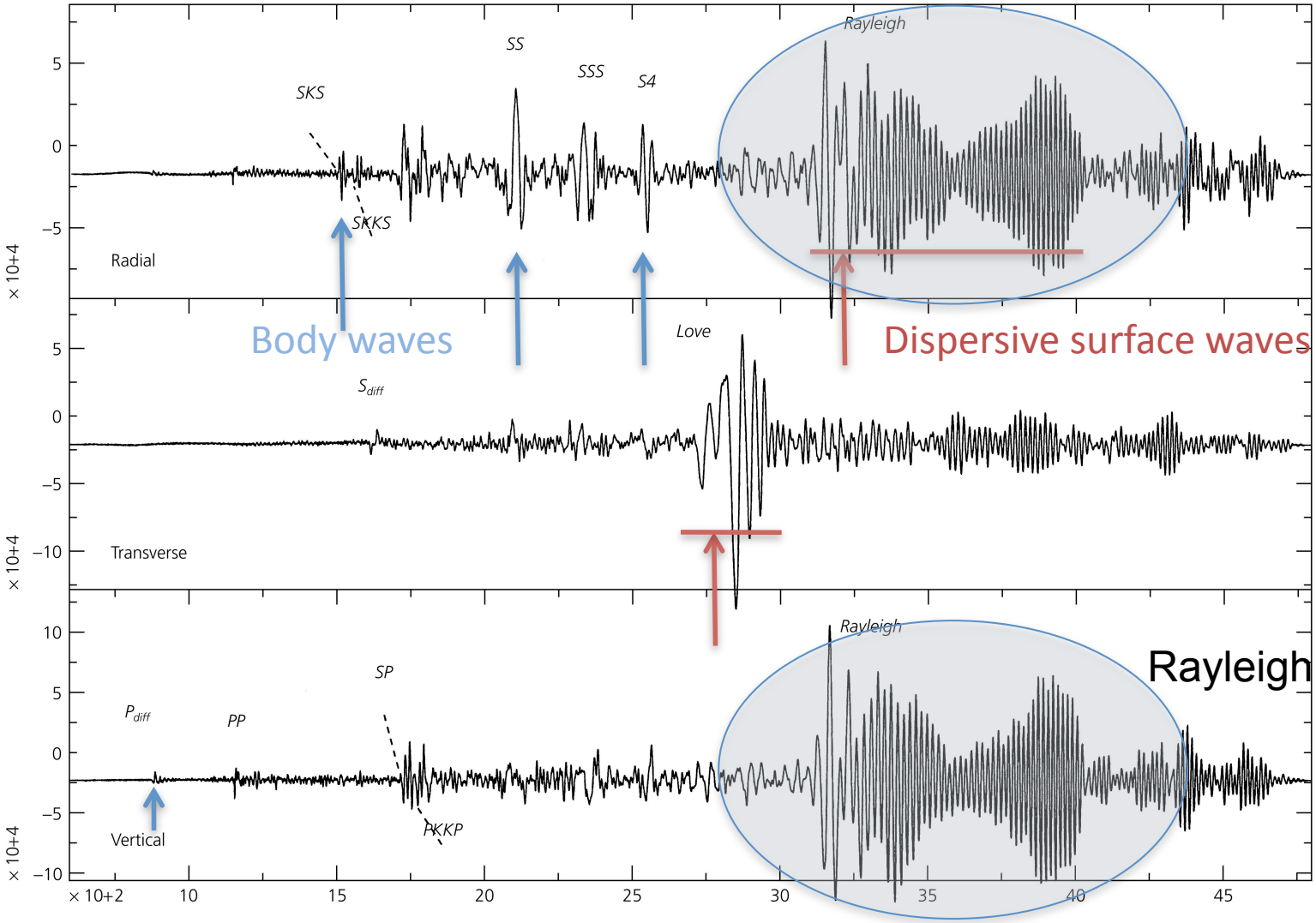

From Stein and Wysession

‘Surface and guided waves’: waves trapped in the shallow layers or a wave guide (such as Love waves in the Earth, acoustic waves in the oceanic SOFAR, ….)

Also in elasticity the Rayleigh wave at the surface of an half-space

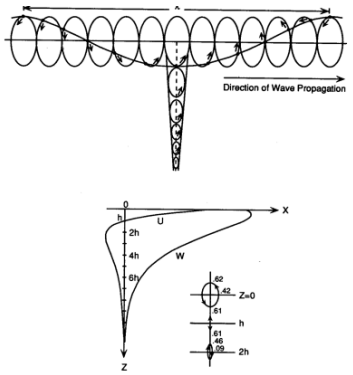

Eigenfunction

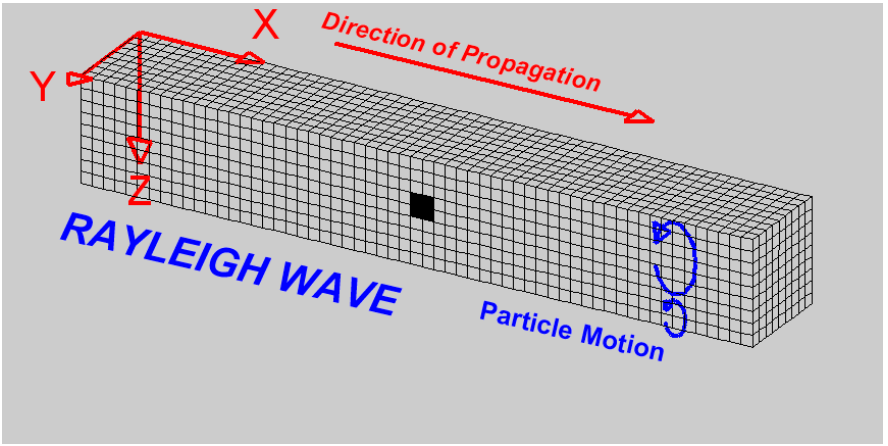

Courtesy: Campillo (Cargese, 2011)

‘Surface and guided waves’: waves trapped in the shallow layers or a wave guide (such as Love waves in the Earth, acoustic waves in the oceanic SOFAR, ….)

Also in elasticity the Rayleigh wave at the surface of an half-space

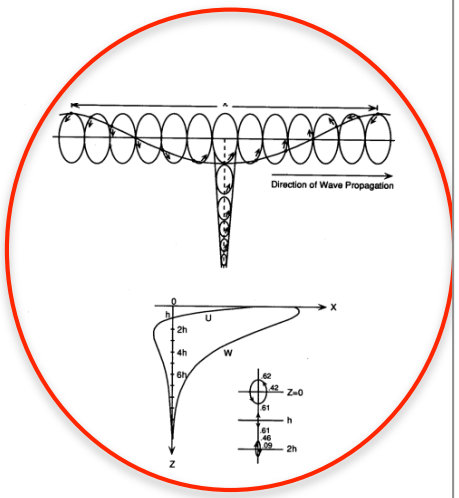

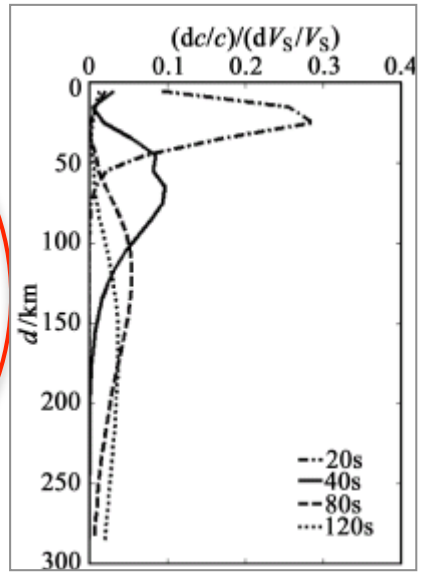

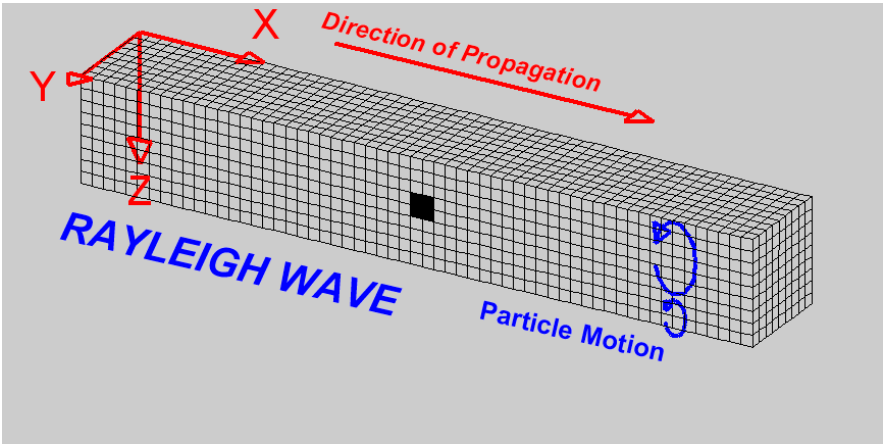

frequency proxy for depth

Courtesy: Campillo (Cargese, 2011)

Traditional Approach to Tomography

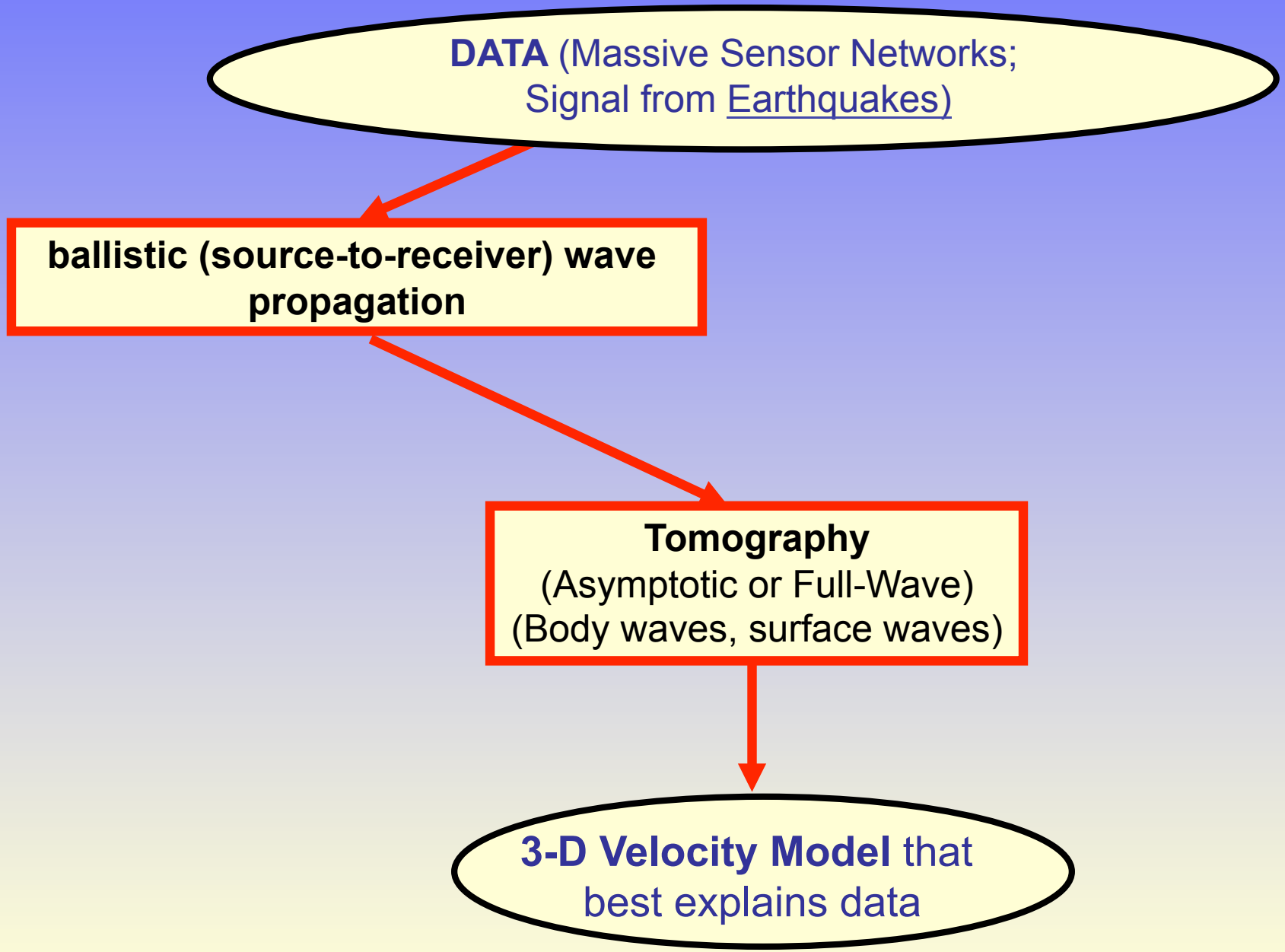

Lebedev and Van der Hilst (*GJI*, 2008)

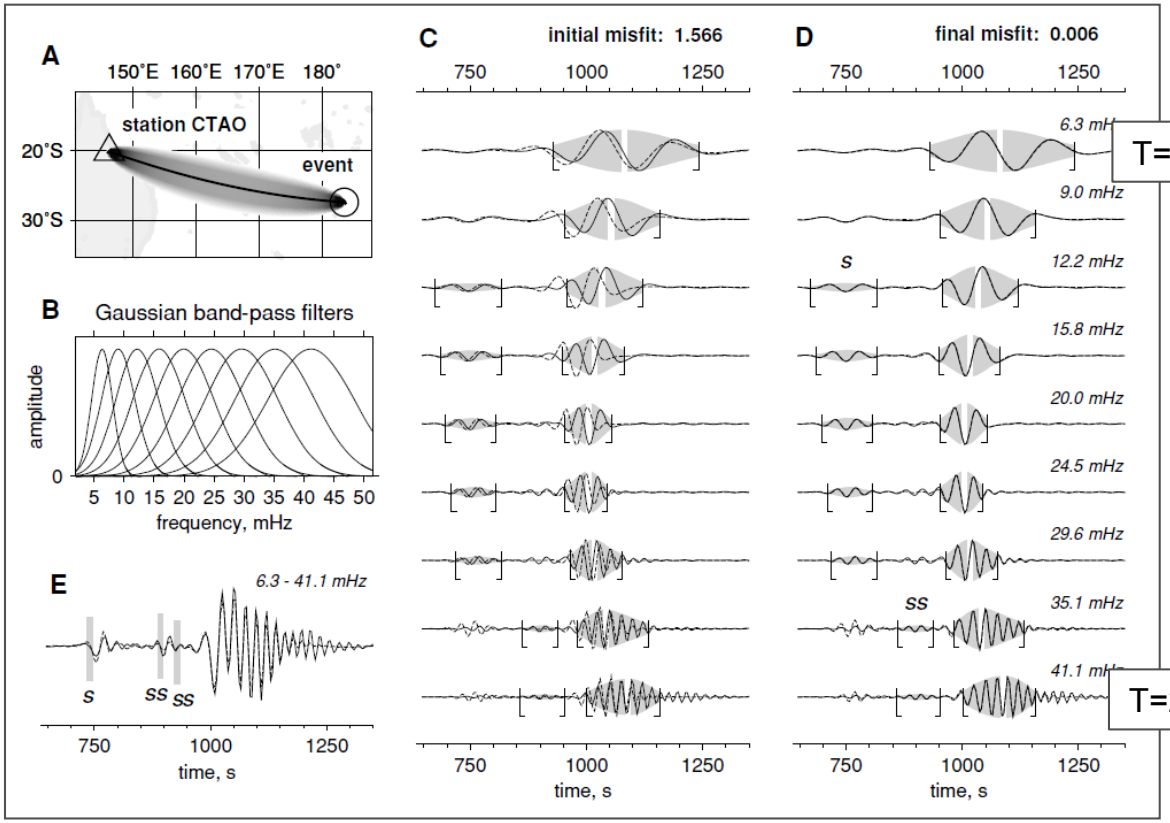

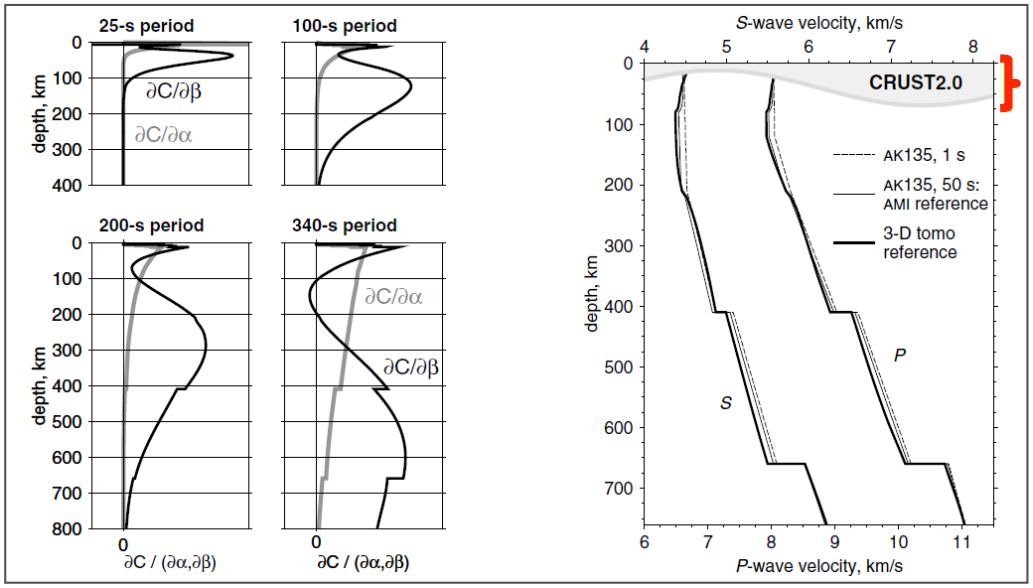

Crust = Problem!

Examples from traditional surface wave tomography with earthquake waves: relatively low frequencies → deep structures

T > 30 s → upper mantle

Simons and Van der Hilst (*EPSL*, 2008)

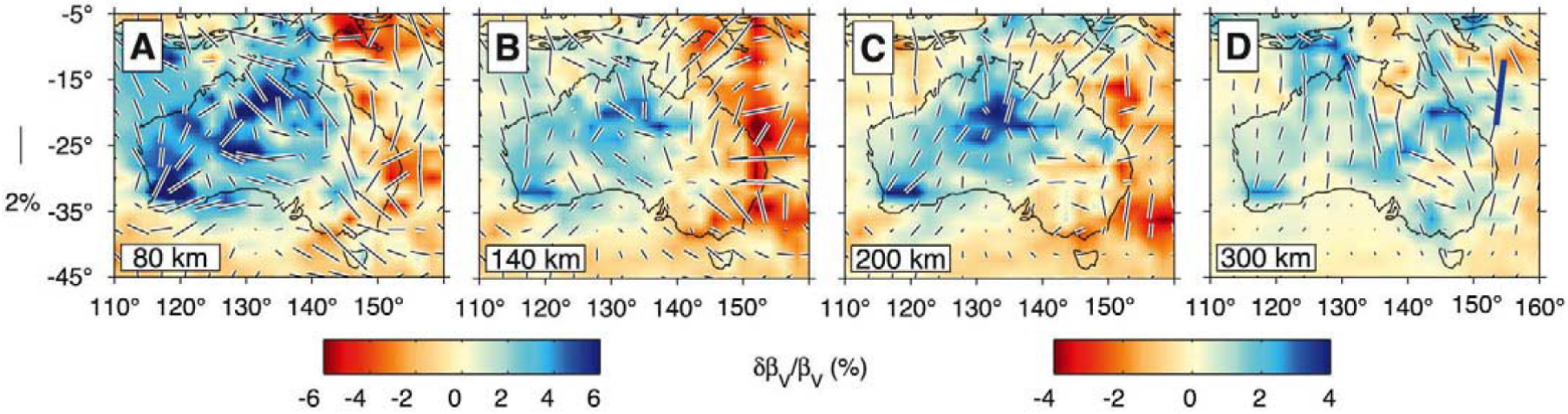

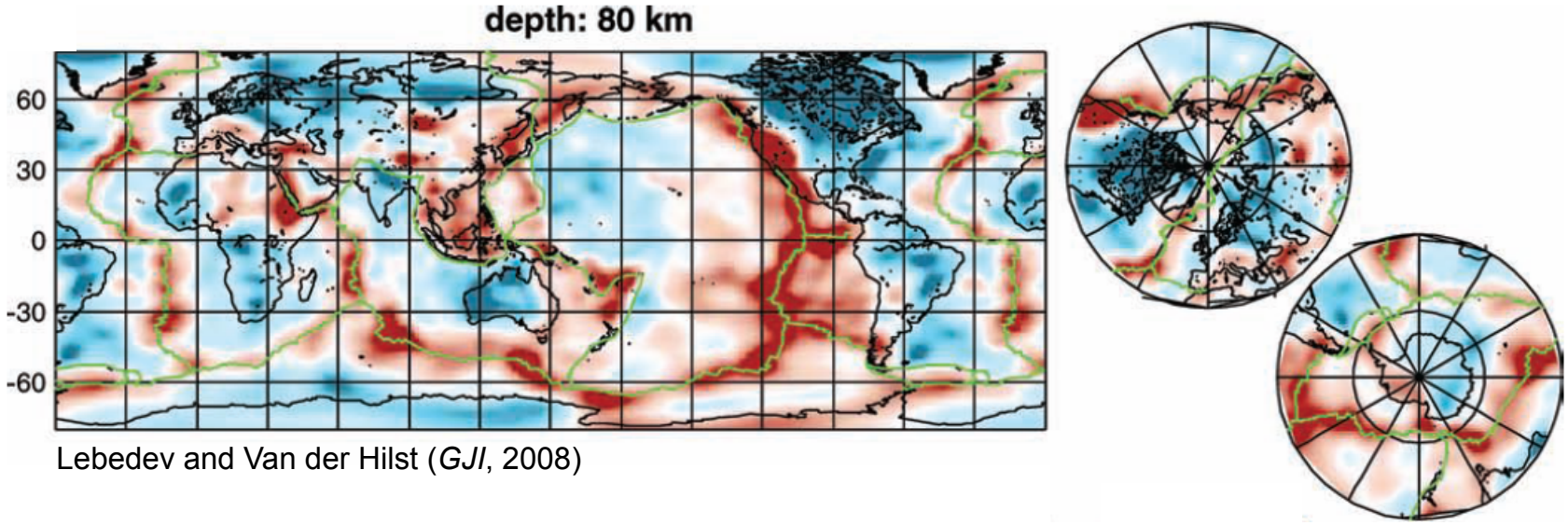

Lebedev and Van der Hilst (*GJI*, 2008)

Ambient Noise Tomography

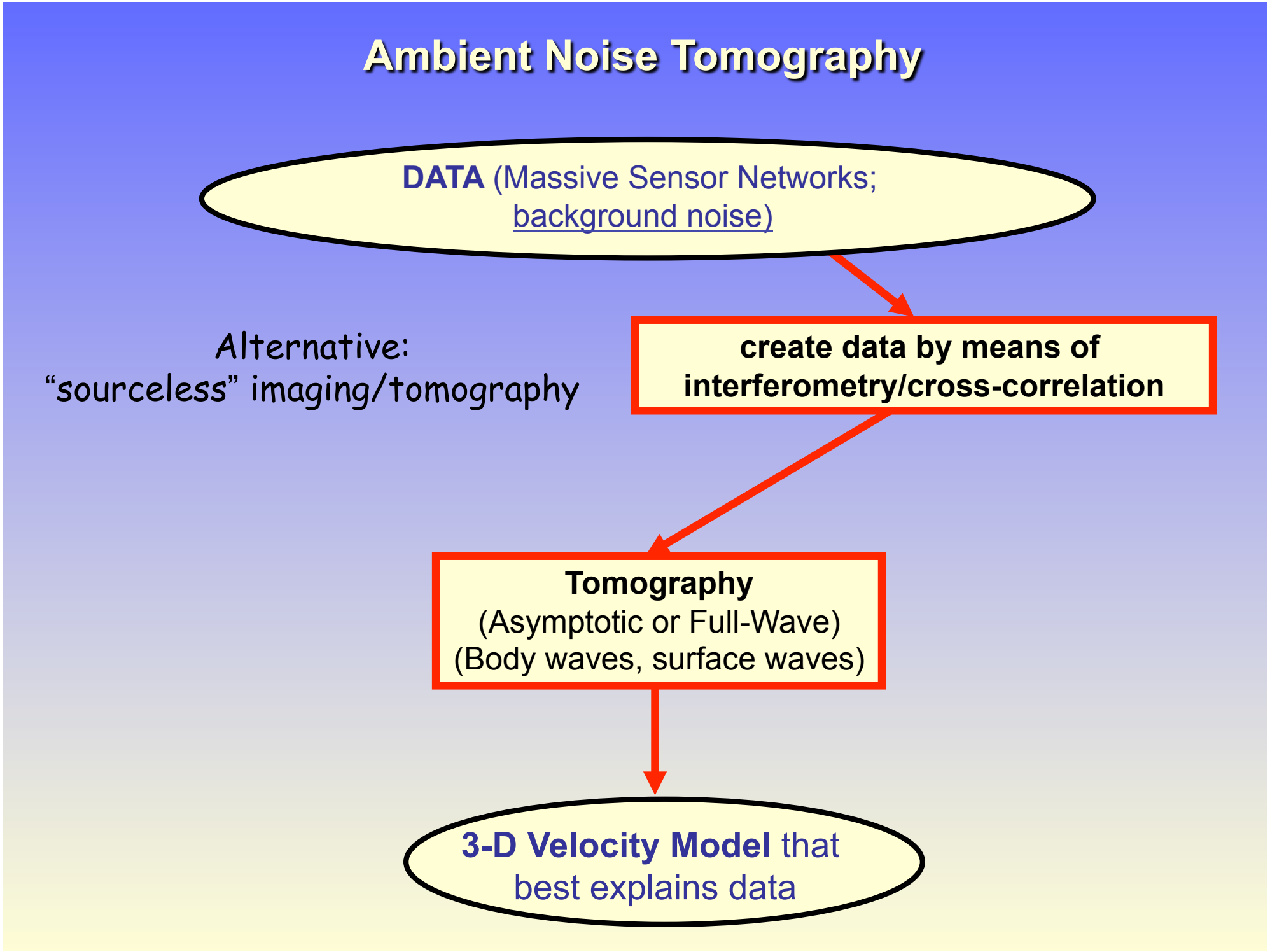

Shapiro, N.M., M. Campillo, L. Stehly, and M.H. Ritzwoller, 2005, High-Resolution Surface-Wave Tomography from Ambient Seismic Noise: Science **307**:1615-1618

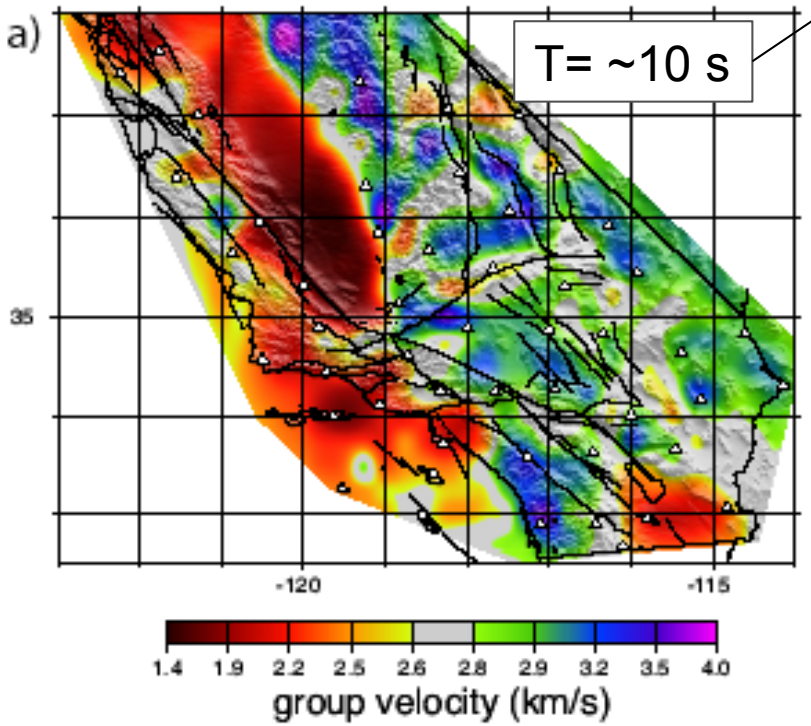

T < 30 s → Crust

A map of Surface-wave Velocity in California

Obtained from correlating seismic noise

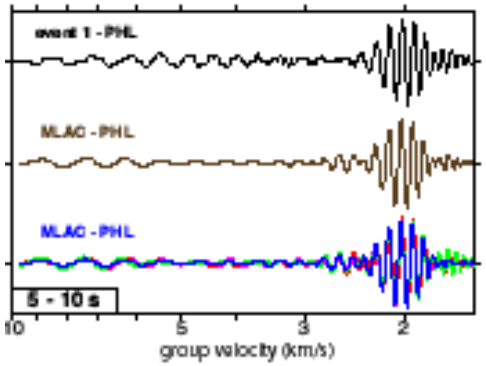

earthquake

1 year of correlations

4 one-month correlations

also Sabra, et al Surface wave tomography from microseisms in Southern California Geophys Res Lett **32** (2005)

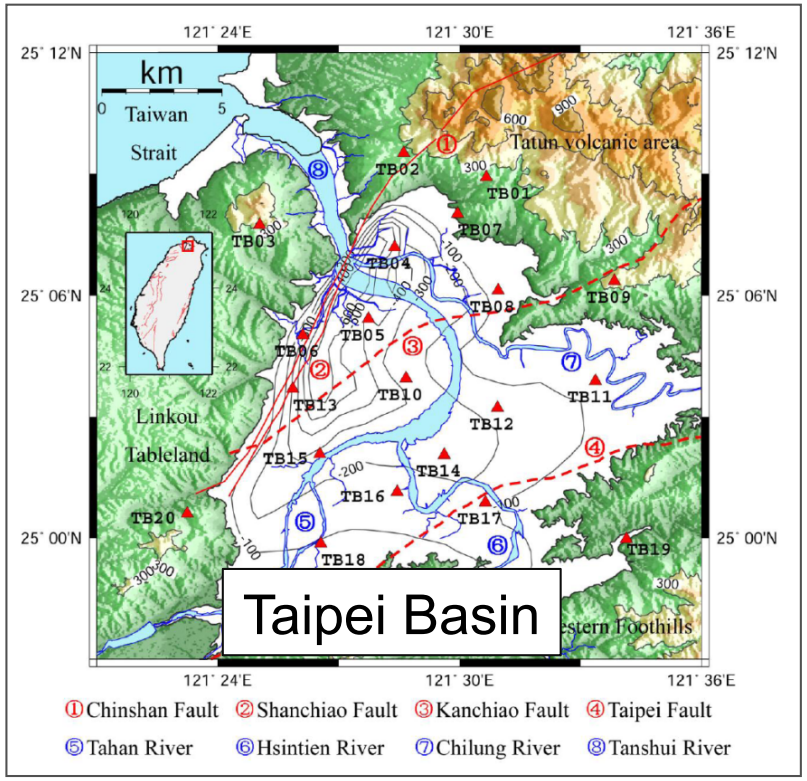

Huang et al. (BSSA, 2010)

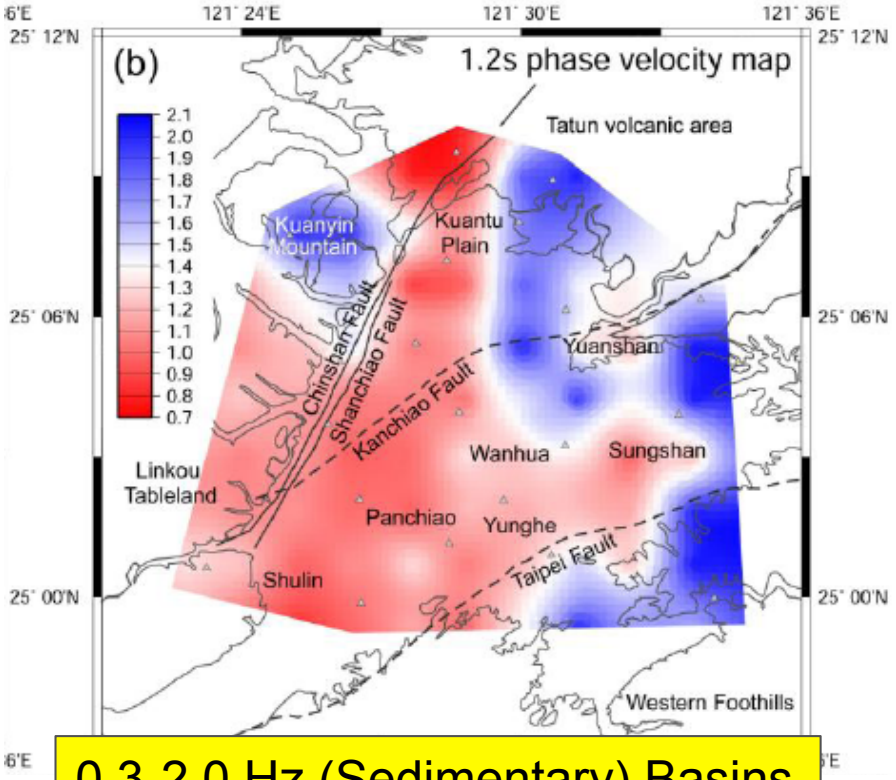

0.3-2.0 Hz (Sedimentary) Basins

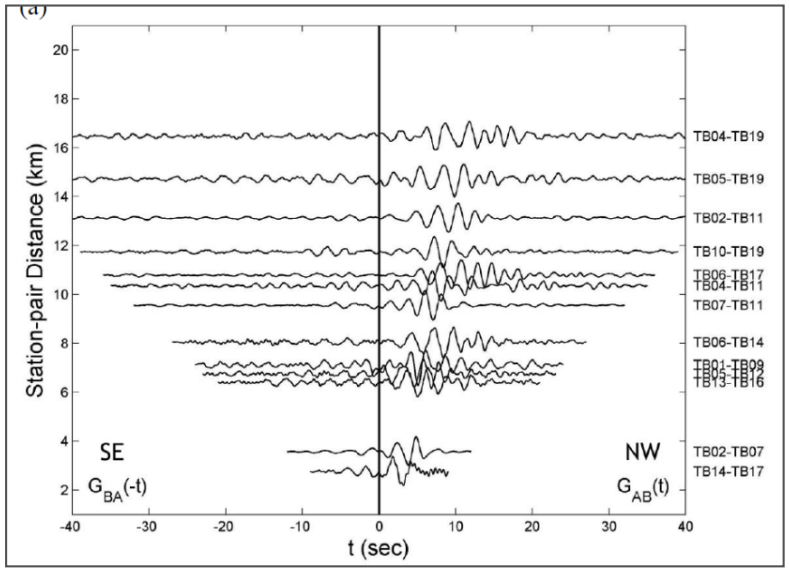

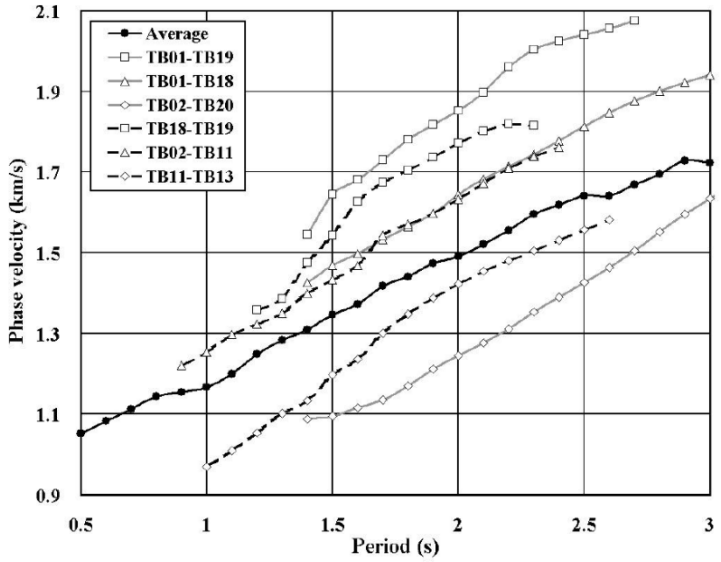

Frequency	**Mhz-kHz**	**10000-100Hz**	**100-10Hz**	**10Hz-1Hz**	**1-0.01Hz**
Domain	Laboratory acoustics	Und acou			
Applications	NDT Monitoring	Ton Sou dete			
Wave type	elastic waves, also sound in water	Acoustic waves	Elastic waves	Elastic waves	Elastic waves
Propagation	Reverberant, andMultiple-Scattering	Weak scattering	Strong attenuation	Weak (crust) to strong (volcanoes) scattering	Weak scattering

Boundaries are blurring

broader frequency bandwidth → larger depth rang
(when arrays are available …)

Surface geology ↔ Deeper dynamic processes

Field Projects Sichuan & Yunnan Provinces and E. Tibet (2003-2004)

Crust-Mantle study E Tibet – SW China

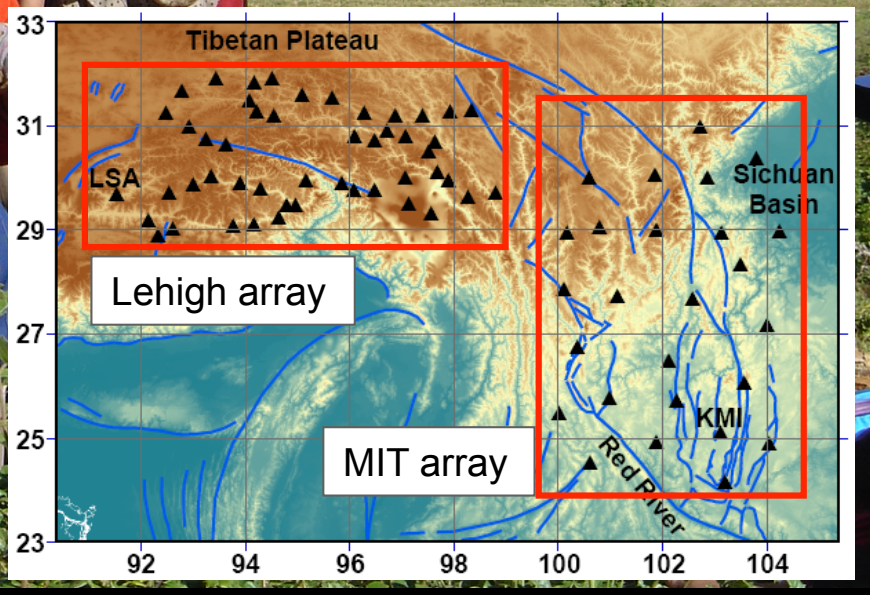

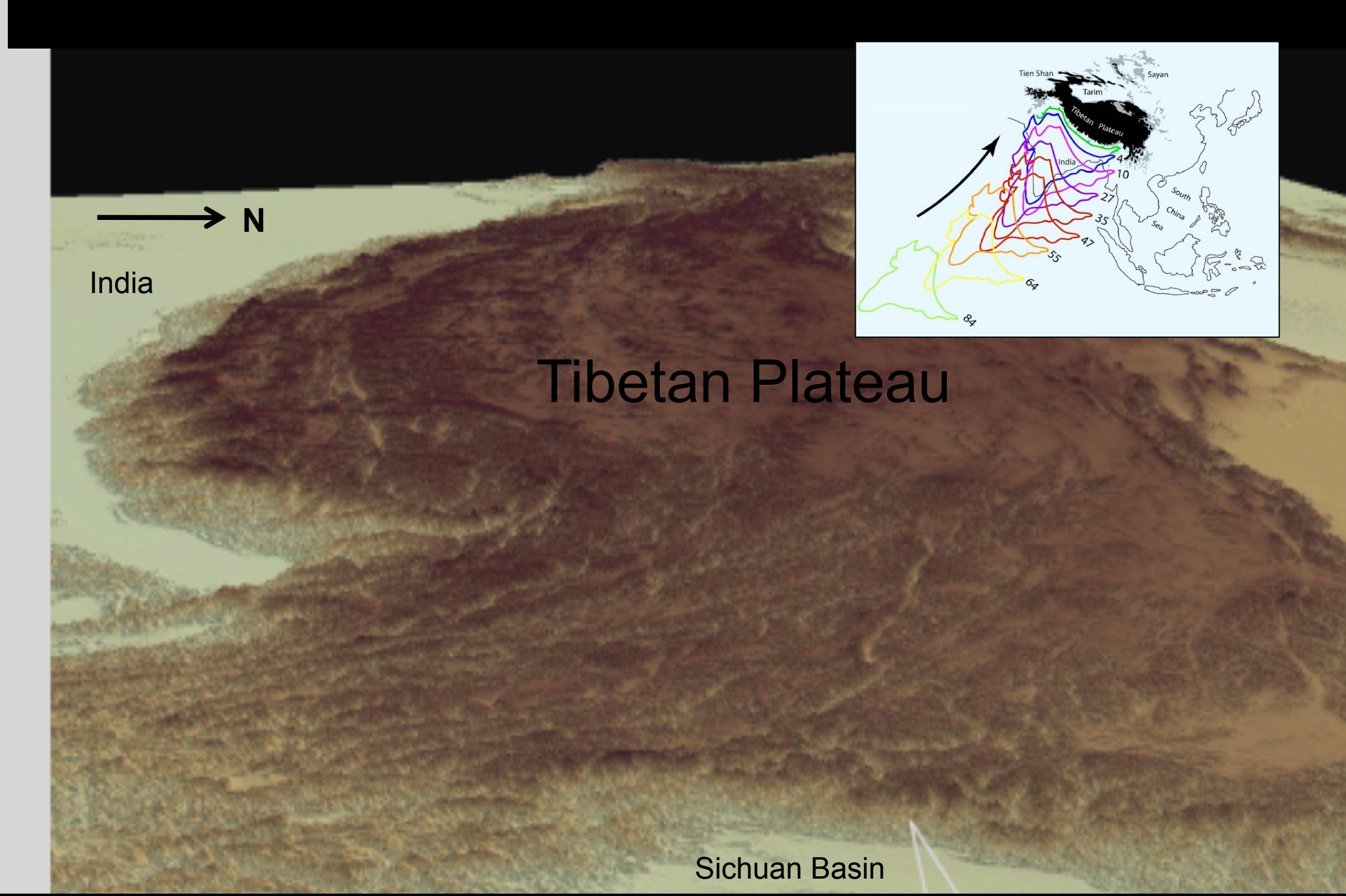
N
India
Tien Shan
Sayan
Tarim
Tibetan Plateau
India
4
10
27
35
47
55
64
84
South
China
Sea
Tibetan Plateau
Sichuan Basin

Why SE Tibet?
1. understanding eastward expansion of plateau

N

India

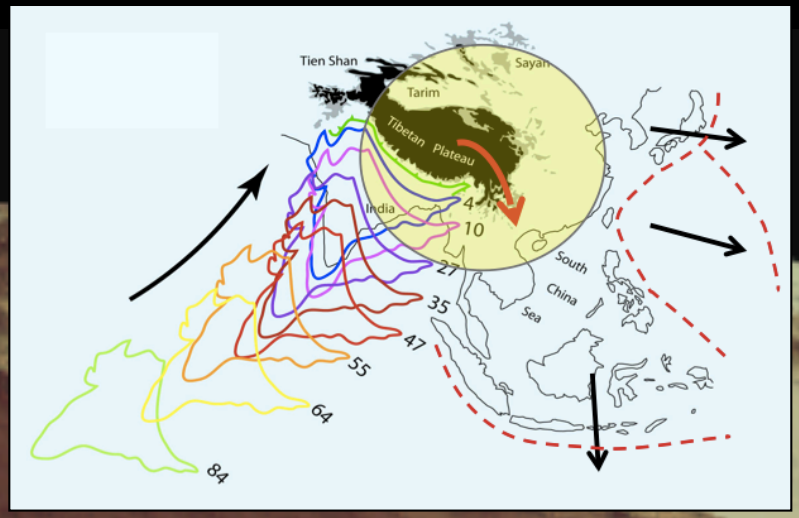

Tibetan Plateau

Rigid block model?

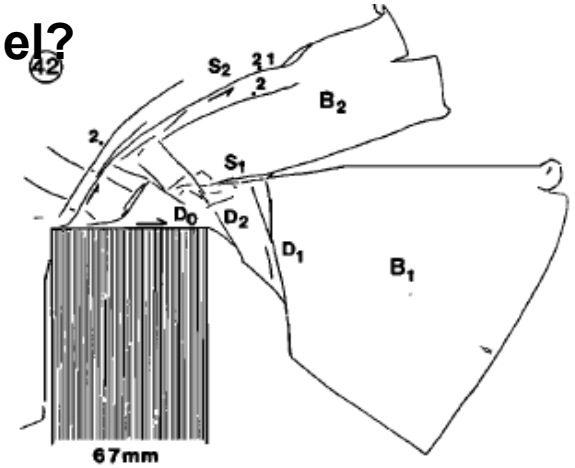

Peltzer and Tapponnier (1988)

Crustal (channel) flow?

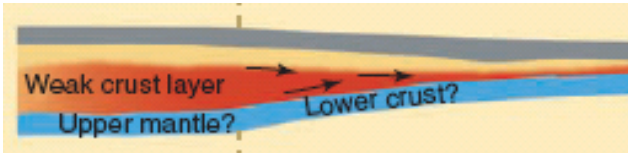

Royden et al. (1996)

How does this work?

Rigid blocks? Crustal flow?

Need to know structure of the crust!

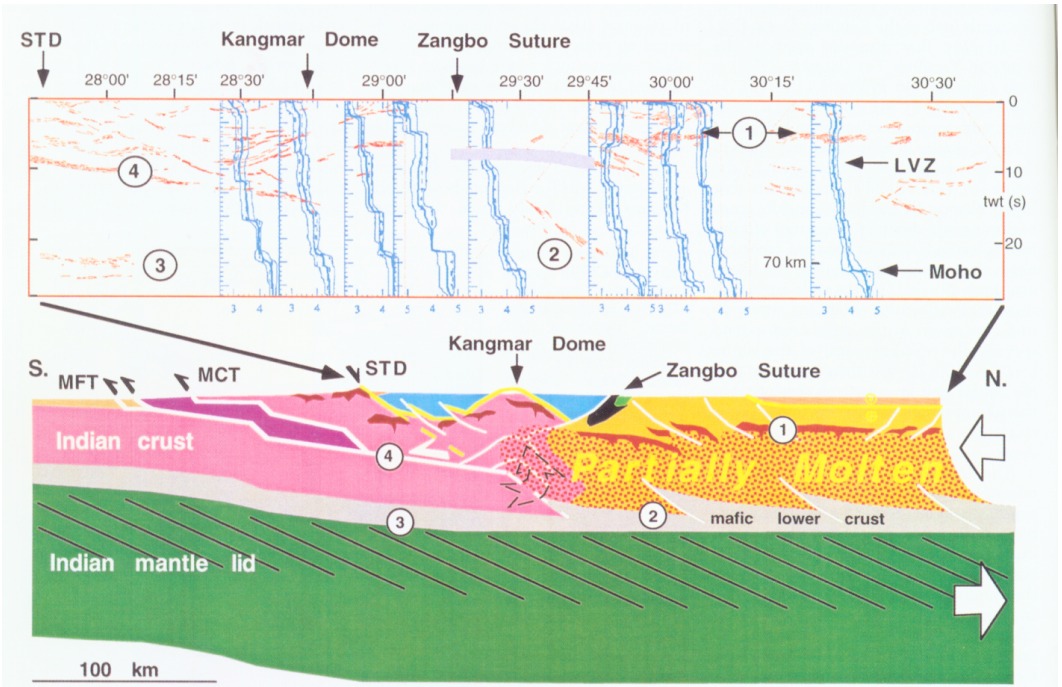

Fig. 2. (**Top**) Composite of selected INDEPTH geophysical observations along the Yadong-Gulu rift in southern Tibet; red, composite north-south CMP profile described in (6); blue, one-dim… profiles derived from broadband earthquake d… reflection observed in CMP data gap beneat… suture; LVZ, midcrustal low-velocity zone evident in shear-wave velocity profiles north of the Zangbo suture. (**Bottom**) Interpretive lithosphere-scale … text). MFT, Main Frontal … tan detachment system.

Nelson et al. (*Science*, 1996)

Why SE Tibet?

2. Southern end of Trans China Seismicity Belt

E.g. Sichuan, 12 May 2008
~80,000 people killed …

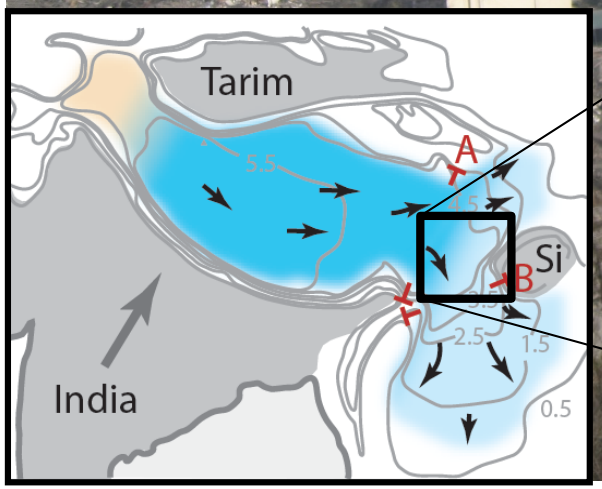

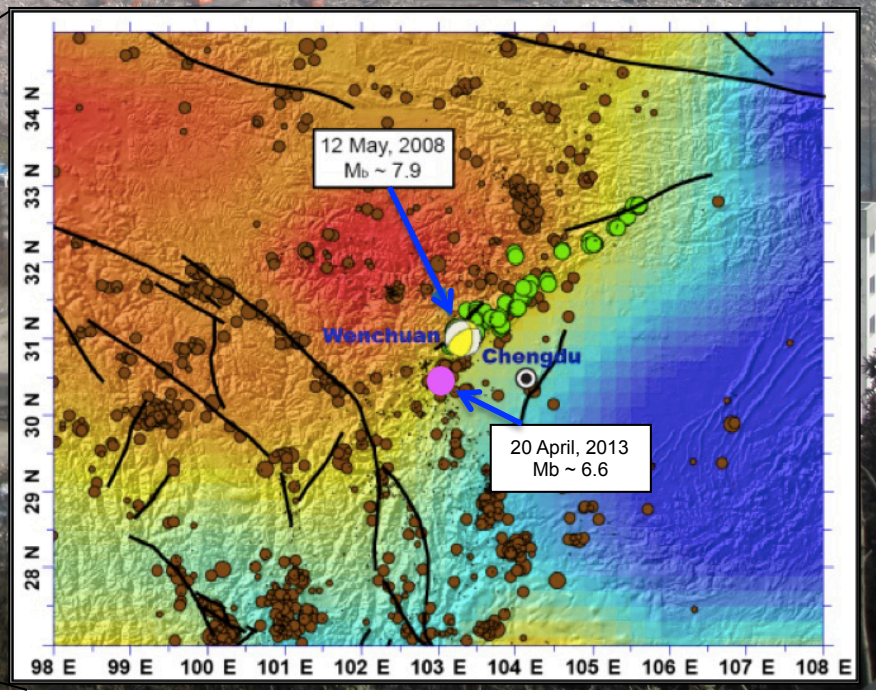

Overview of lecture:

1. Introduction/background
2. Ambient noise and surface wave tomography
3. Reverse time migration of converted waves
4. Interferometry of teleseismic (coda) waves

Interferometry:

long-term noise correlation → new data for crustal tomography

$$\frac{dC_{AB}(t)}{dt} \approx -\hat{G}_{AB}(t) + \hat{G}_{BA}(-t) \approx -G_{AB}(t) + G_{BA}(-t).$$

G = Green's function

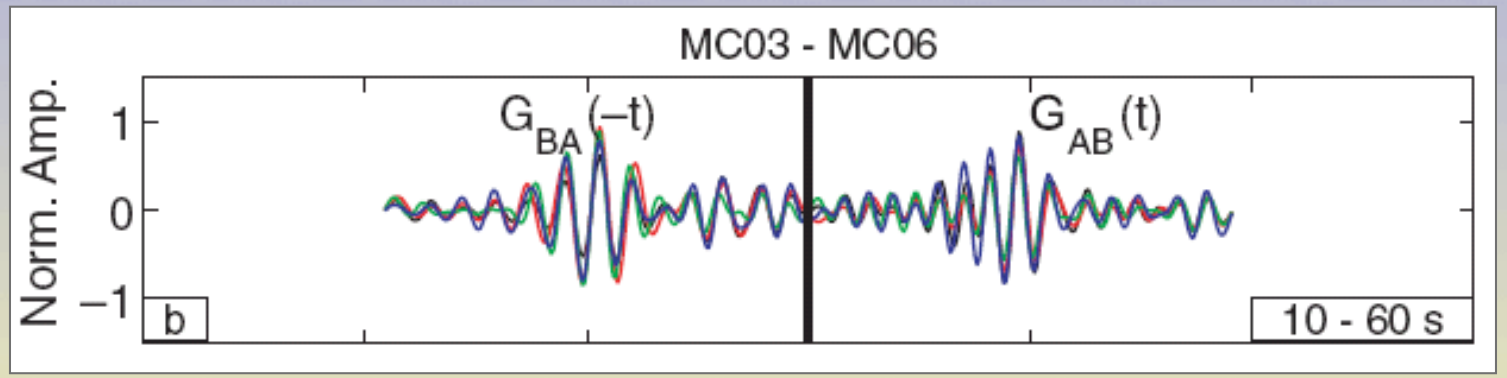

Yao et al. (*GJI*, 2006)

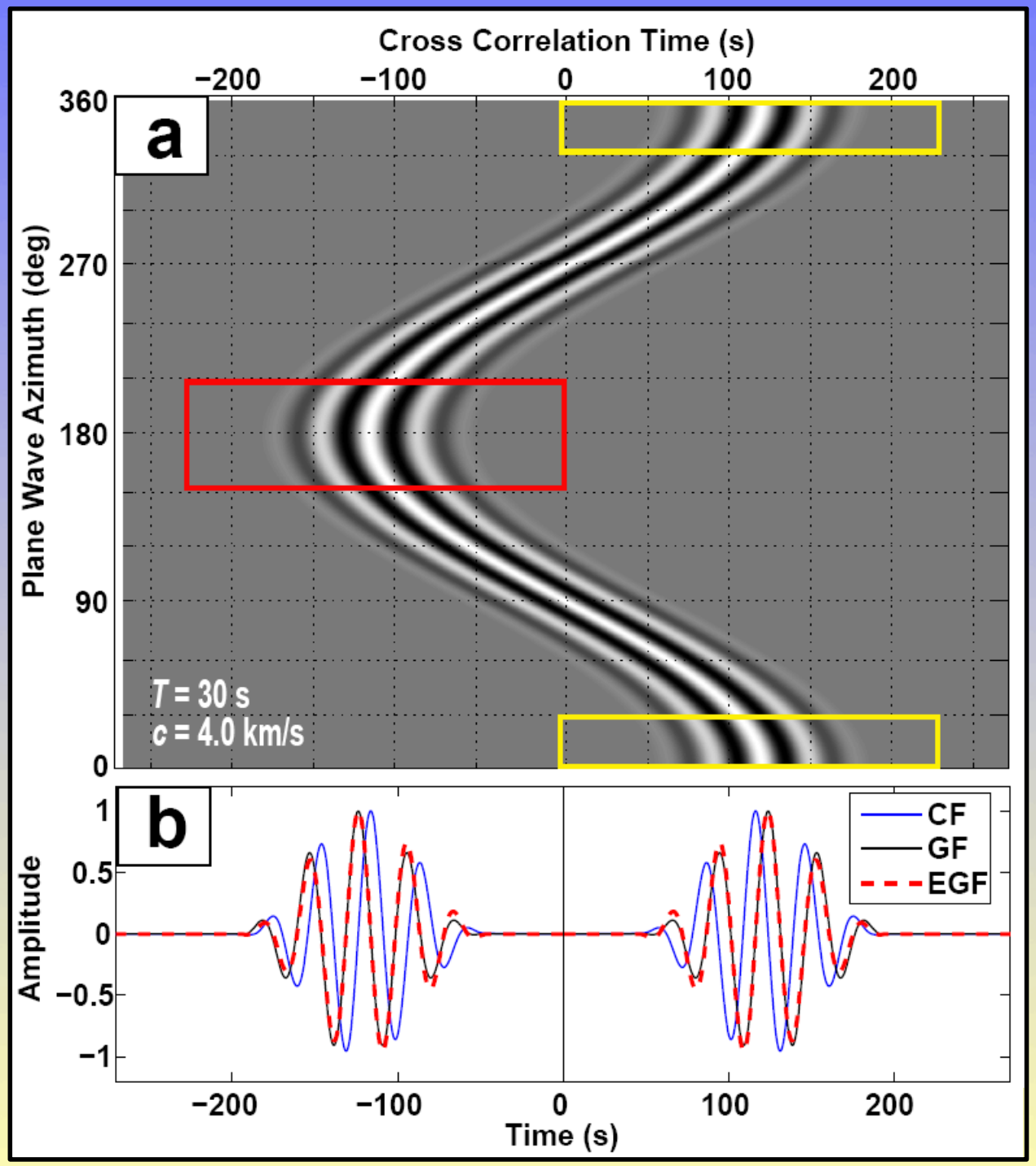

Recovery of surface waves (2D case)

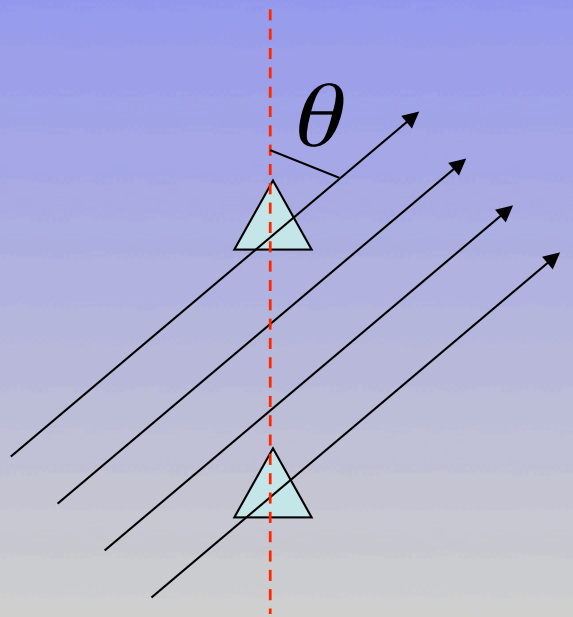

Homogen. + iso medium

isotropic incident plane wave

Yao & Van der Hilst (2009)

Interferometry:

long-term noise correlation → new data for crustal tomography

(simple in concept, but devil is in the detail …)

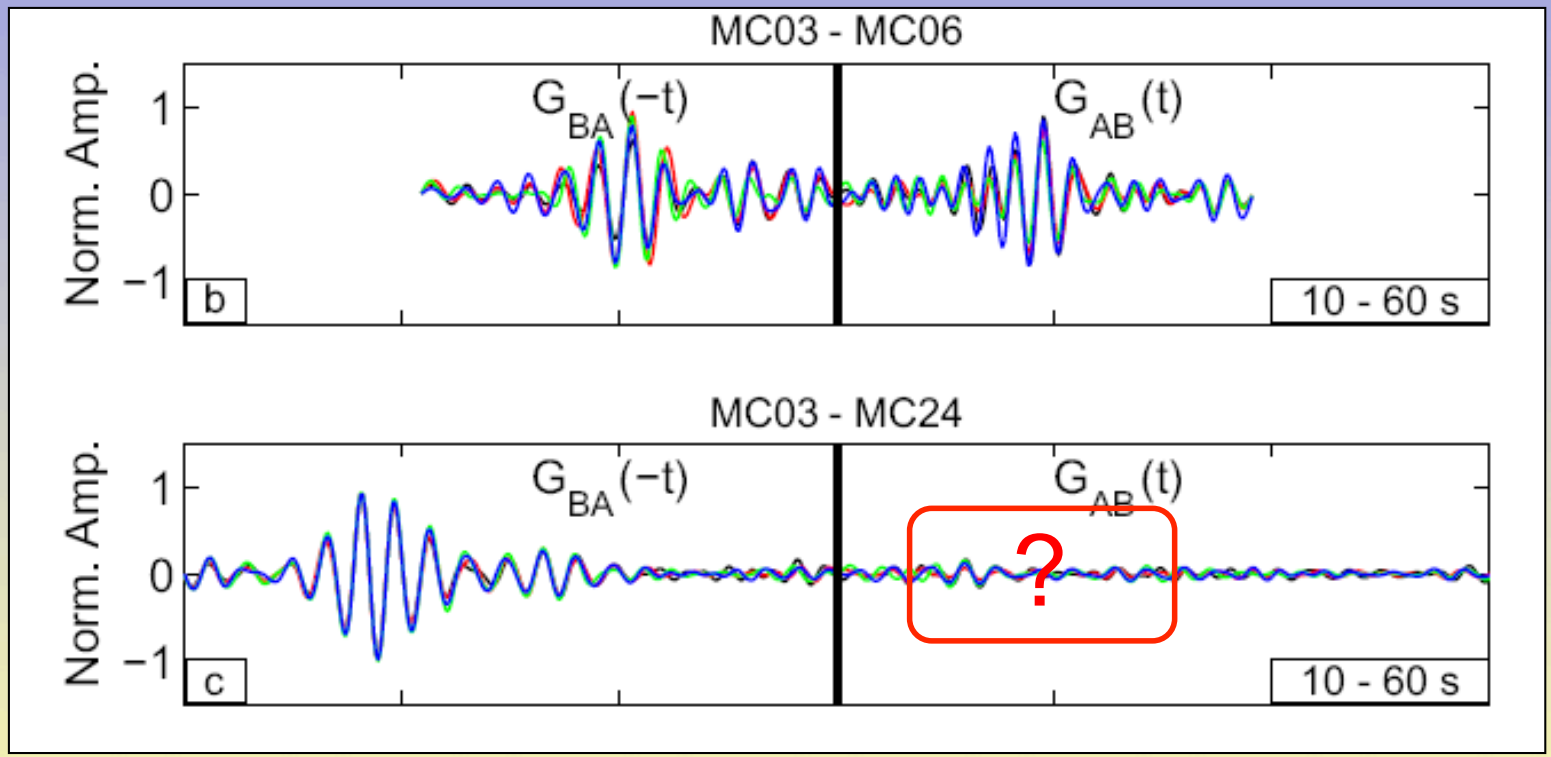

Yao et al. (*GJI*, 2006)

Crust and Lithosphere:
Multi-resolution surface wave tomography

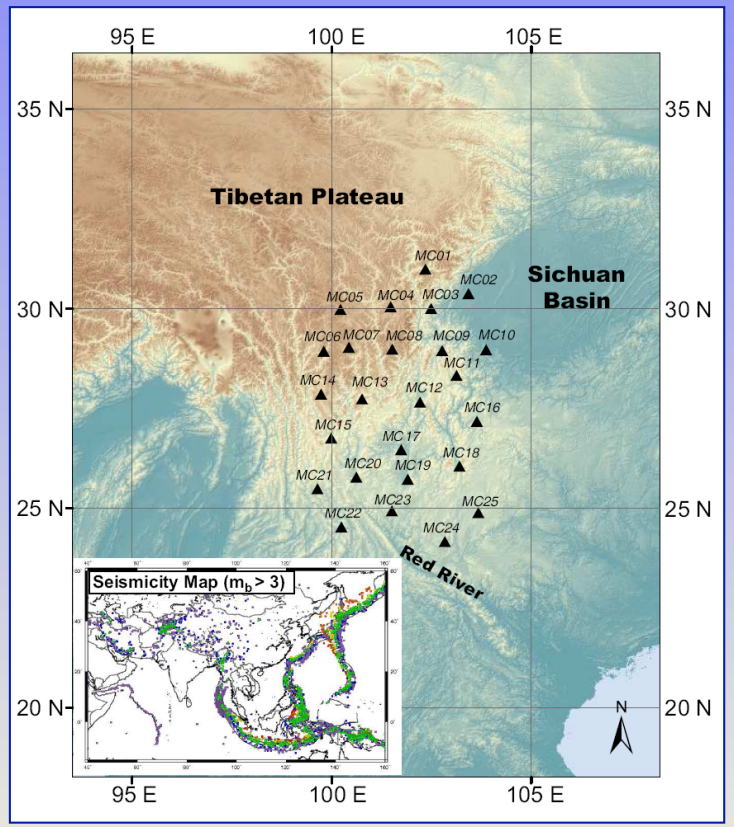

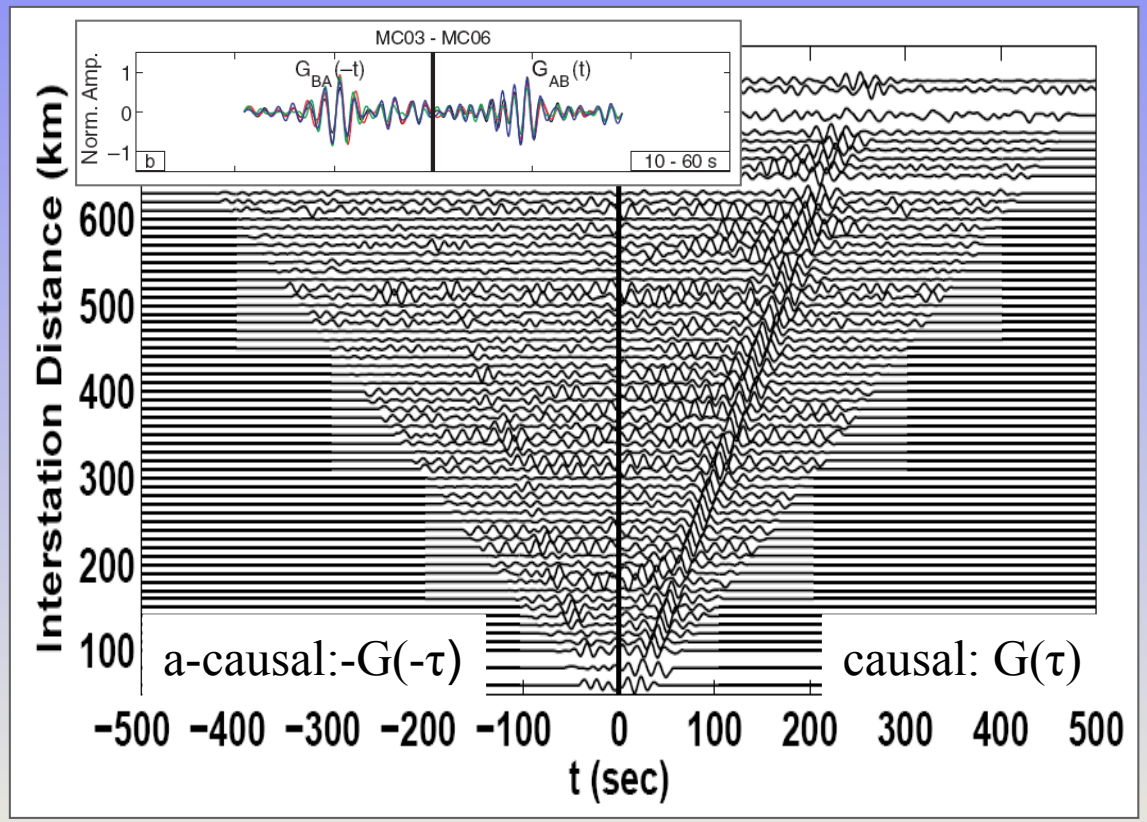

Seismic interferometry → estimate data from background "noise"

(NB we ignore asymmetry and sum causal and a-causal signals)

Example: “ambient noise” surface wave tomography

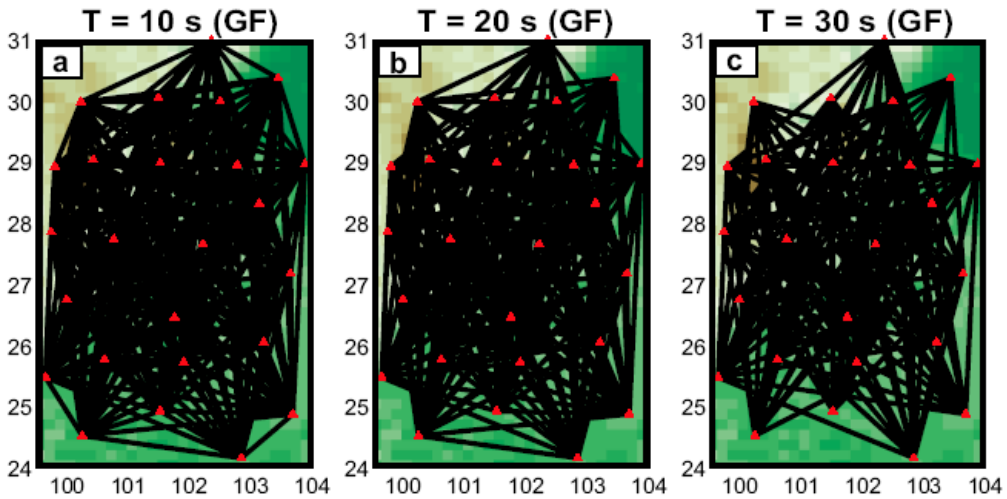

“source”-receiver pairs at different periods

Interferometry (scattering) → works well for relatively short periods (high frequency)

Yao, Van der Hilst, and De Hoop (*GJI*, 2006)

Example: “ambient noise” surface wave tomography

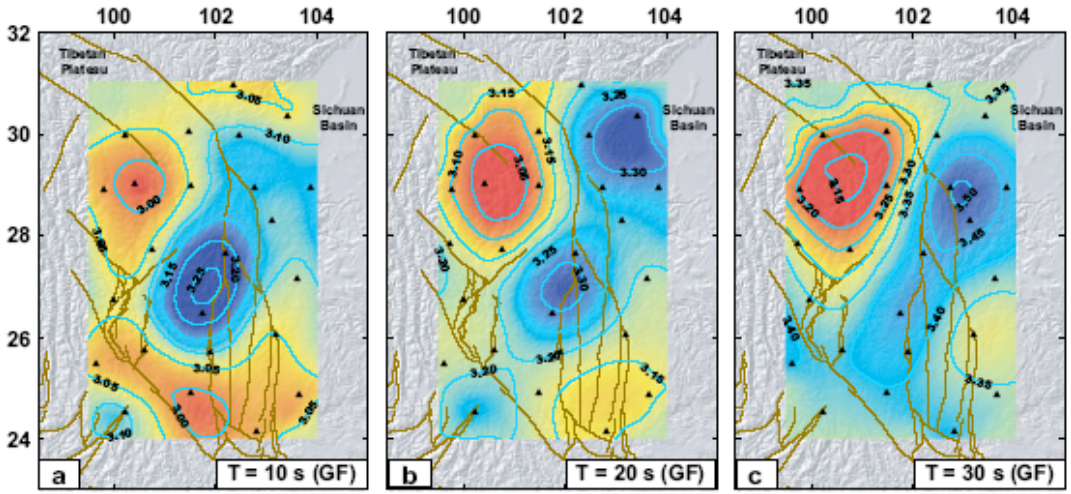

Phase velocity maps at different periods

Interferometry (scattering) → relatively short periods (high frequency)

For surface wave tomography that means: “shallow” sub-surface

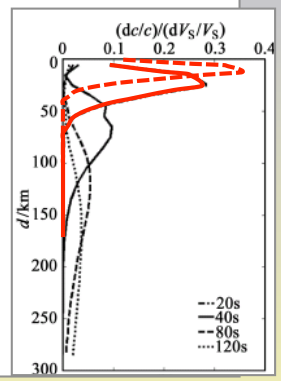

Use both ‘active’ and ‘passive’ data

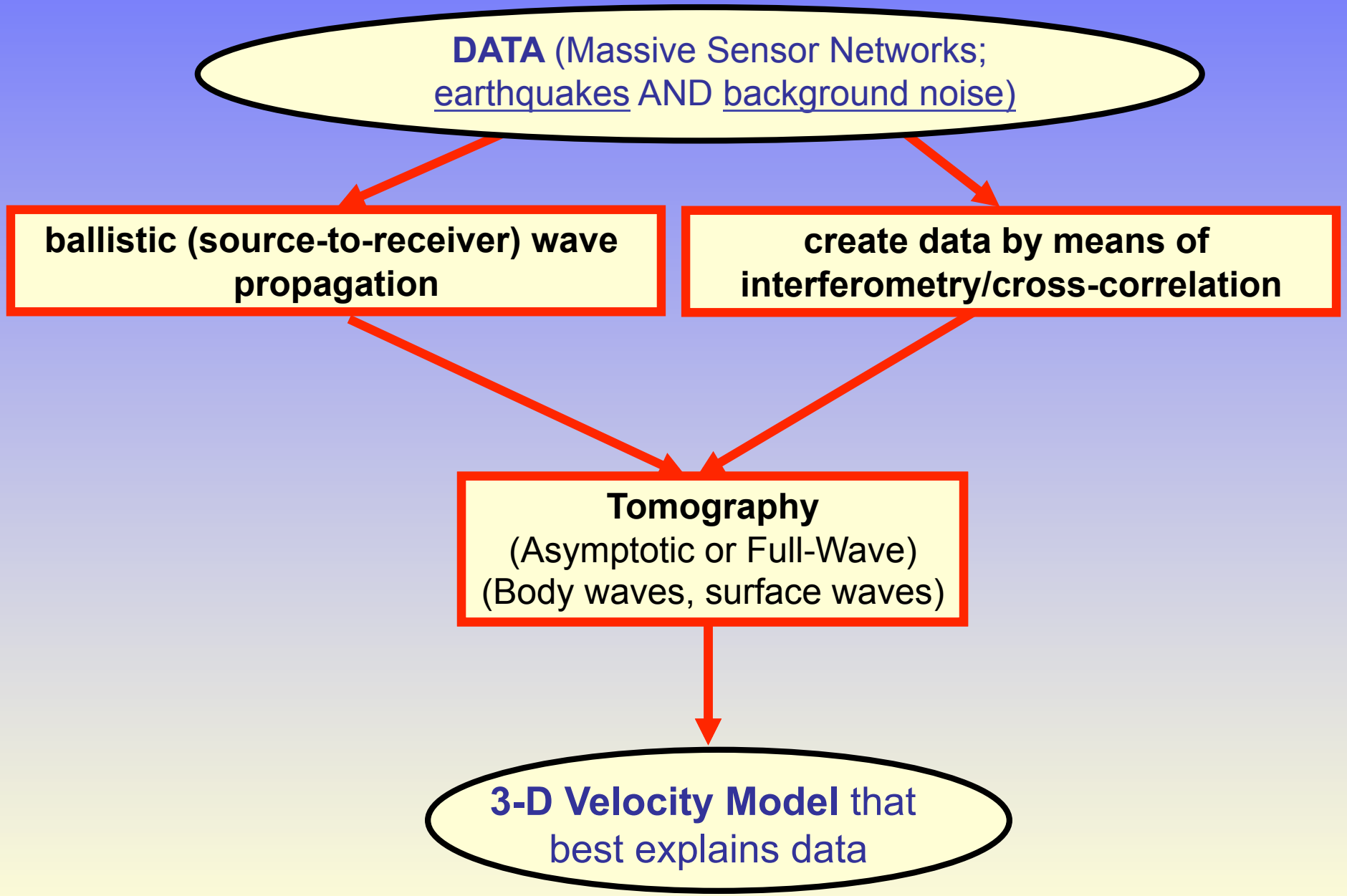

Combination of ambient noise and earthquake data:
extend frequency range → extend depth range

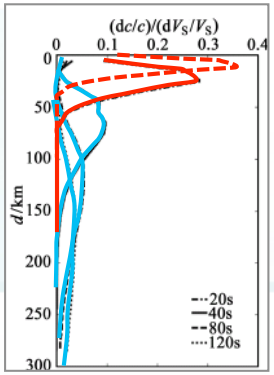

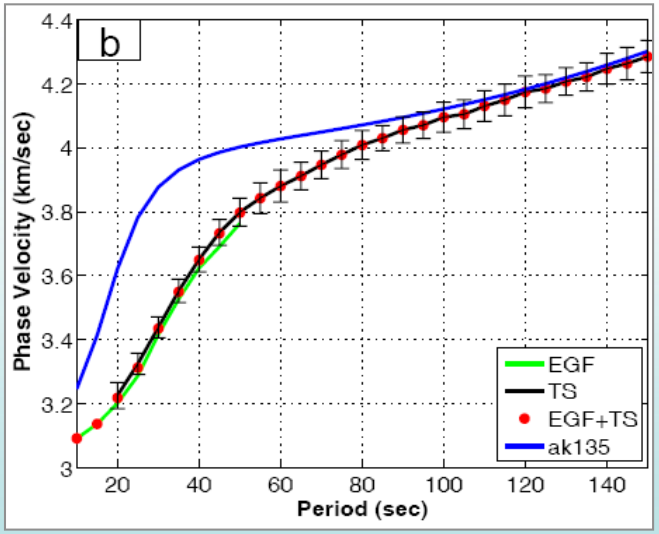

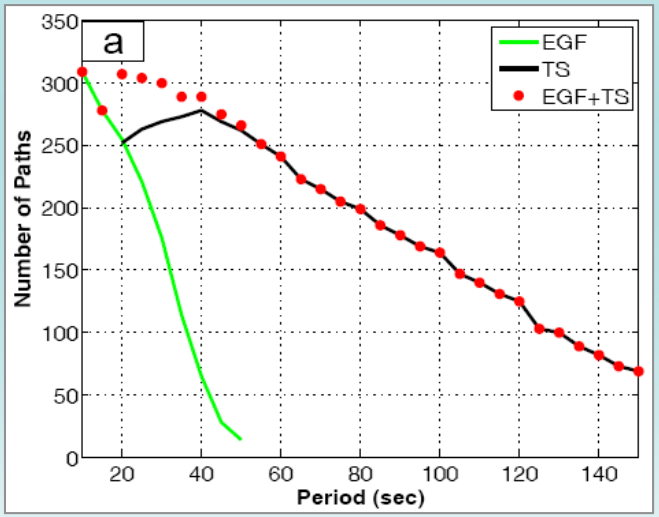

At overlapping periods, Rayleigh wave phase velocities from EGF (from 10 months Z-comp. data) and TS analyses are similar

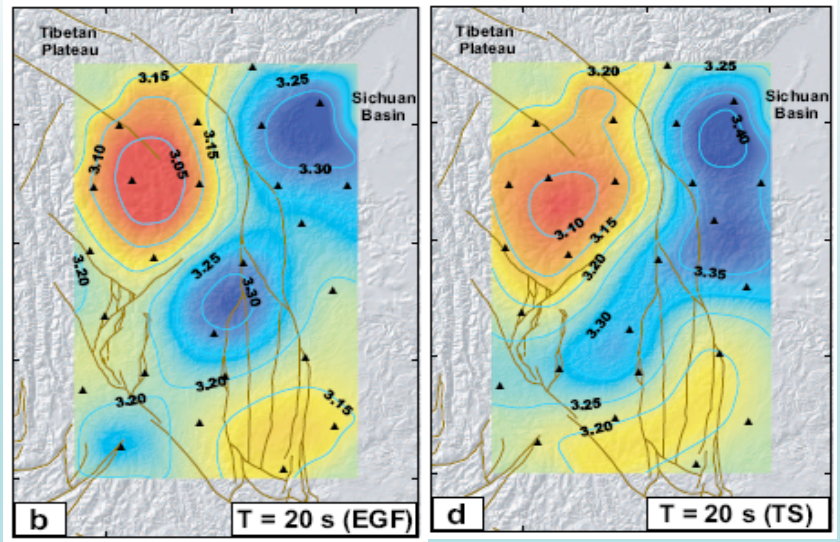

- TS slightly higher (< 0.7%) due to differences in finite frequency effect
- Difference << medium perturbations (< 10%)

Yao, van der Hilst, de Hoop, 2006

Multi-resolution surface wave tomography

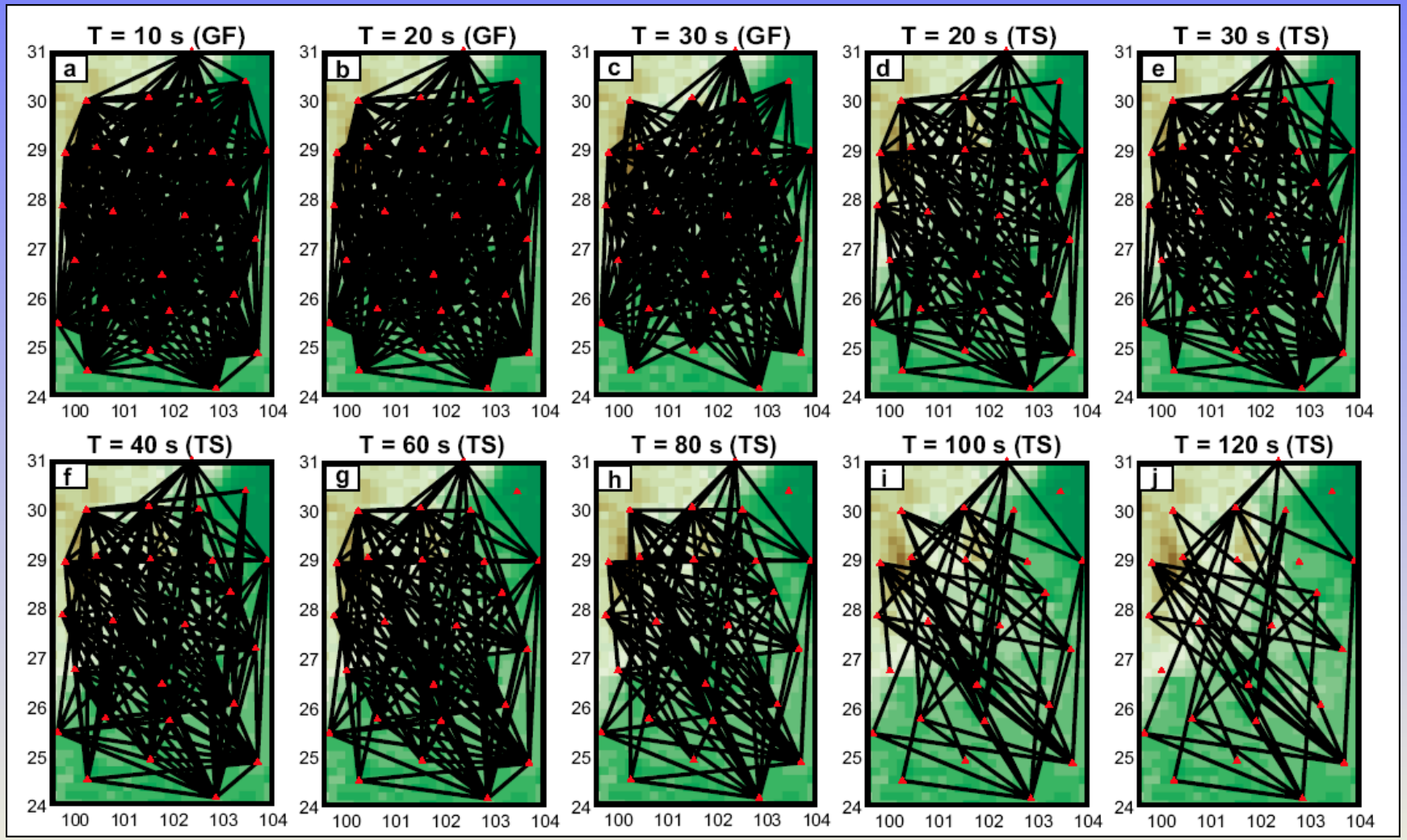

Yao, Van der Hilst, and De Hoop (*GJI*, 2006)

Phase velocity maps at different periods

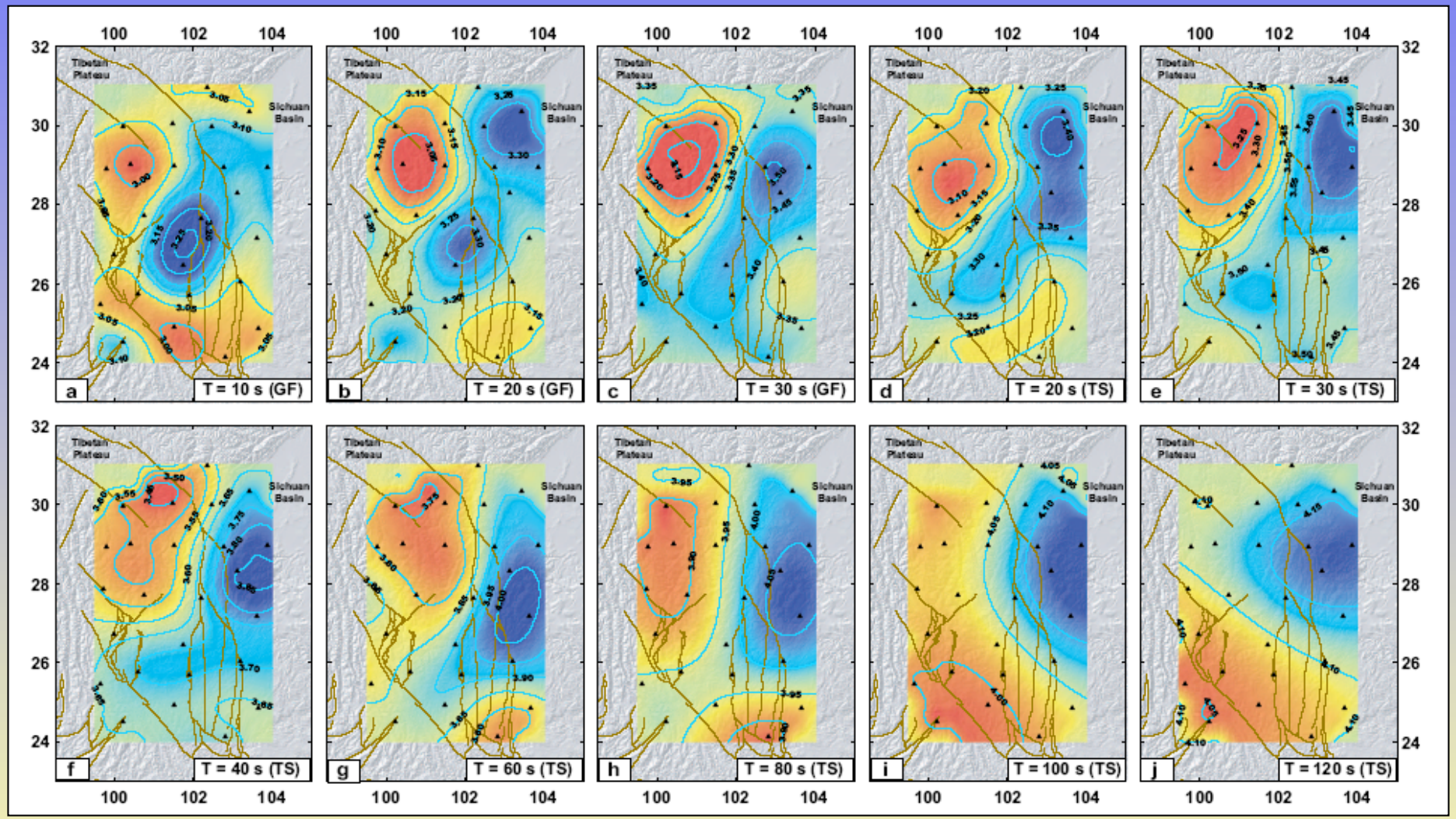

Yao, Van der Hilst, and De Hoop (*GJI*, 2006)

Multi-resolution surface wave tomography

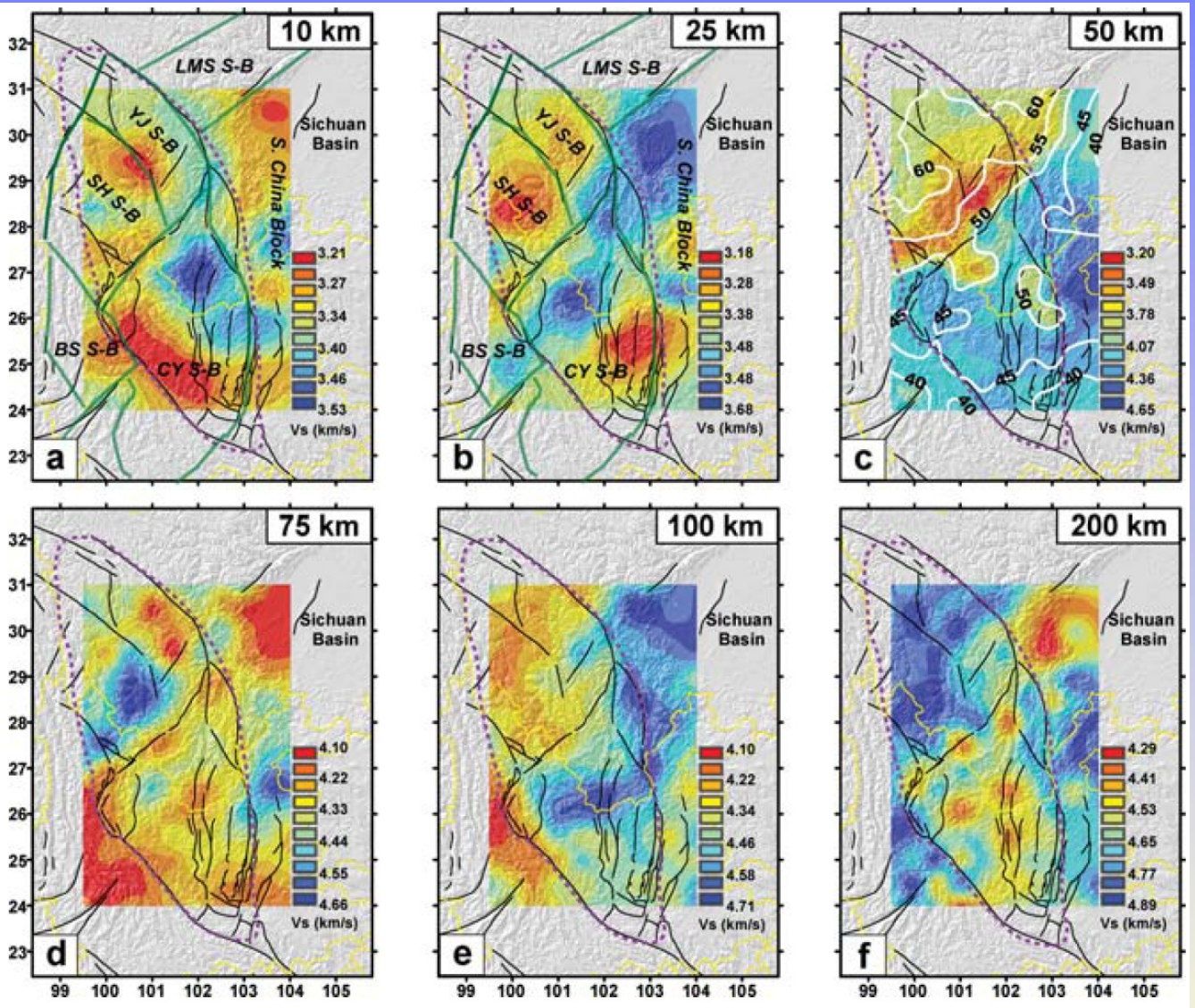

Yao, Beghein, and Van der Hilst (*GJI*, 2008)

Path coverage and lateral resolution of phase velocity maps

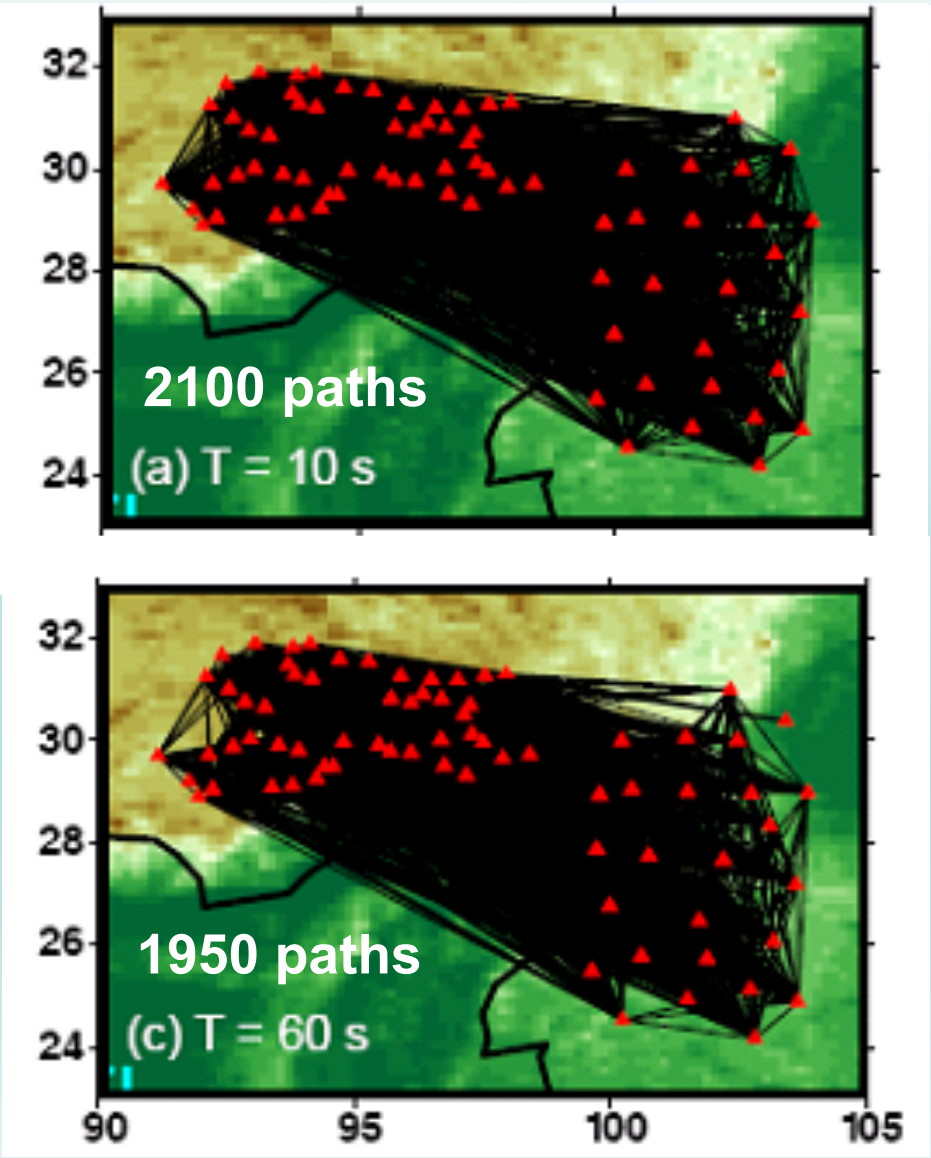

1°x1° input

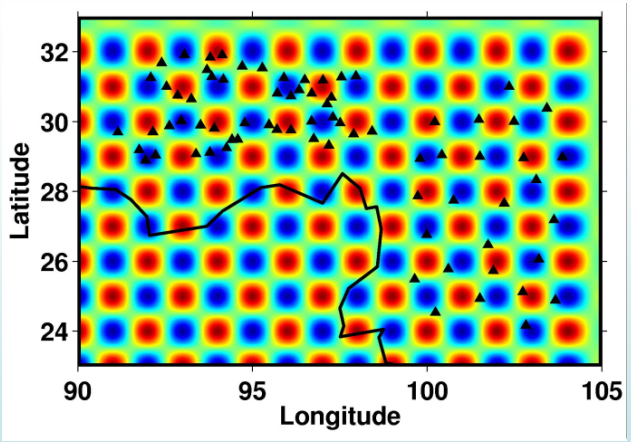

1°x1° output

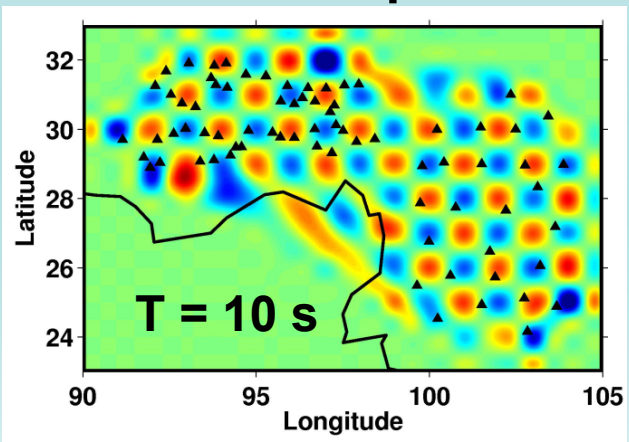

Horizontal resolution ~100 km

Crustal wavespeeds in SE Tibet and Sichuan Province (from Ambient Noise – Rayleigh wave – tomography)

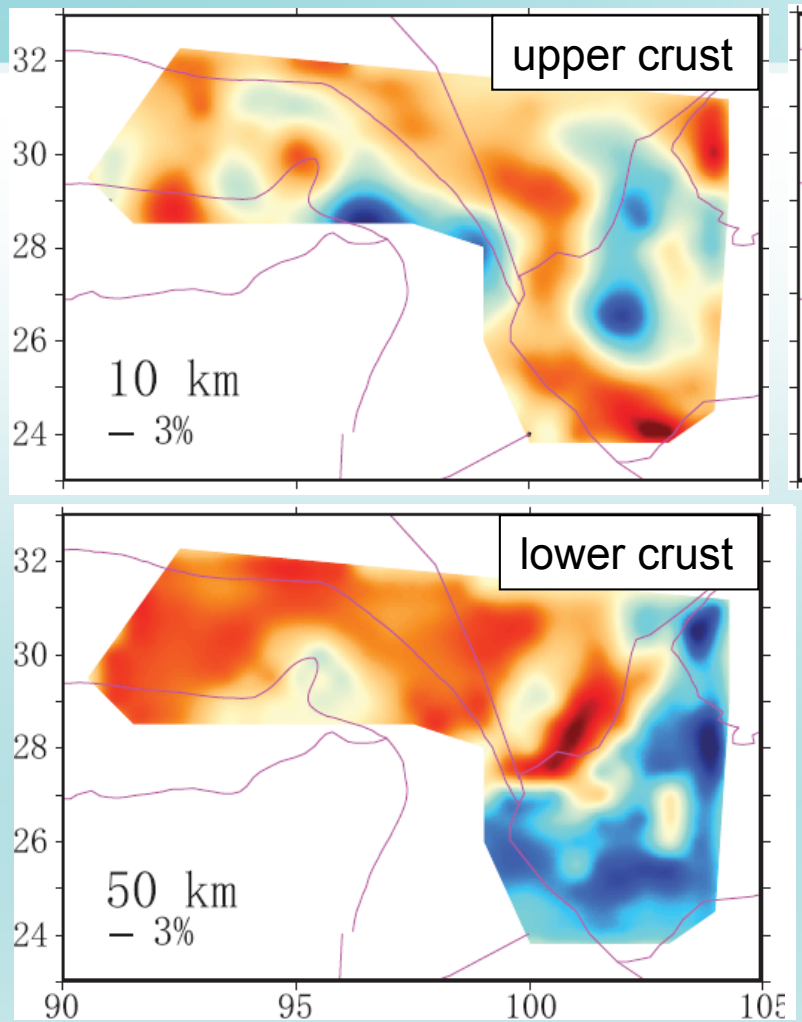

Yao, Van der Hilst, and Montagner (*JGR*, 2010)

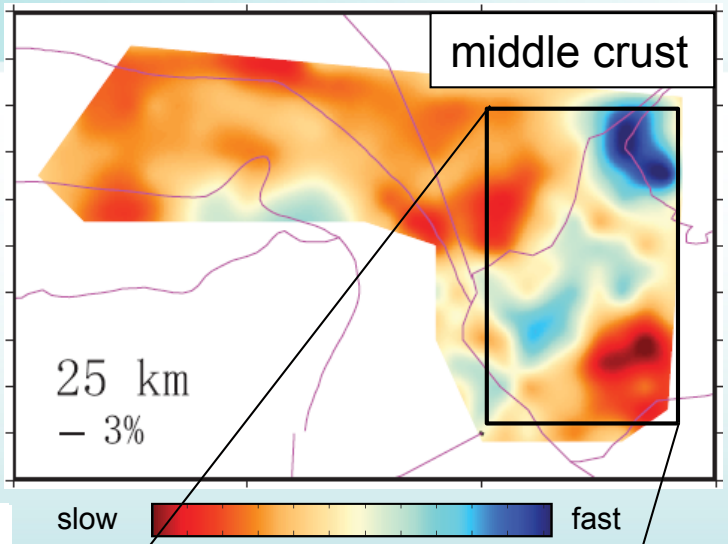

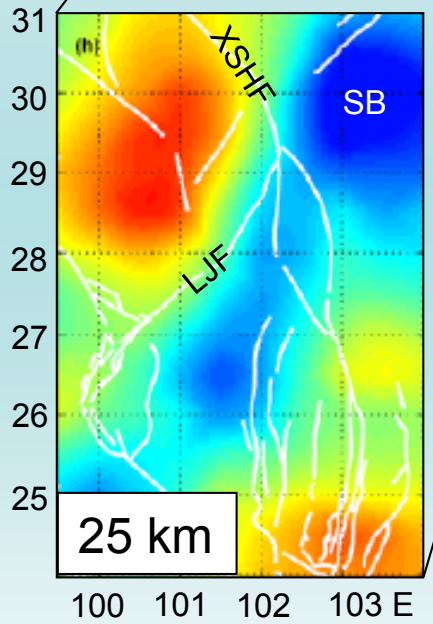

Complex 3D pattern of low velocity layers

Huang, Yao, Van der Hilst (*GRL*, 2010)
(average Love-Rayleigh speed)

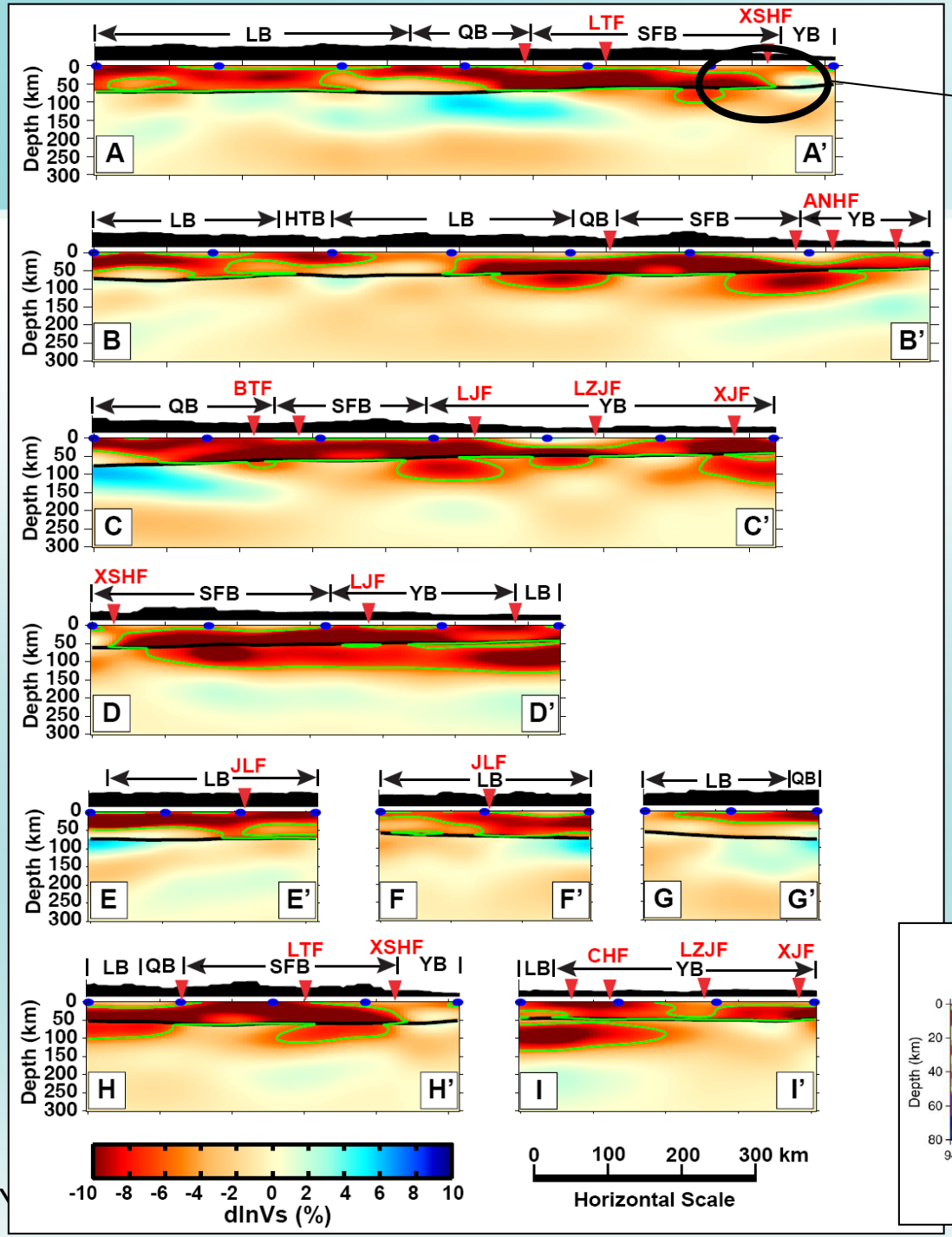

Yao, Van der Hilst, and Montagner (JGR, 2010)

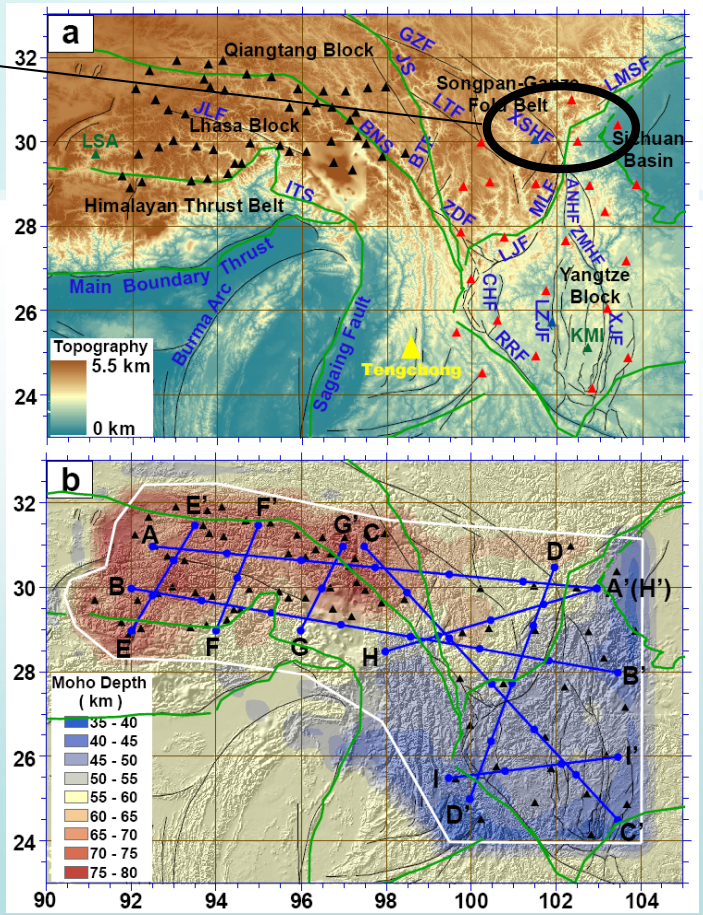

Receiver Functions – Wang et al. *(EPSL, 2010)*

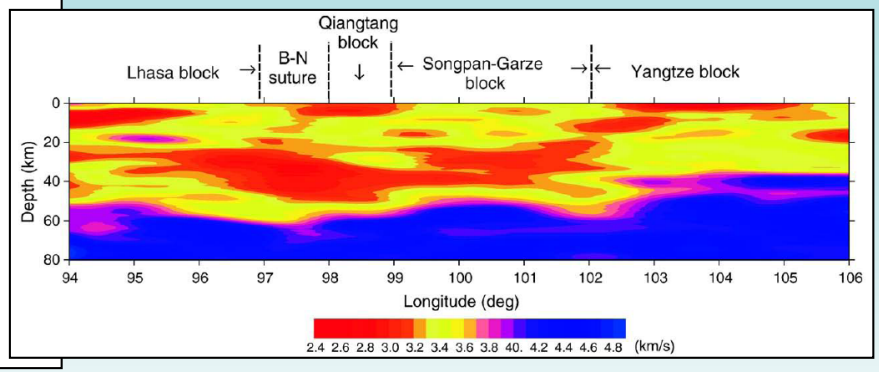

Topographic gradients on plateau margin reflect the strength (effective viscosity) of the weakest layer in the underlying crust

Figure: Royden (MIT)

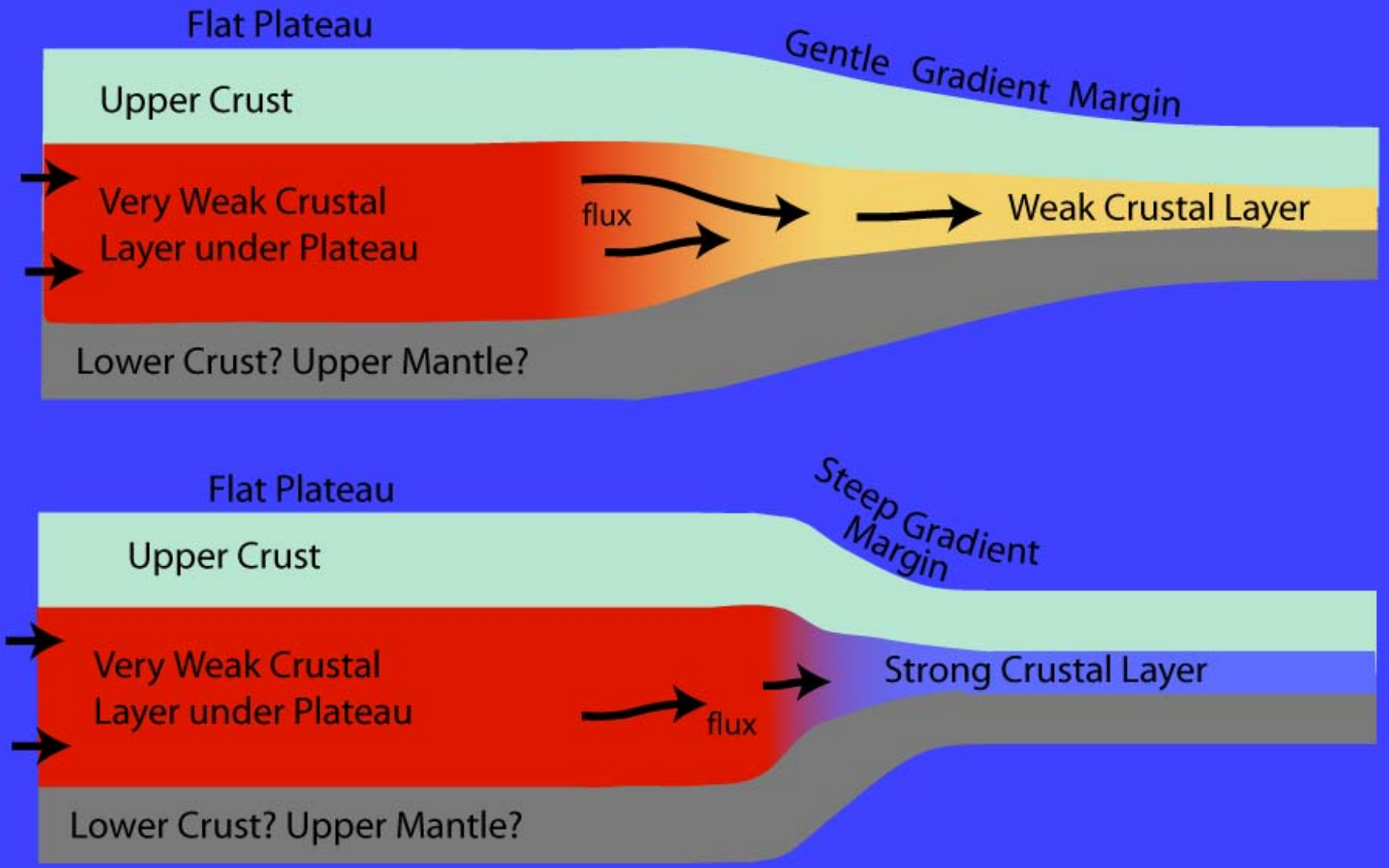

Regional variation in topographic gradient at the margins of the Tibetan Plateau

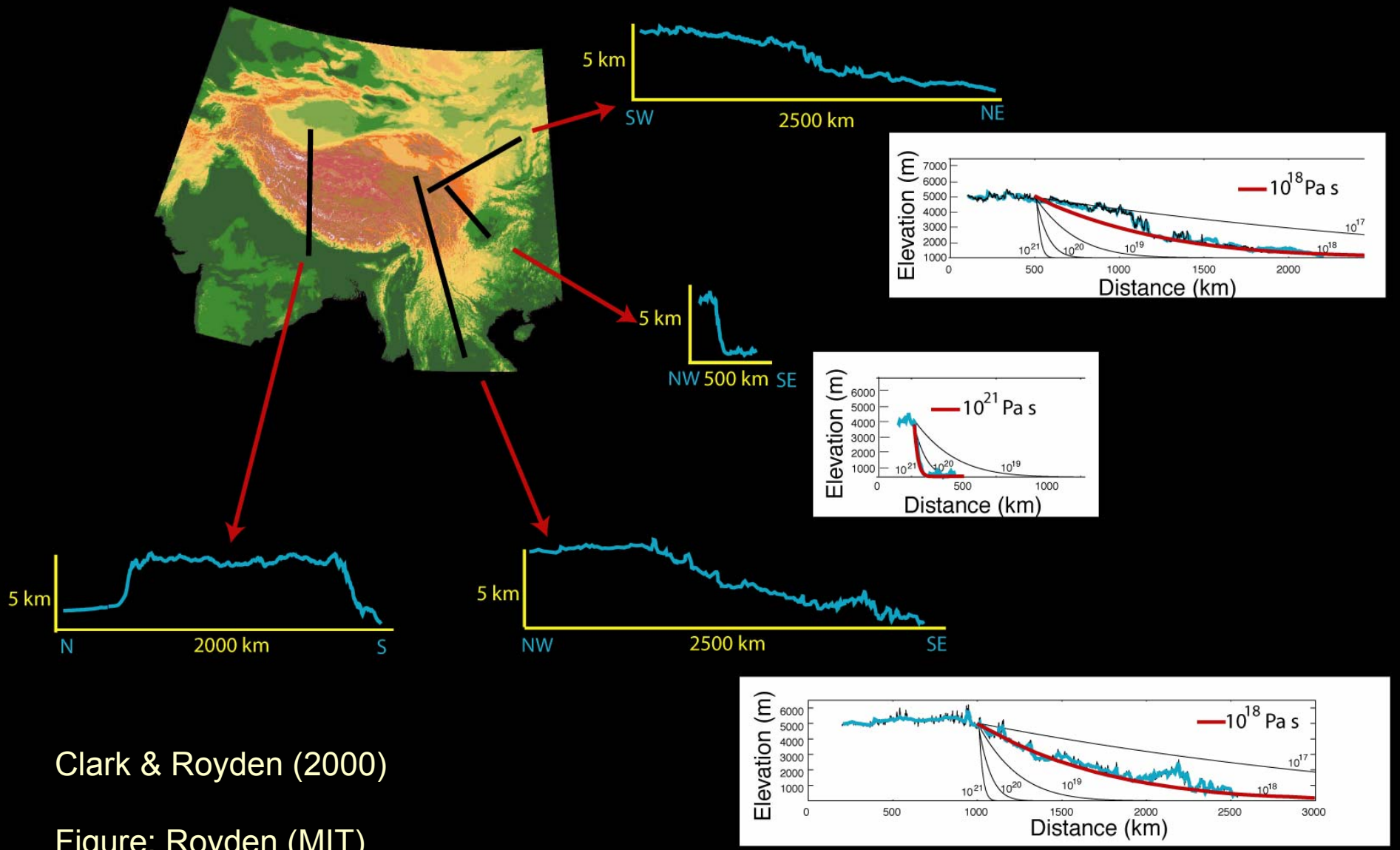

Clark & Royden (2000)

Figure: Royden (MIT)

Yao, Van der Hilst, Montagner (*JGR,* 2010)

Anisotropy I: Azimuthal Anisotropy

(i.e., dependence of wavespeed on direction of propagation in horizontal plane)

- Step 1: inter-station phase velocities from **EGF** → azimuthally anisotropic phase velocity maps

$$c(\omega,\psi) = c_0(\omega)[1 + a_0(\omega) + a_1(\omega)\cos 2\psi + a_2(\omega)\sin 2\psi]$$

- Step 2: phase velocity maps → shear wave speed & anisotropy

$$\delta c_R(x,y,\omega,\psi) \approx \int_0^H \left[\frac{\partial c_R}{\partial L}\left(\delta L + G_c \cos 2\psi + G_s \sin 2\psi\right)\right]\frac{dz}{\Delta h}$$

At each point (x,y), the reference crustal thickness is constrained from receiver functions (Xu et al., 2007; Zurek et al, 2005)

$$\hat{\beta}_{SV} \approx \beta_{SV}\left(1 + \frac{G_c}{2L}\cos 2\psi + \frac{G_s}{2L}\sin 2\psi\right)$$

Transverse isotropic V_{SV}: $\beta_{SV} = \sqrt{L/\rho}$

Magnitude of azimuthal aniso: $A_{SV} = \frac{1}{2L}\sqrt{(G_c)^2 + (G_s)^2}$

Fast axis of azimuthal aniso: $\phi = \frac{1}{2}\tan^{-1}(G_s/G_c)$

3D lithospheric heterogeneity & azimuthal anisotropy

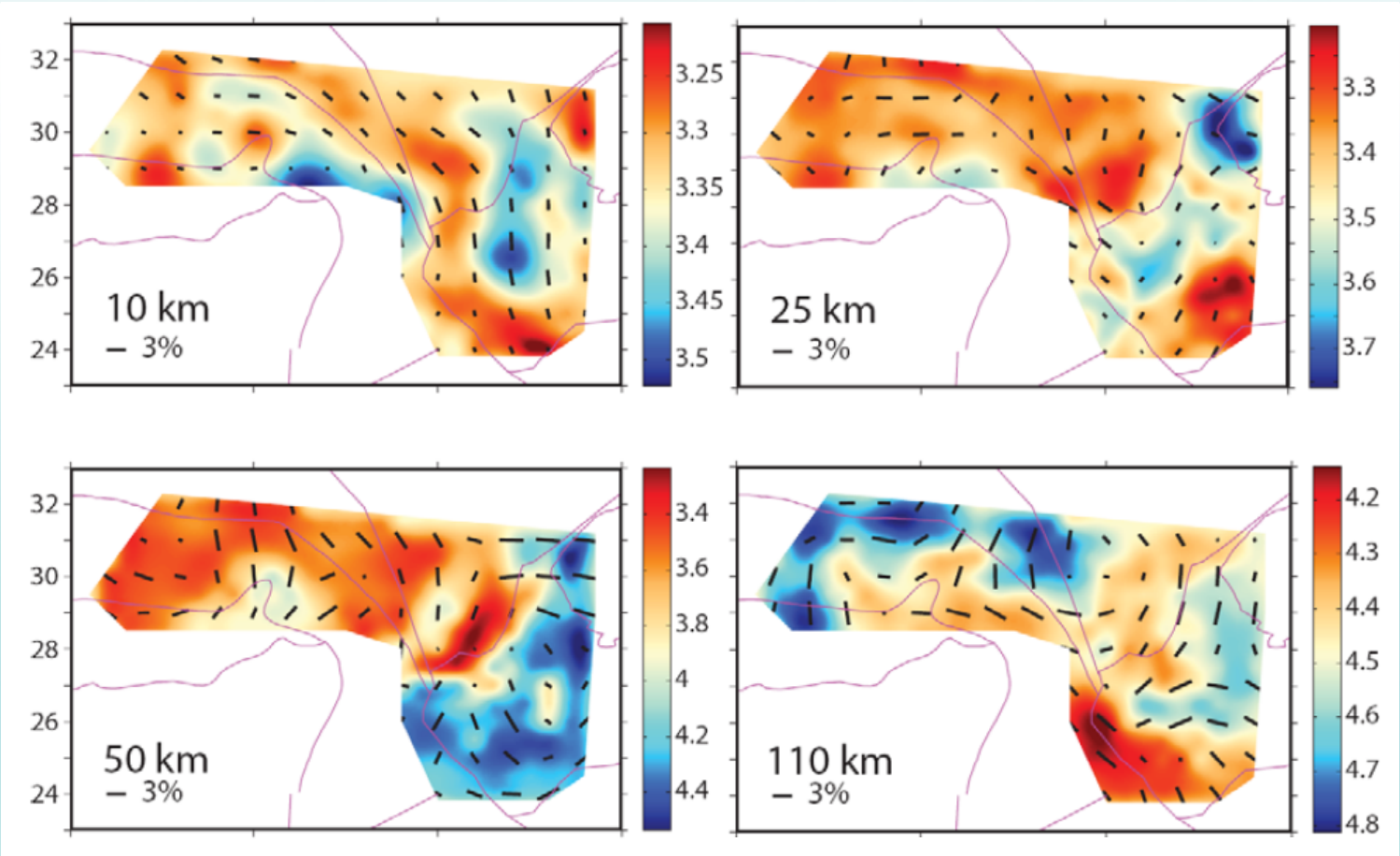

Yao, Van der Hilst, and Montagner (JGR, 2010)

Complicated deformation pattern:

Upper crust: consistent with clockwise rotation (GPS)

Uppermost mantle: fast direction along the LVZ of the margin of Yangtze block

SKS splitting (~ azimuthal anisotropy) and GPS (purple arrows)

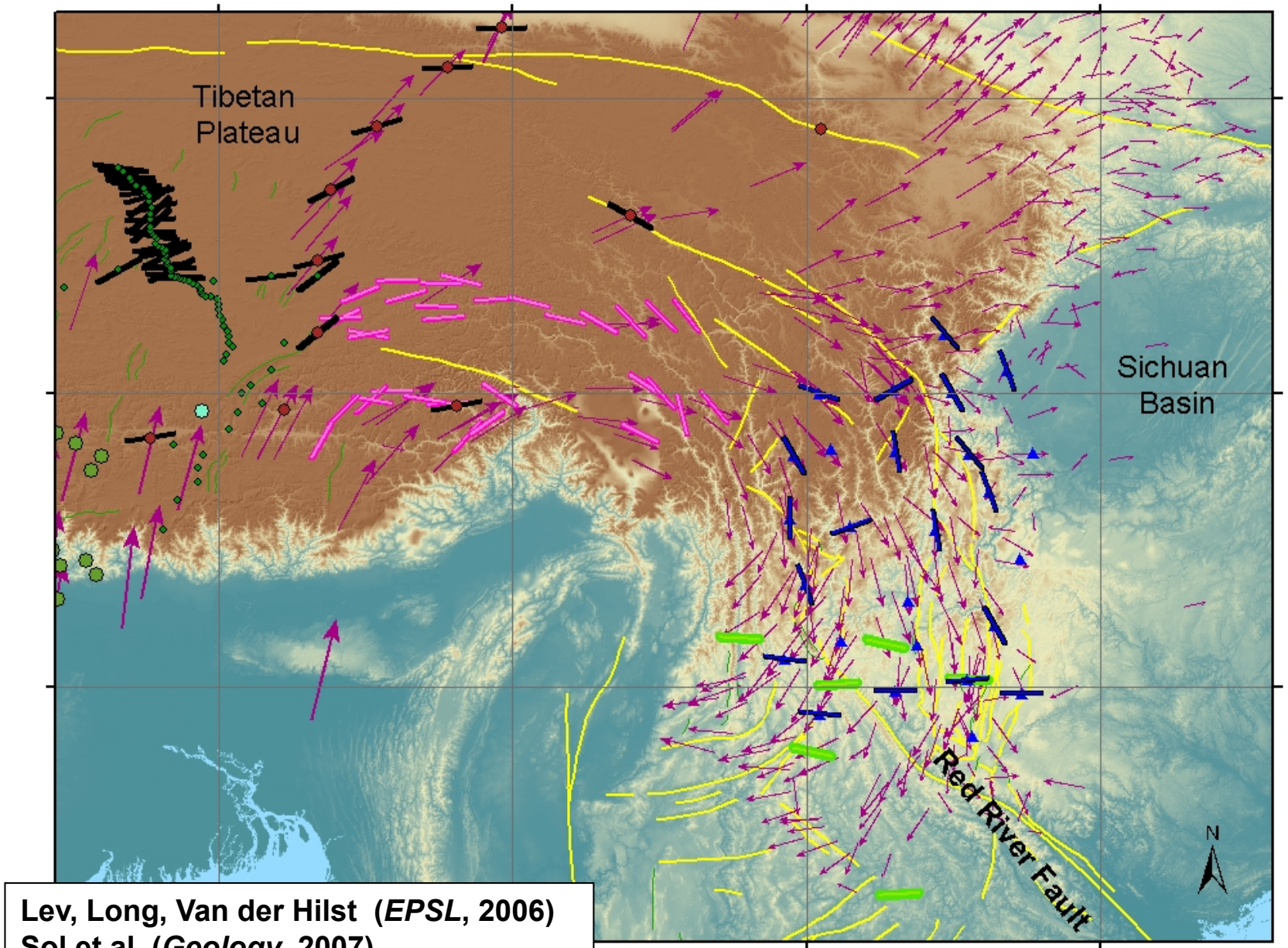

Lev, Long, Van der Hilst (*EPSL*, 2006)
Sol et al. (*Geology*, 2007)

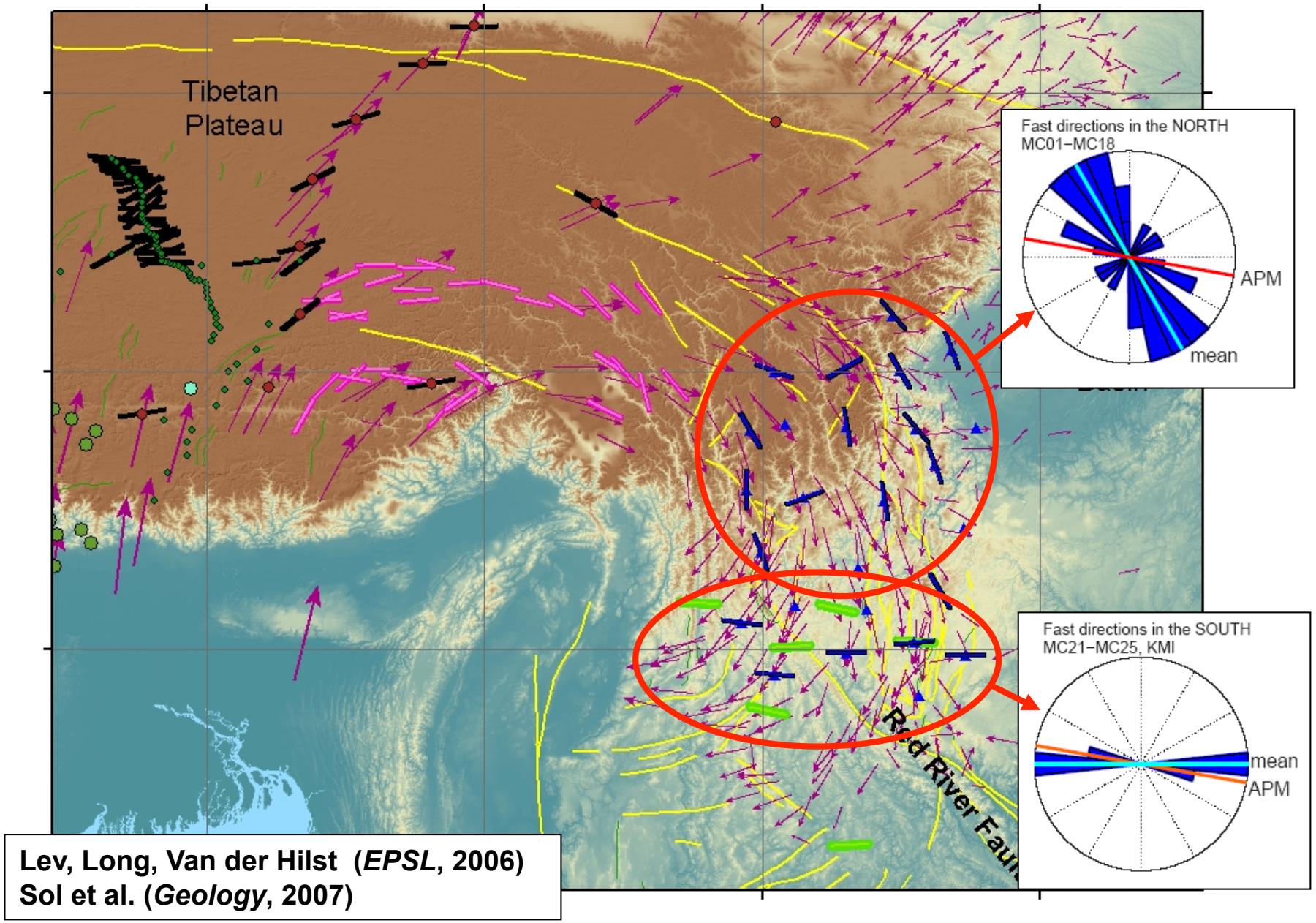

Lev, Long, Van der Hilst (*EPSL*, 2006)
Sol et al. (*Geology*, 2007)

strong variation of azimuthal anisotropy with depth

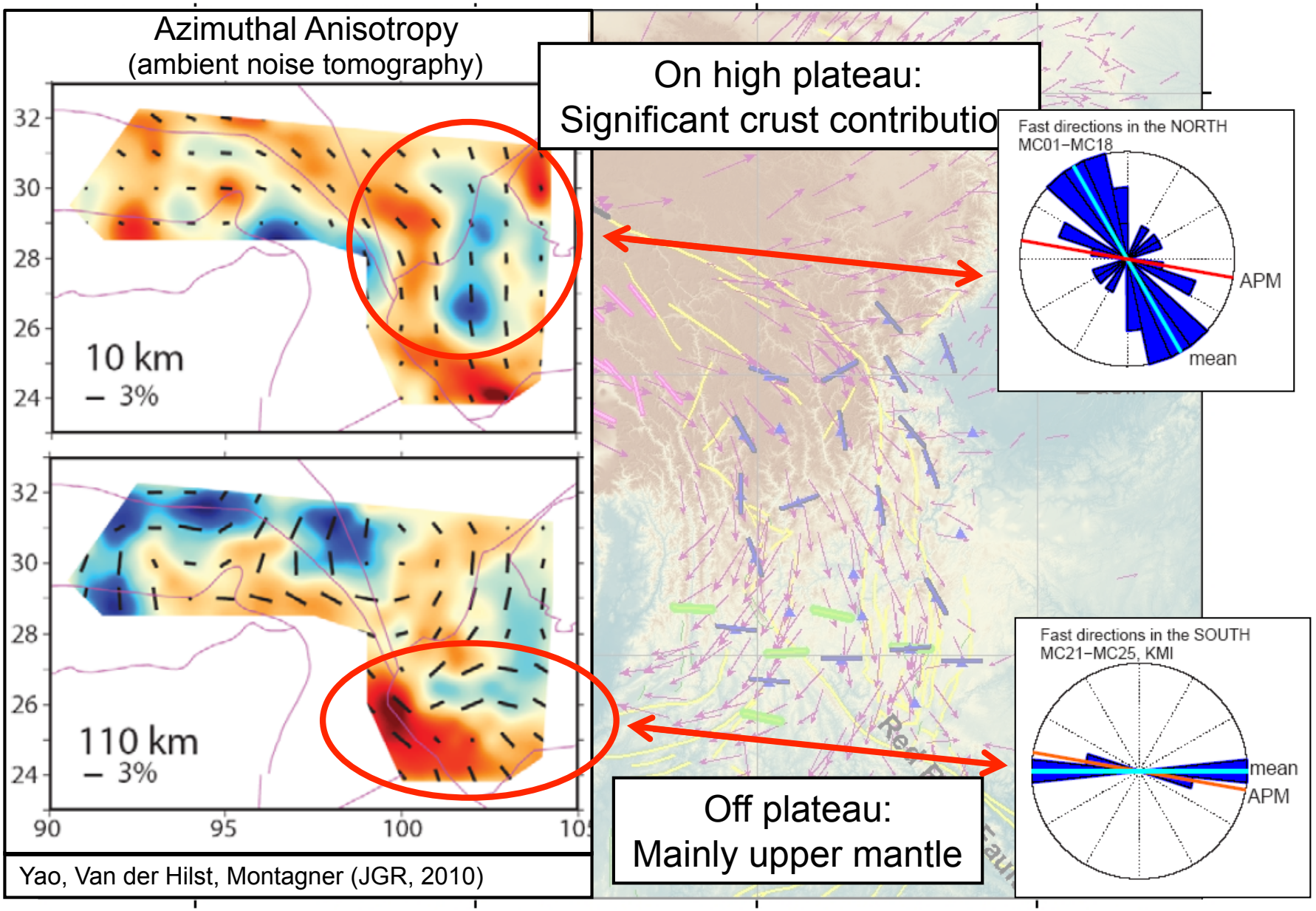

strong variation of azimuthal anisotropy with depth

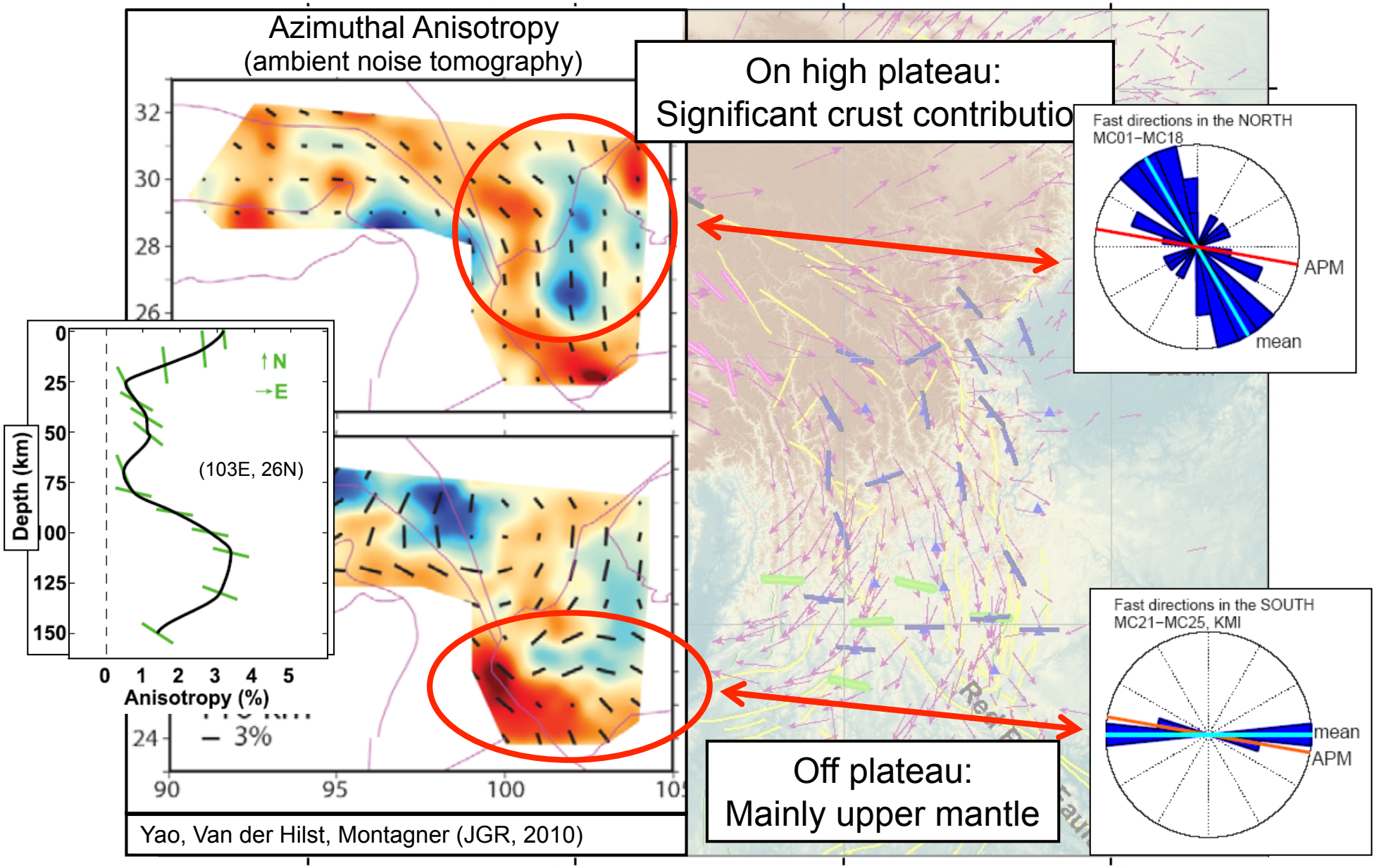

Radial Anisotropy from joint inversion of Love and Rayleigh wave dispersion (empirical Green's functions for noise correlation).

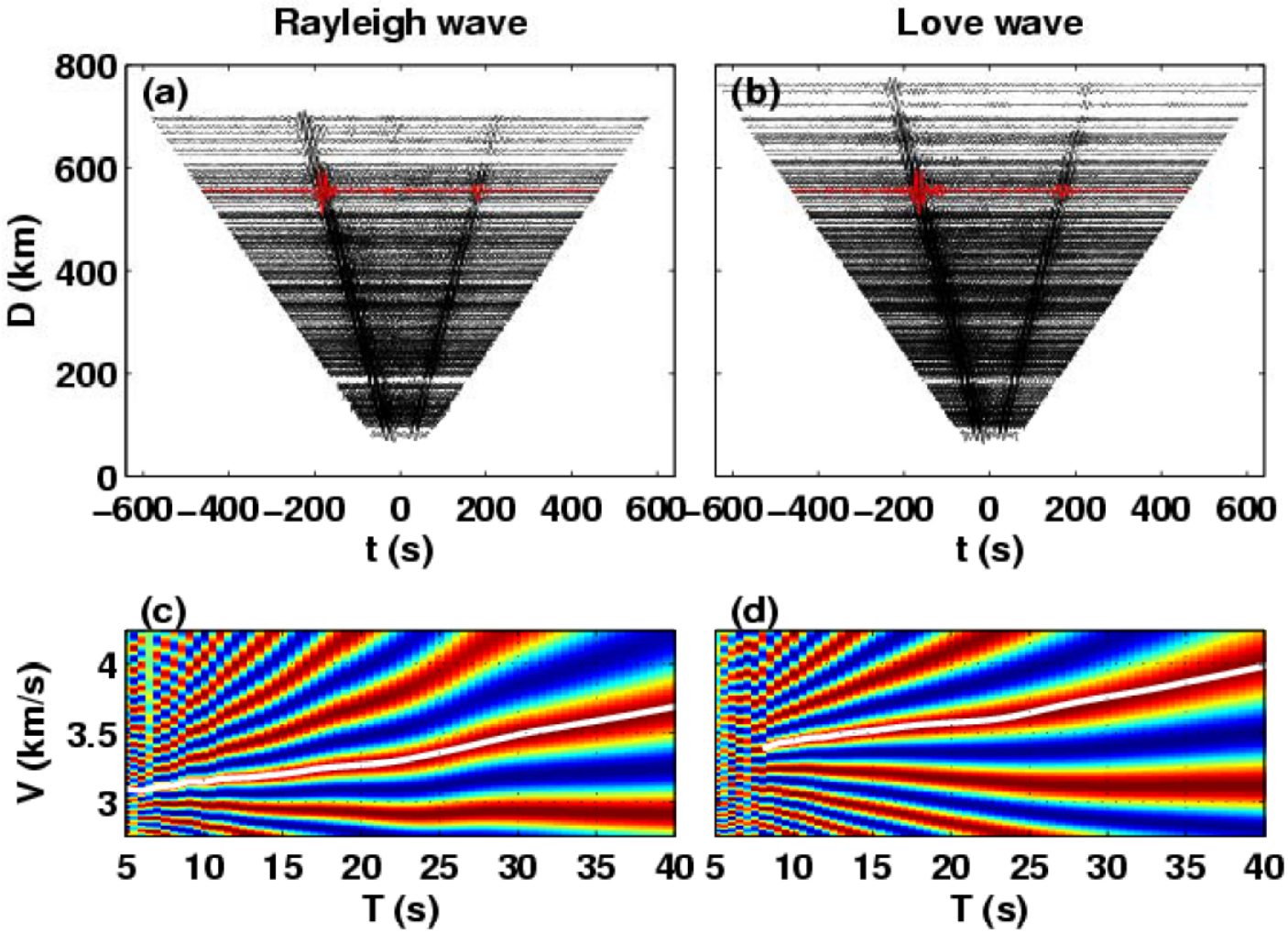

Huang, Yao, and Van der Hilst (GRL, 2010)

Anisotropy II: Radial Anisotropy (or: transverse *isotropy*)

(i.e., difference between wavespeed of horizontally and vertically polarized waves)

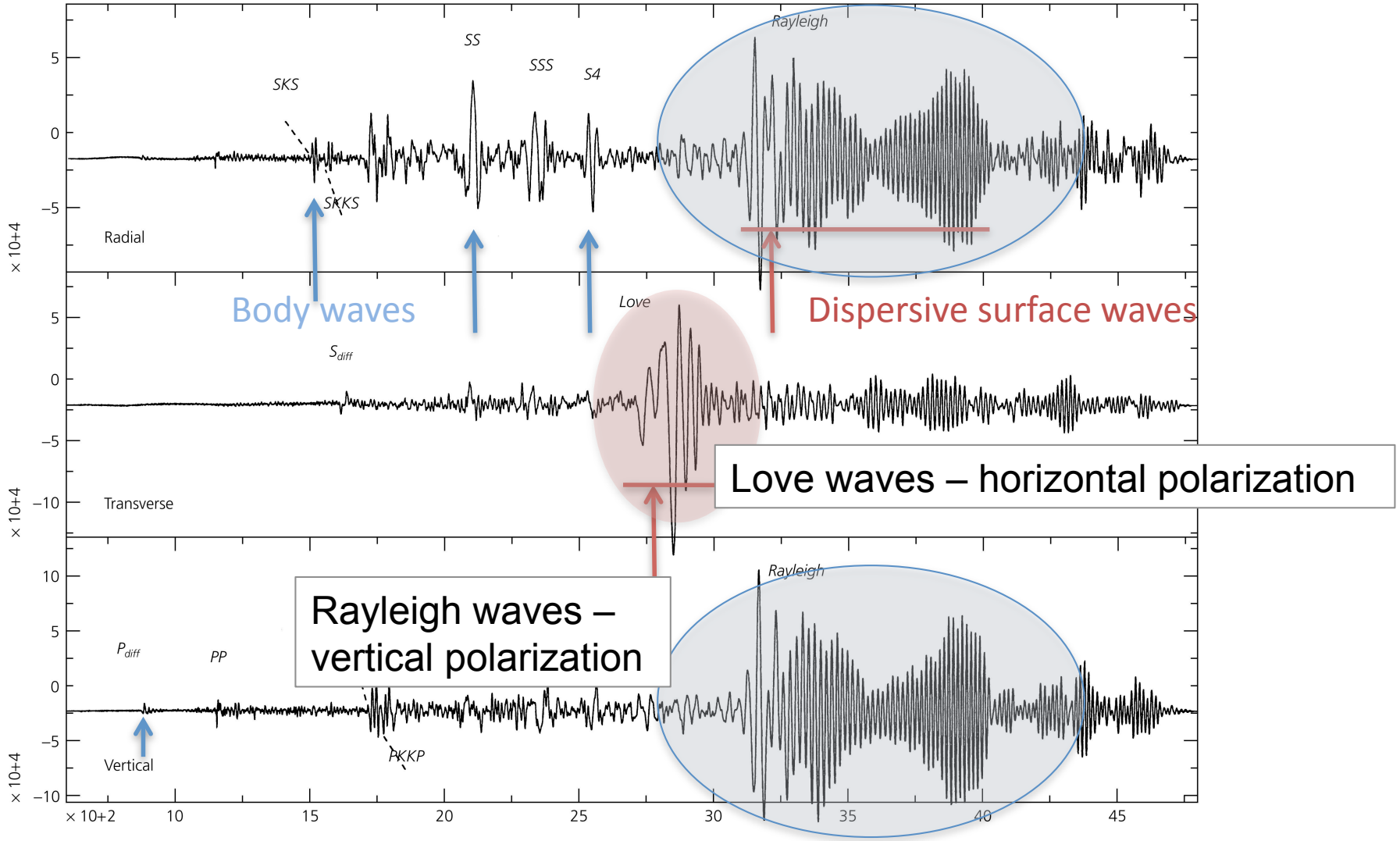

From Stein and Wysession

Radial Anisotropy (from Love and Rayleigh wave dispersion)

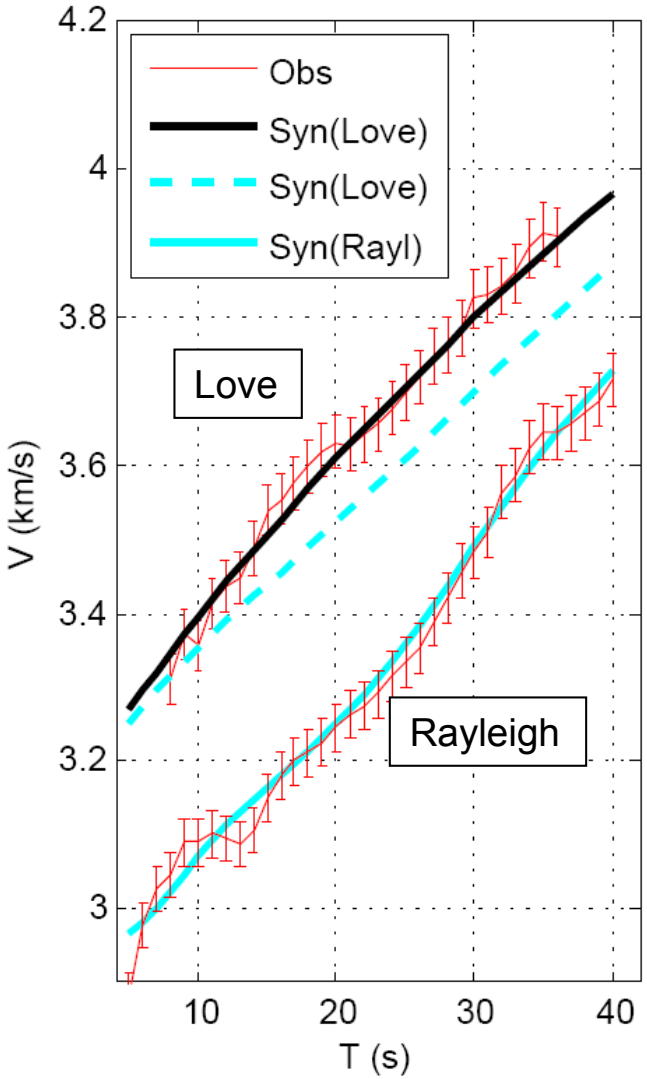

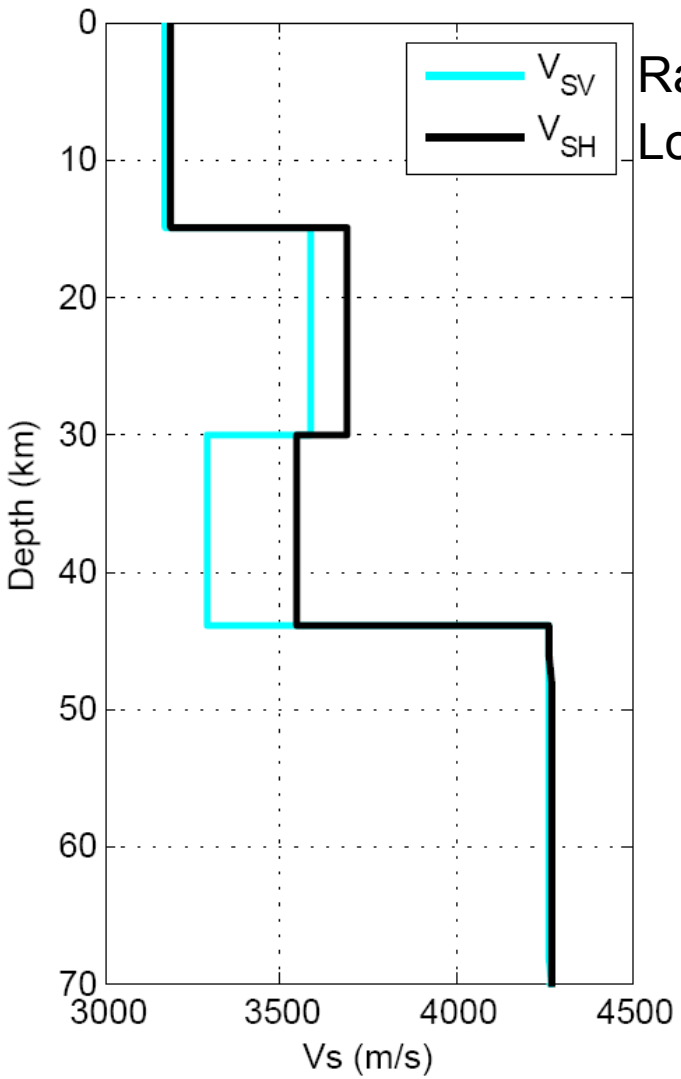

Rayleigh waves

Love waves

Huang, Yao, and Van der Hilst (GRL, 2010)

Huang, Yao, and Van der Hilst (GRL, 2010)

Strong correlation with LVZs → horizontal flow in weak zones?

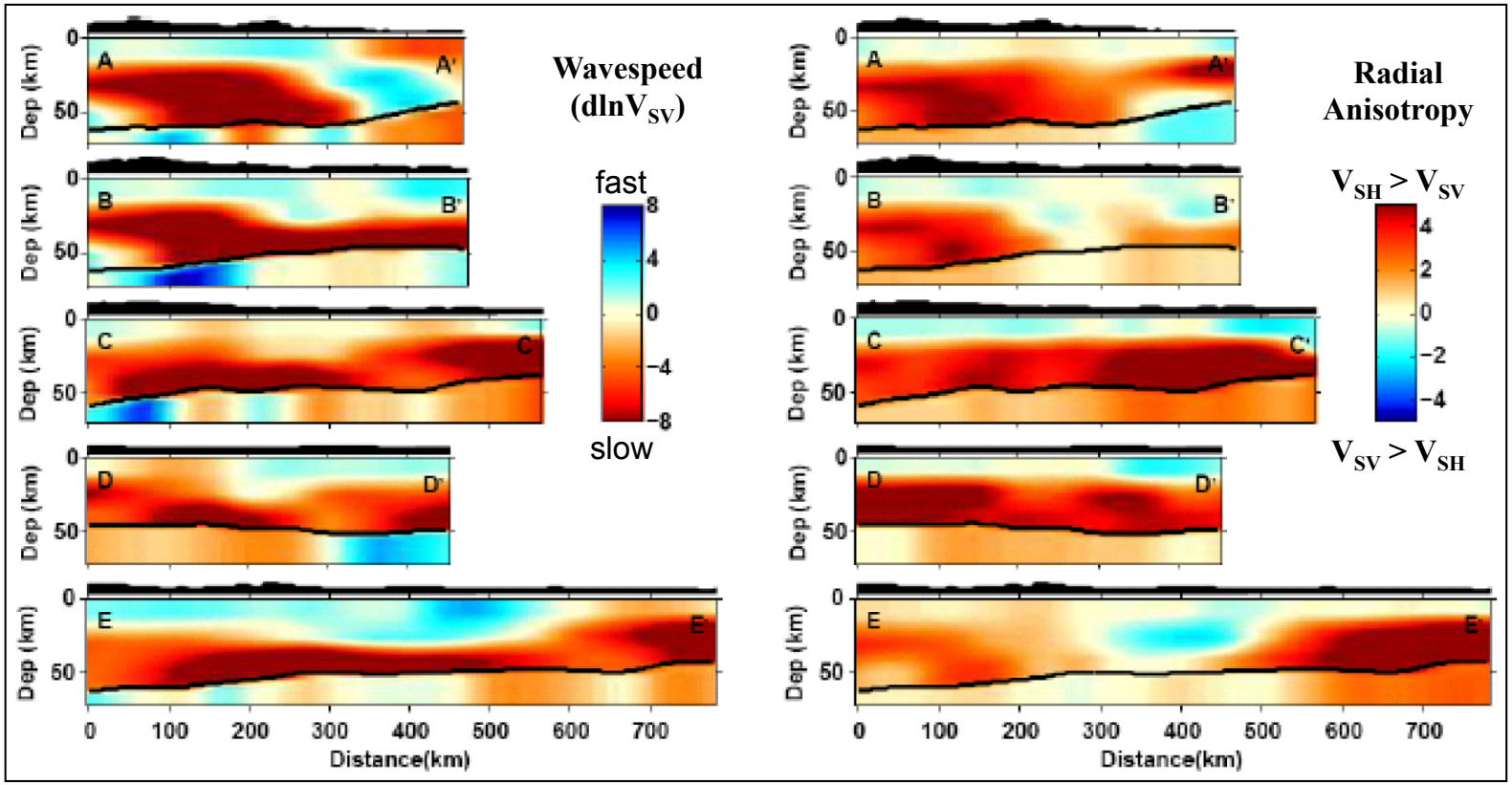

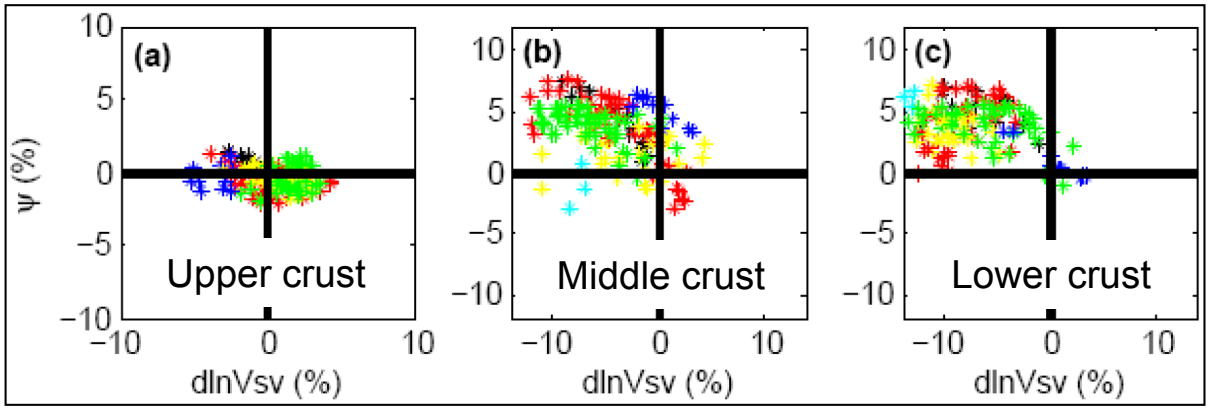

High resolution studies with dense seismograph arrays

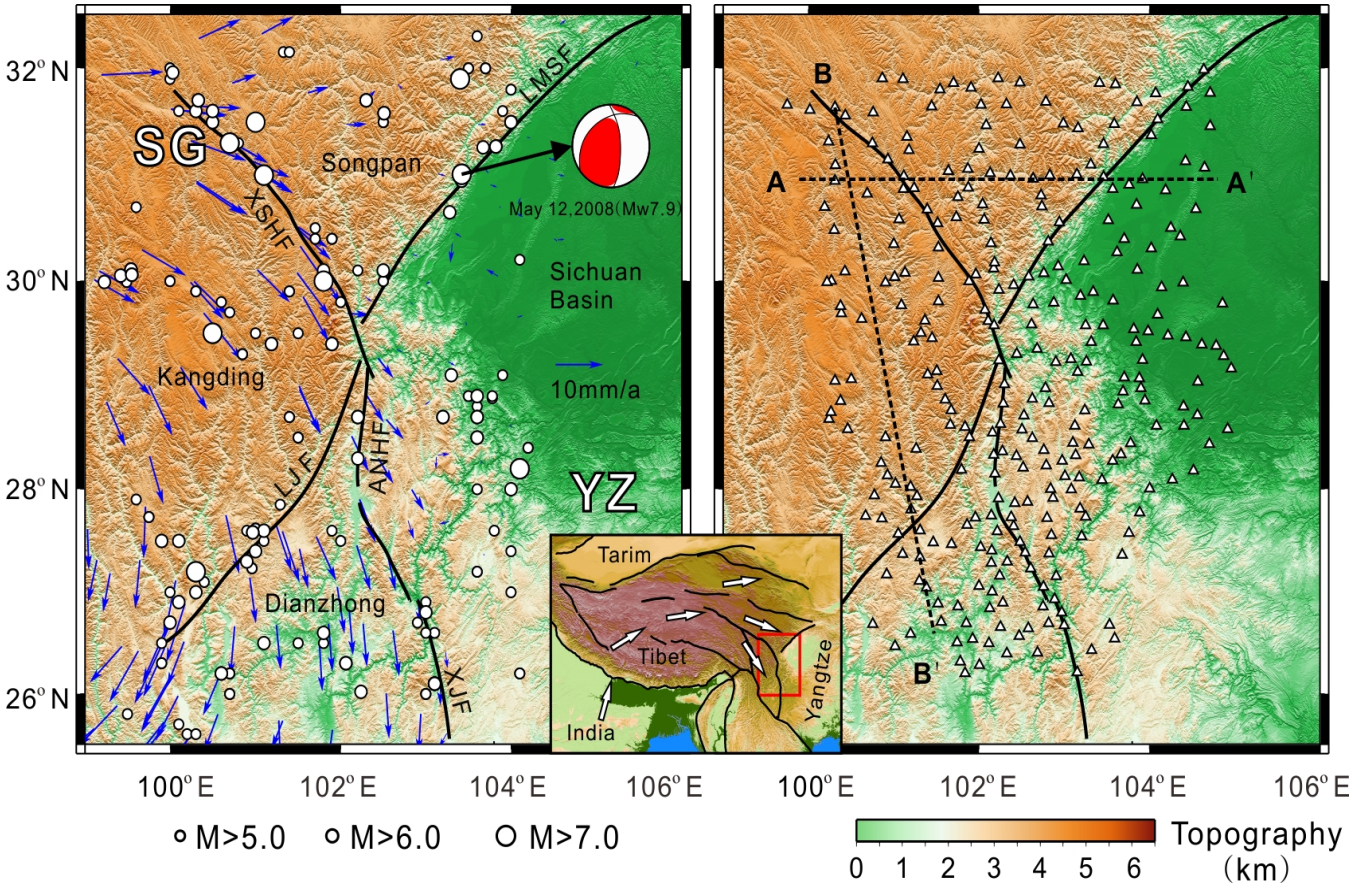

Geological setting and station map of the movable dens seismic array in western Sichuan (State Key Laboratory of Earthquake Dynamics, Institute of Geology, China Earthquake Administration). Black solid lines: major faults; blue triangles: stations; yellow circles: earthquakes (Ms ≥ 5.0,1901-2010, 2008 Wenchuan focal mechanism); blue arrows: crustal motion relative to the Yangze craton from GPS; red dash lines: seismic profile.

[SB=Sichuan Basin; YZ=Yangtze block; CD=Chundian unit; SG= Songpan-Ganze unit]
[XSH=Xiangshuihe; LMS=Longmen Shan; ANH=Anninghe; LJ=Lijiang fault]

Liu et al. (2013)

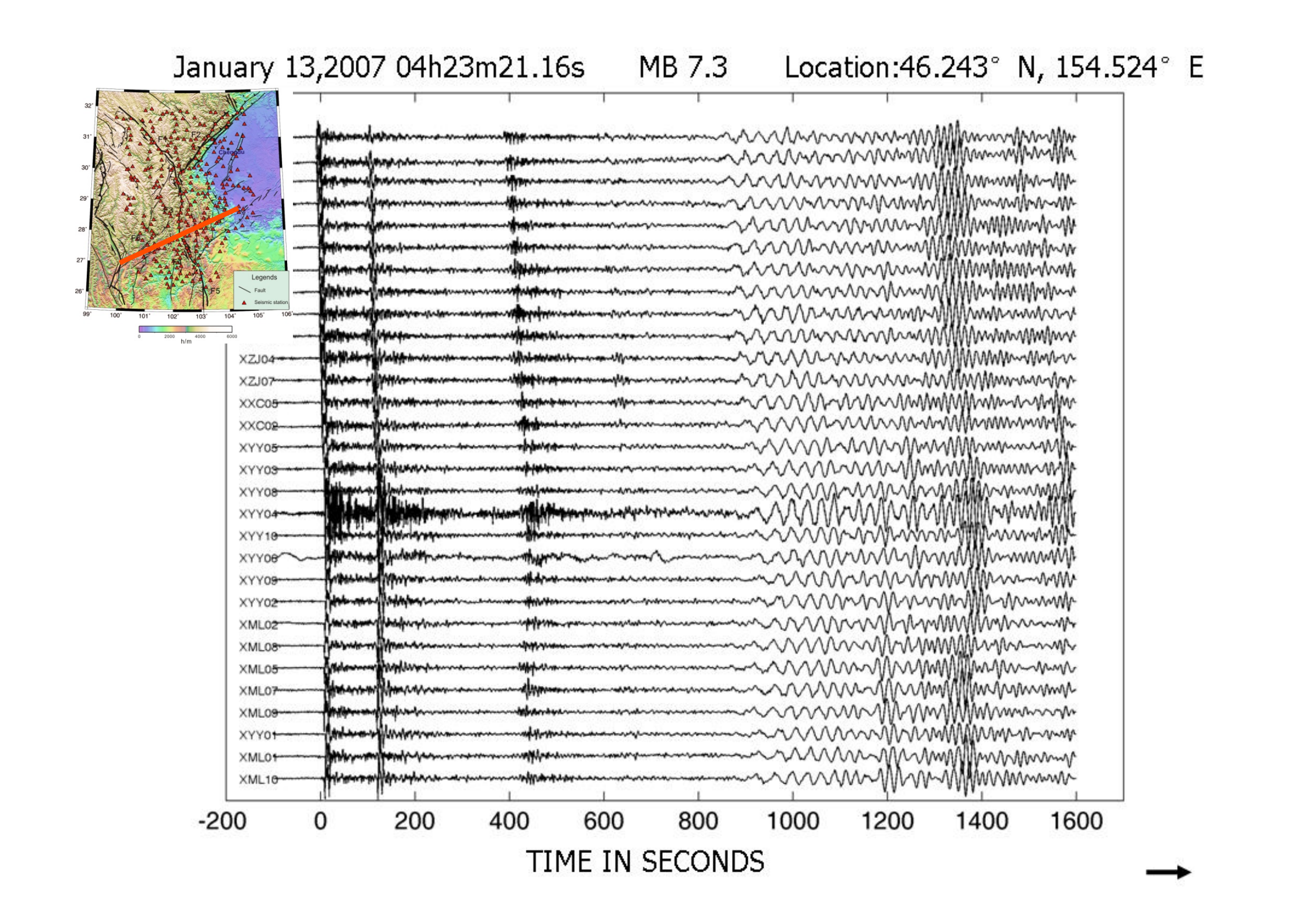
January 13,2007 04h23m21.16s MB 7.3 Location:46.243° N, 154.524° E
F1
F2
F3
F4
F5
Chengdu
Legends
Fault
Seismic station
h/m
XZJ04
XZJ07
XXC05
XXC02
XYY05
XYY03
XYY08
XYY04
XYY10
XYY06
XYY09
XYY02
XML02
XML08
XML05
XML07
XML09
XYY01
XML01
XML10
-200
0
200
400
600
800
1000
1200
1400
1600
TIME IN SECONDS

Ambient Noise Tomography (with Moho depth constrained by receiver functions)

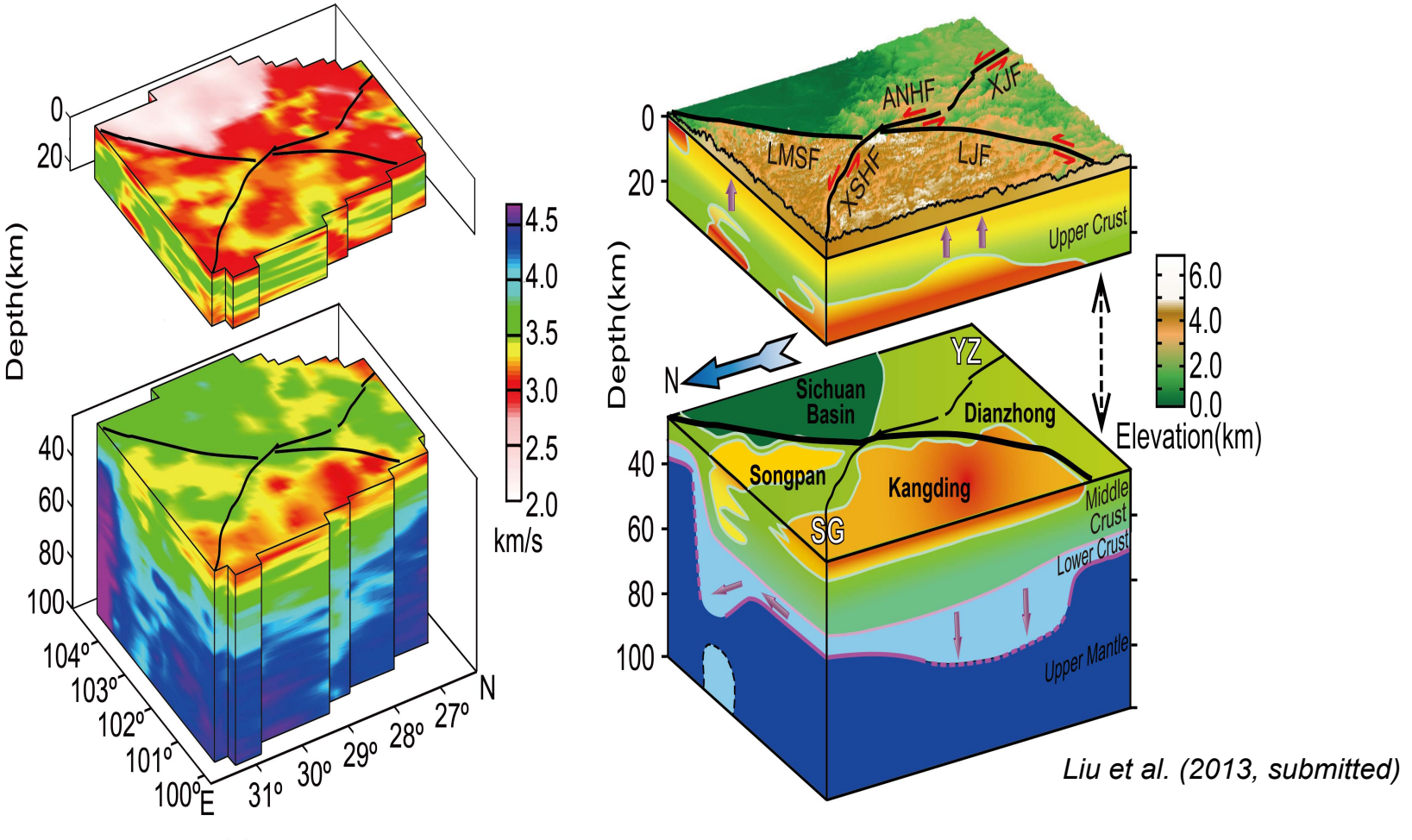

Liu et al. (2013, submitted)

3D perspectives of lithospheric shear-wavespeed variations in relation to surface topography and major fault systems in the region. Left: wavespeeds from joint inversion; Right: cartoon summarizing the main structural and topographic features.

[SB=Sichuan Basin; YZ=Yangtze block; CD=Chundian unit; SG= Songpan-Ganze unit]
[XSH=Xiangshuihe; LMS=Longmen Shan; ANH=Anninghe; LJ=Lijiang fault]

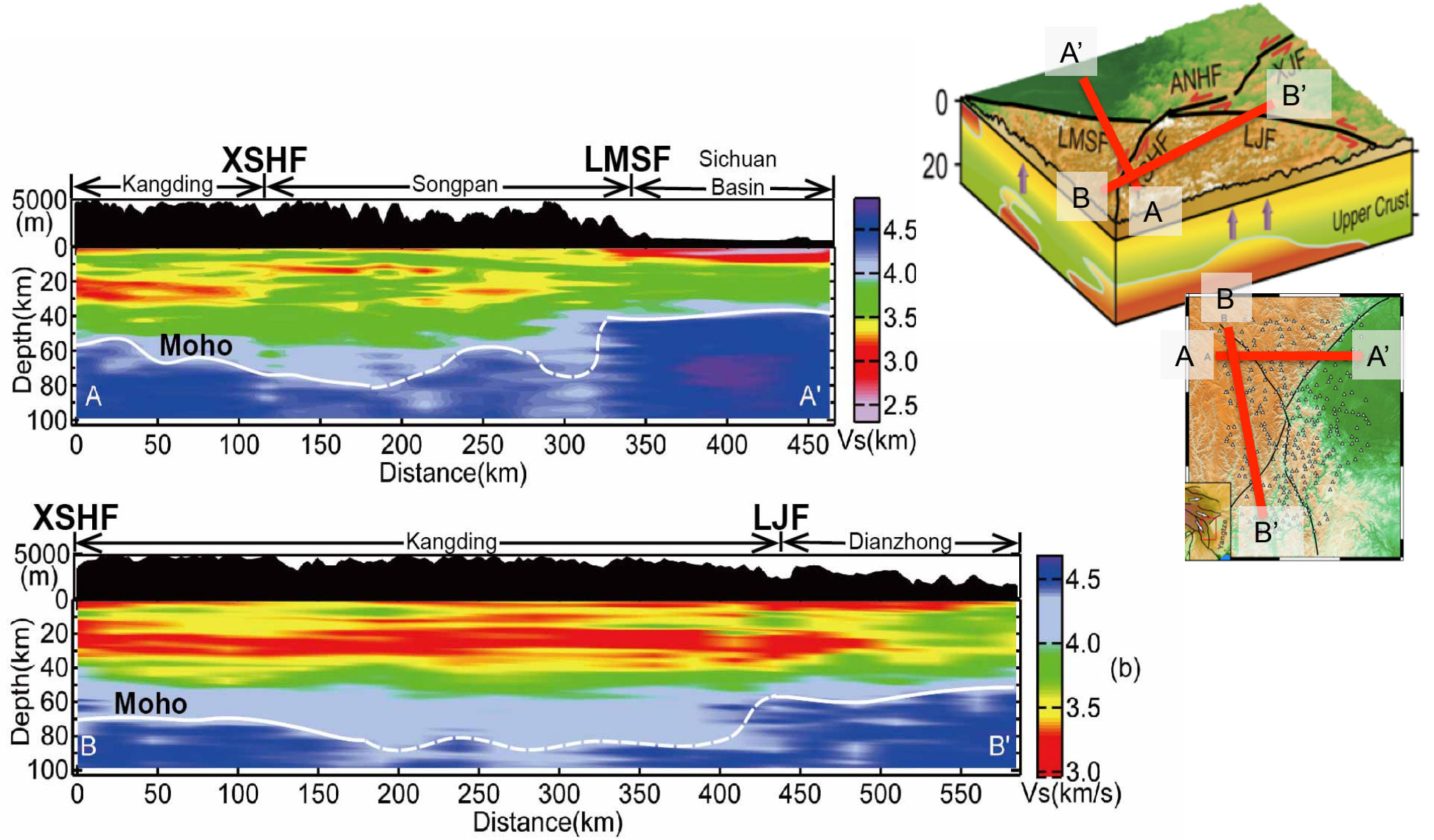

Topography and shear wavespeed variations from joint inversion of P-receiver functions and Ambient Noise (Rayleigh wave) Tomography across region of steep relief (A-A'; top) and gentle topographic gradient (B-B'; bottom).

Liu et al. (2013, submitted)

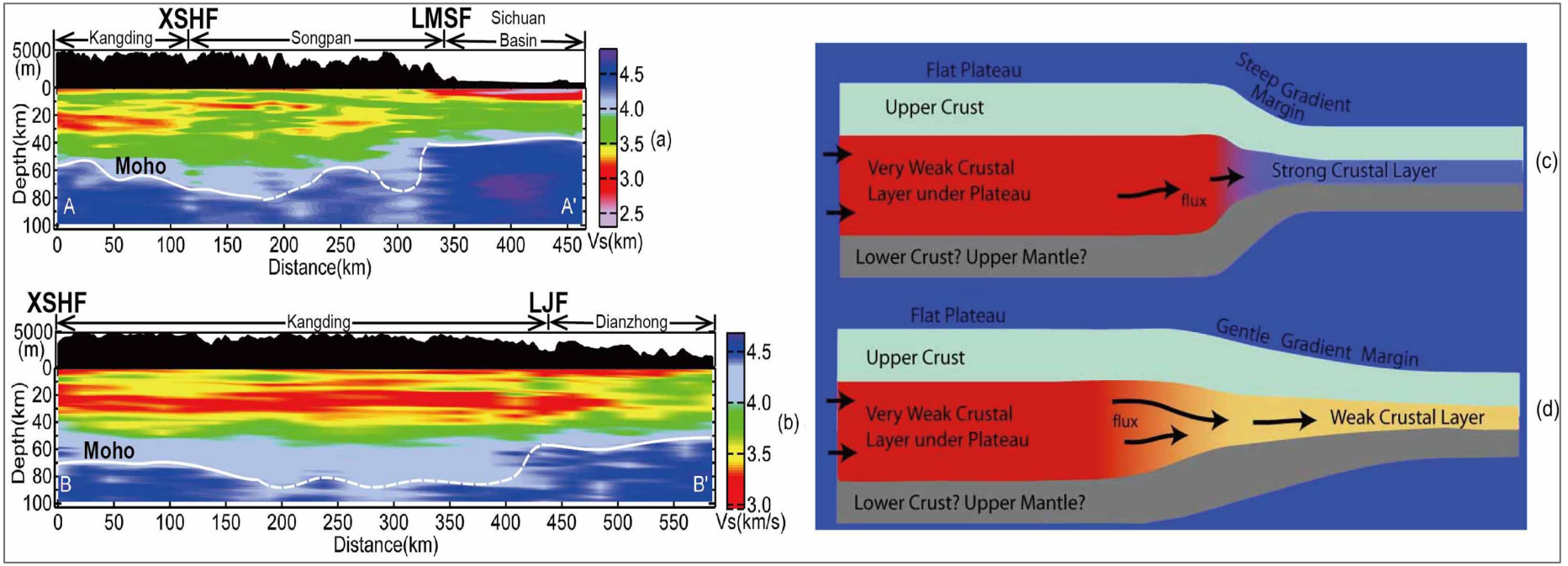

Crustal structure constrained by waveform data obtained by a dense seismography array in western Sichuan.

Concept: canonical channel flow model. (Figure courtesy of L. Royden, MIT).

Liu et al. (2013, submitted)

Overview of lecture:

1. Introduction/background
2. Ambient noise and surface wave tomography
3. Reverse time migration of converted waves
4. Interferometry of teleseismic (coda) waves

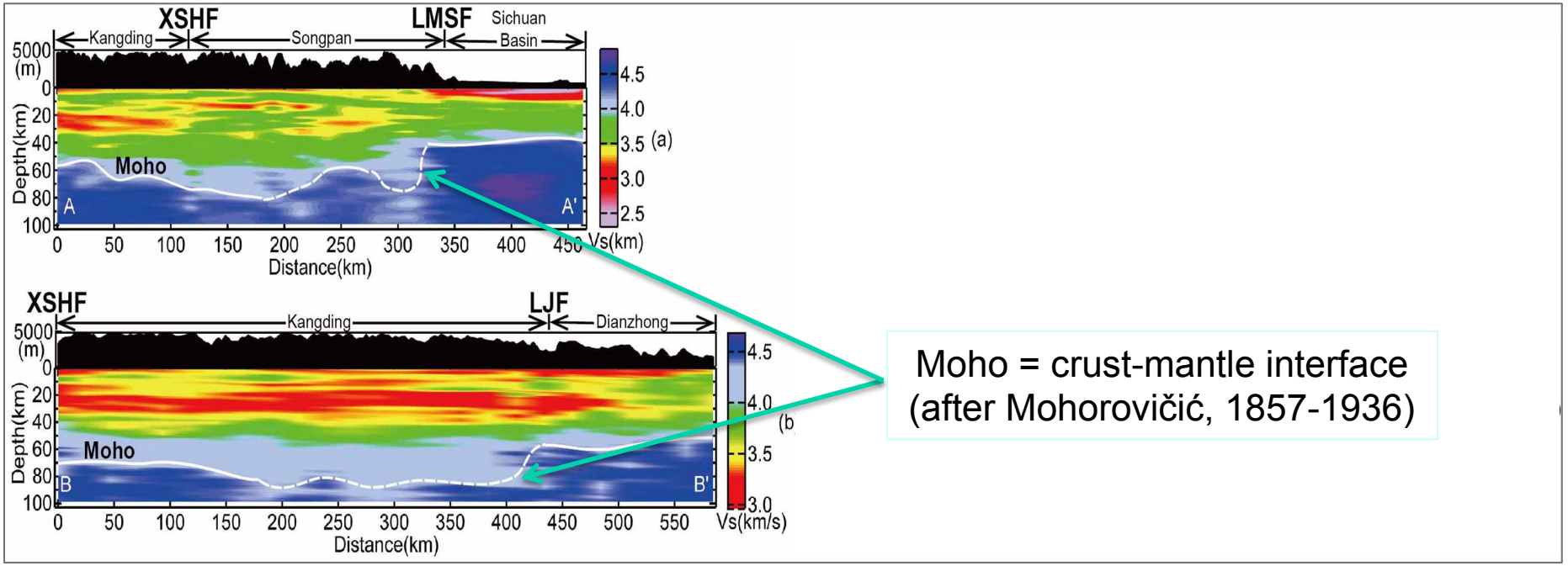

Imaging of the Moho with Converted Waves (*P-to-S* or *S-to-P*)

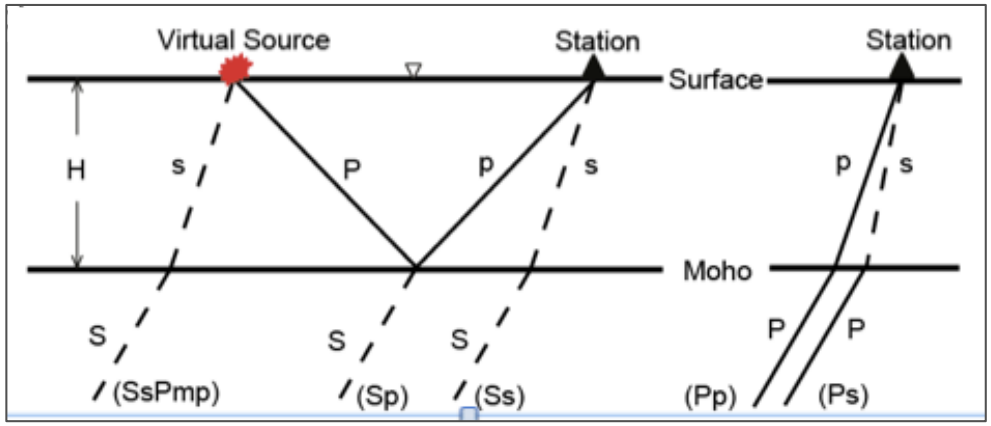

Yu et al.(EPSL, 2012)

Traditional approach (concept)

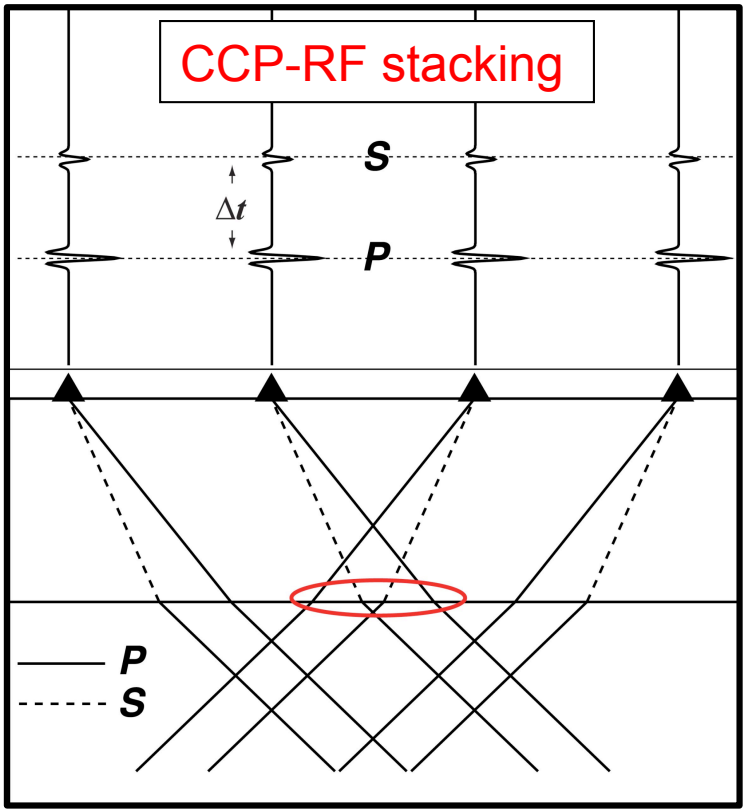

Common **C**onversion **P**oint stacks of converted waves (**R**eceiver **F**unctions):

-Time differences mapped directly to depth

-Horizontal interfaces

Traditional approach (concept)

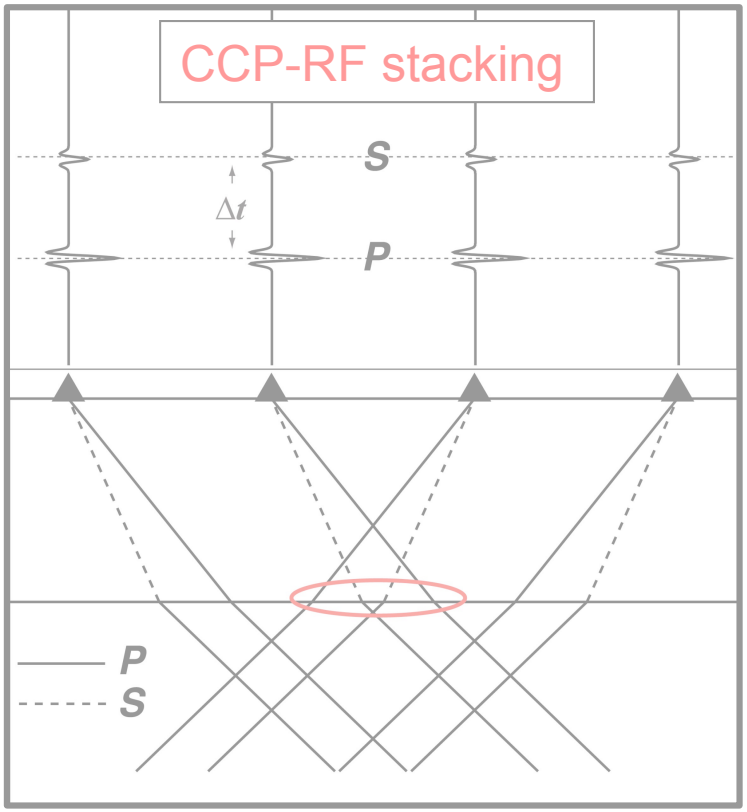

Shang et al. (GRL, 2012)

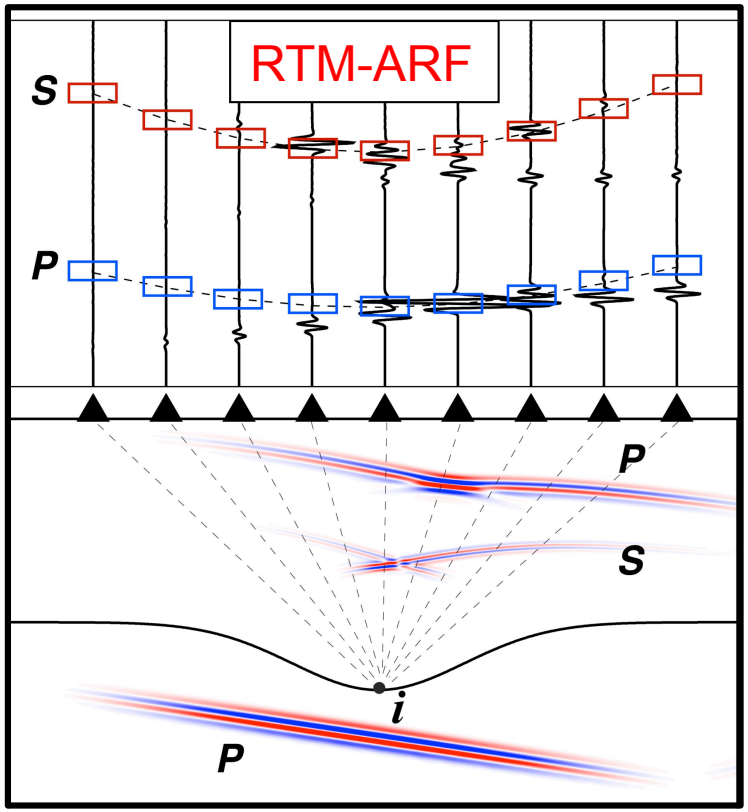

Common **C**onversion **P**oint stacks of converted waves (**R**eceiver **F**unctions):

-Time differences mapped directly to depth

-Horizontal interfaces

Reverse **T**ime **M**igration of **A**rray **R**eceiver **F**unctions:

- Cross-correlations: incoming & time reversed and *P* & *S* waves (“imaging condition“)
- No assumption on structure

Shang, De Hoop, Van der Hilst (GRL, 2012)

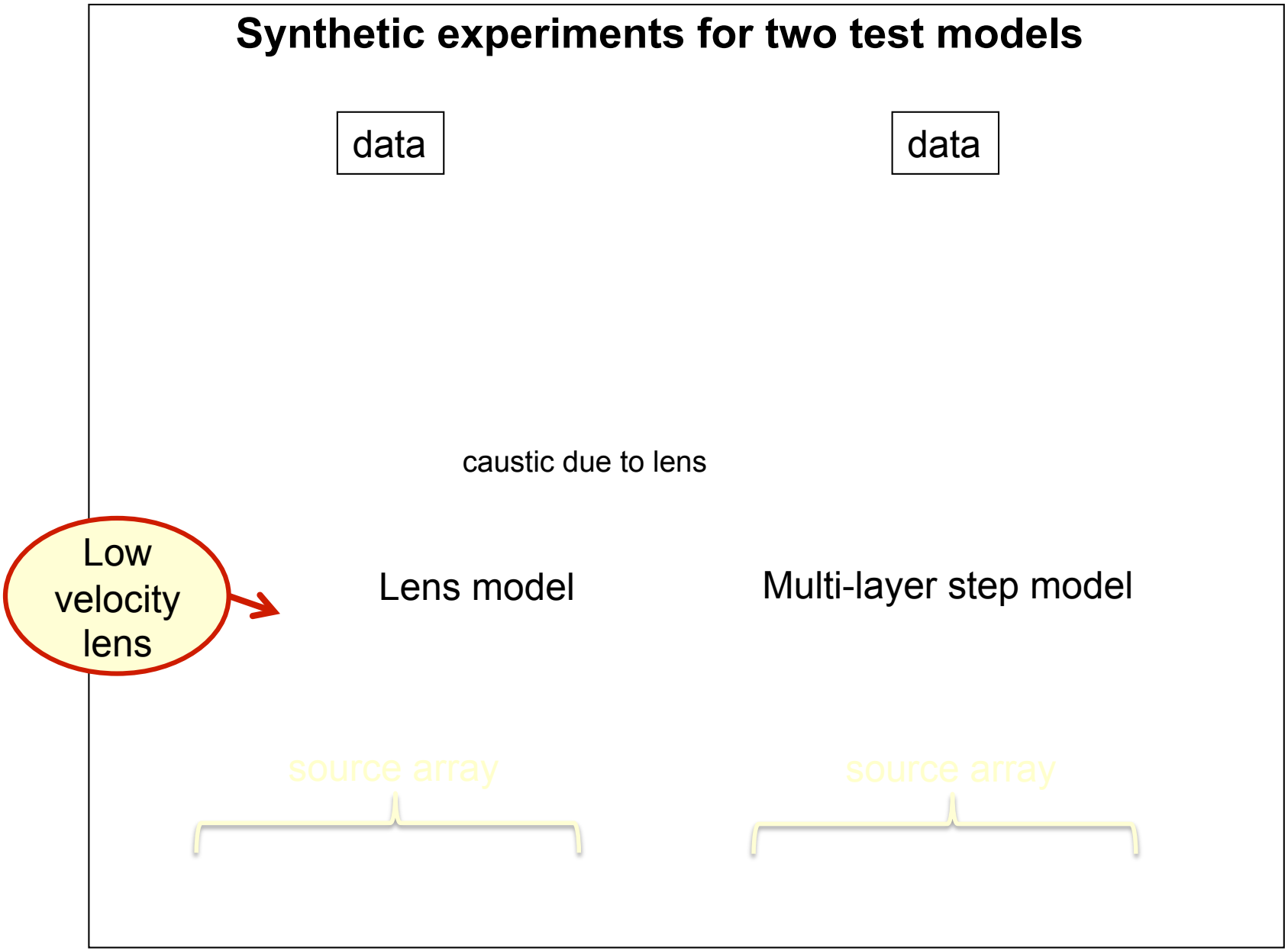

Shang, De Hoop, Van der Hilst (GRL, 2012)

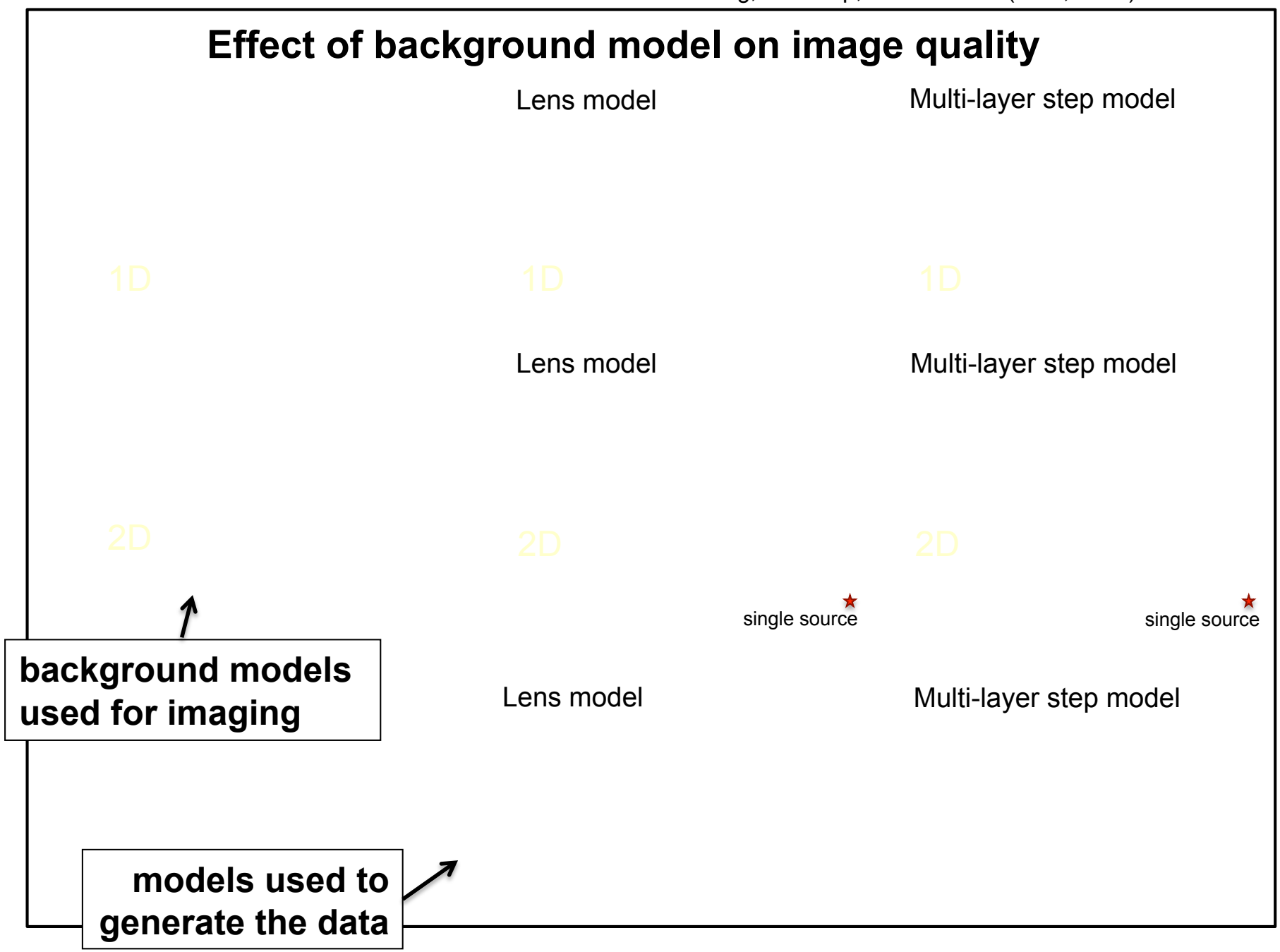

Shang, De Hoop, Van der Hilst (GRL, 2012)

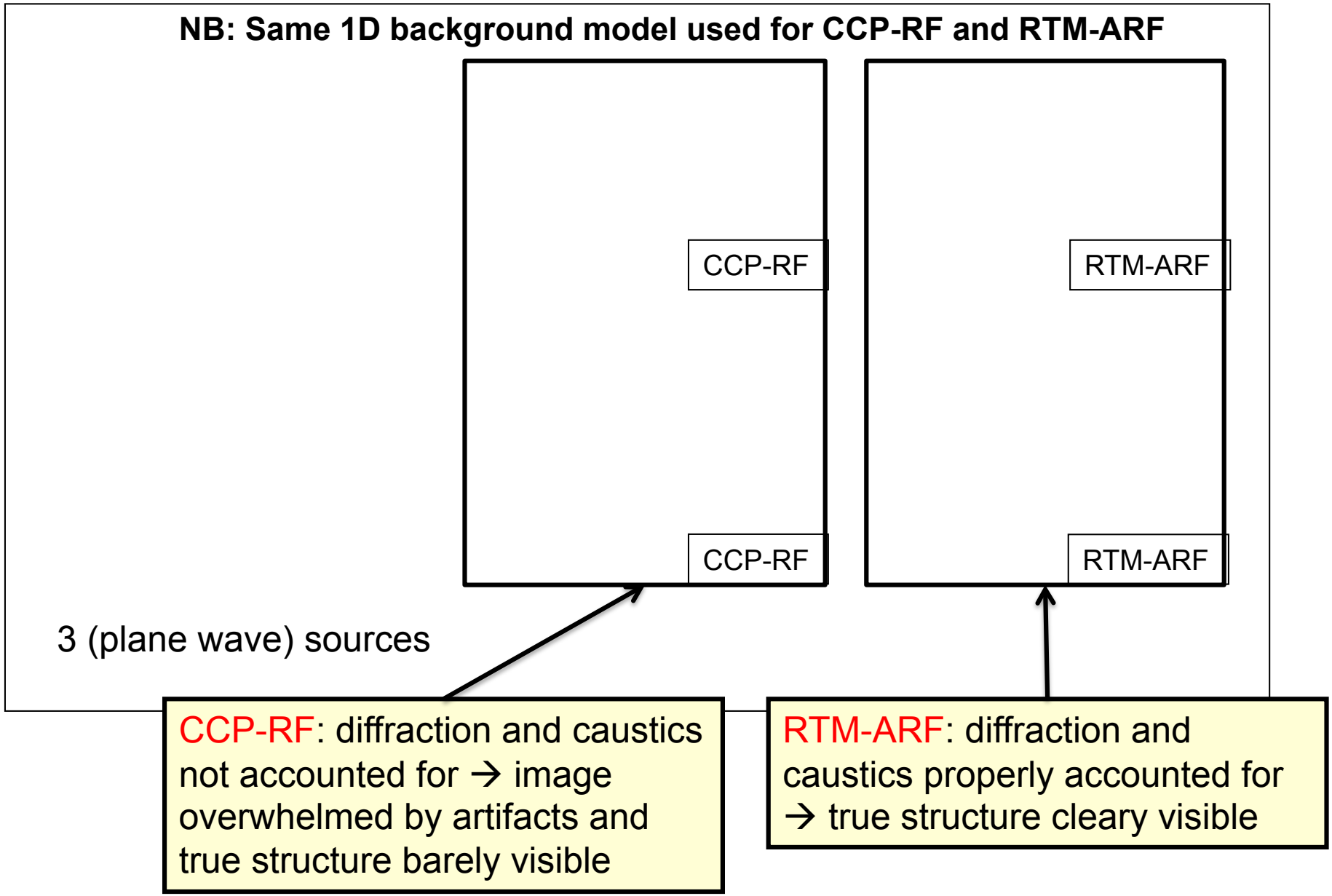

Image accuracy depends on background model

Can be obtained from tomography

E.g., travel time, surface waves, ambient noise …

Or ….

RTM based (teleseimic) reflection tomography

Teleseismic wave-equation reflection tomography using free surface reflected phases

S. Burdick[1], M. V. de Hoop[2], S. Wang[2] R. D. van der Hilst[1]
[1] *Department of Earth, Atmospheric, and Planetary Sciences, Massachusetts Institute of Technology Cambridge, MA 02139, USA*
[2] *Department of Mathematics, Purdue University*

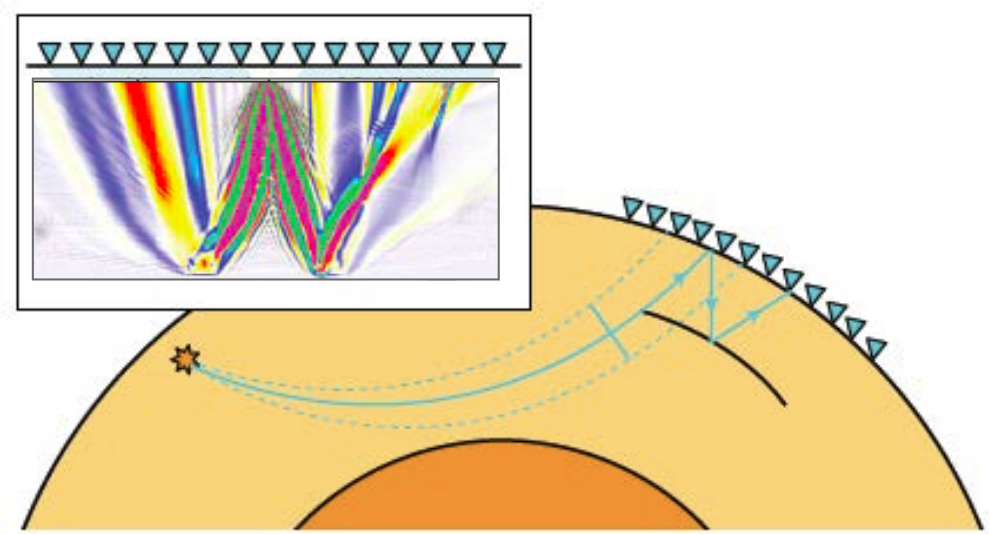

Construct images from converted and multiply-reflected teleseismic phases

Overview of lecture:

1. Introduction/background
2. Ambient noise and surface wave tomography
3. Reverse time migration of converted waves
4. Interferometry of teleseismic (coda) waves

For instance, imaging of the slab interface

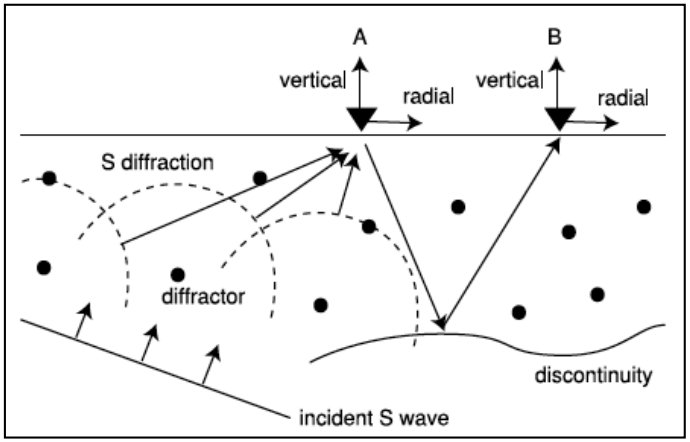

Seismic interferometry of teleseismic *S*-wave coda for retrieval of body waves: an application to the Philippine Sea slab underneath the Japanese Islands

Takashi Tonegawa,[1] Kiwamu Nishida,[1] Toshiki Watanabe[2] and Katsuhiko Shiomi[3]

[1] *Earthquake Research Institute, Univ. of Tokyo,* 1-1-1, *Yayoi, Bunkyo-ku, Tokyo* 113-0032, *Japan. E-mail: tonegawa@eri.u-tokyo.ac.jp*
[2] *Graduate School of Environmental Studies, Nagoya University, Furo-cho, Chikusa-ku, Nagoya* 464-8602, *Japan*
[3] *National Research Institute for Earth Science and Disaster Prevention,* 3-1, *Tennodai, Tsukuba, Ibaraki* 305-0006, *Japan*

Accepted 2009 May 11. Received 2009 April 20; in original form 2009 January 22

Tonegawa et al. (GJI, 2009)

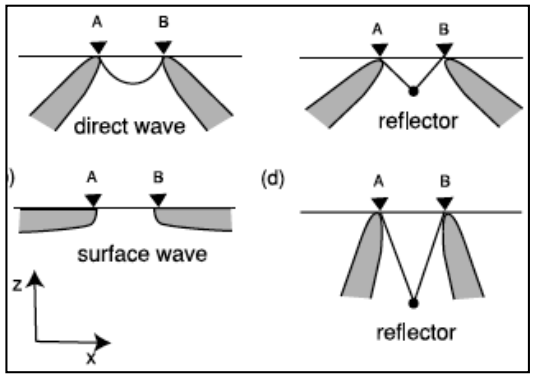

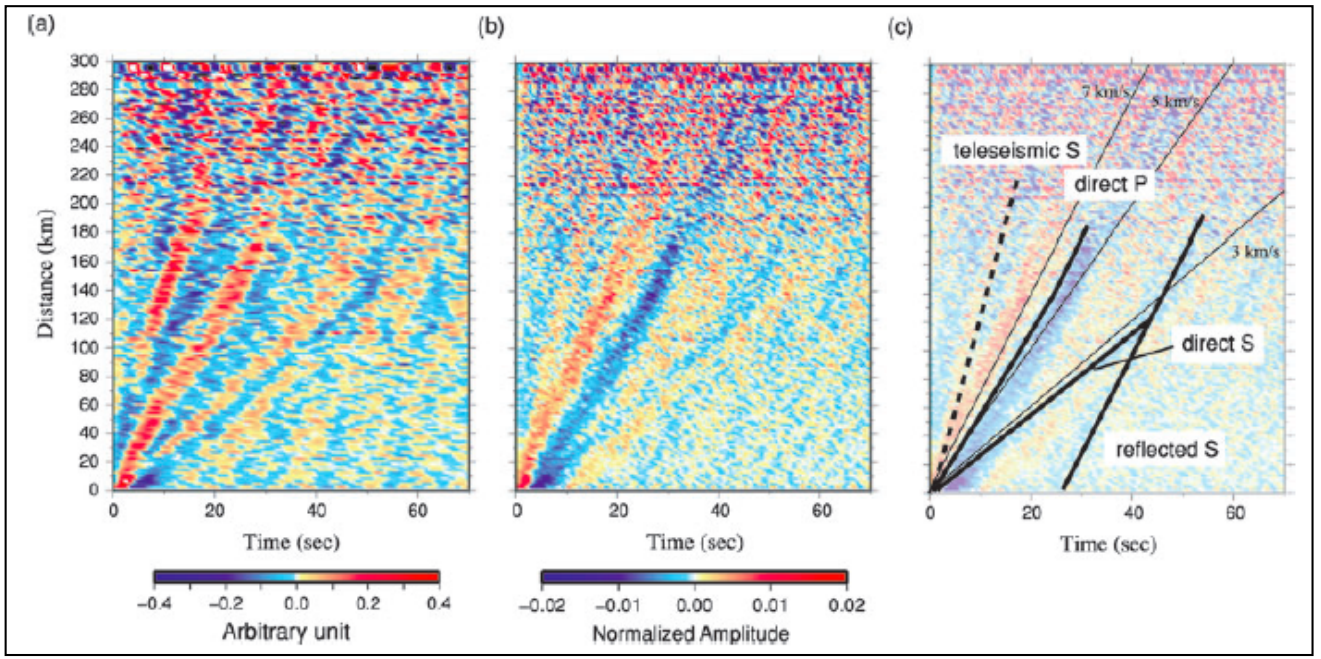

Or passive imaging: Earth's mantle discontinuities from ambient seismic noise.

Poli et al. (Science, 2012)

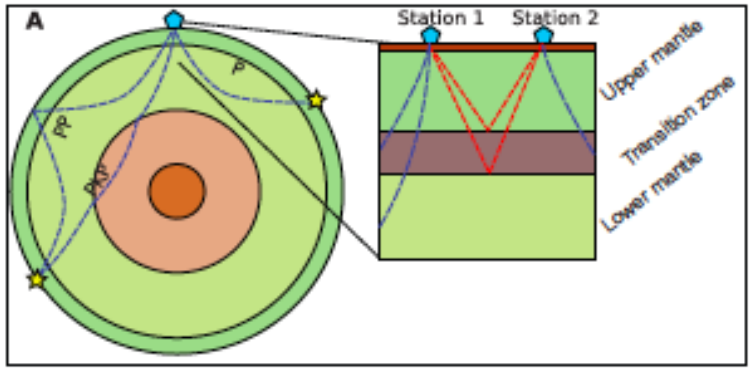

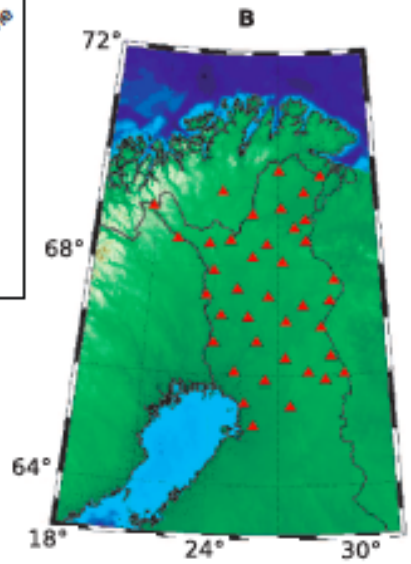

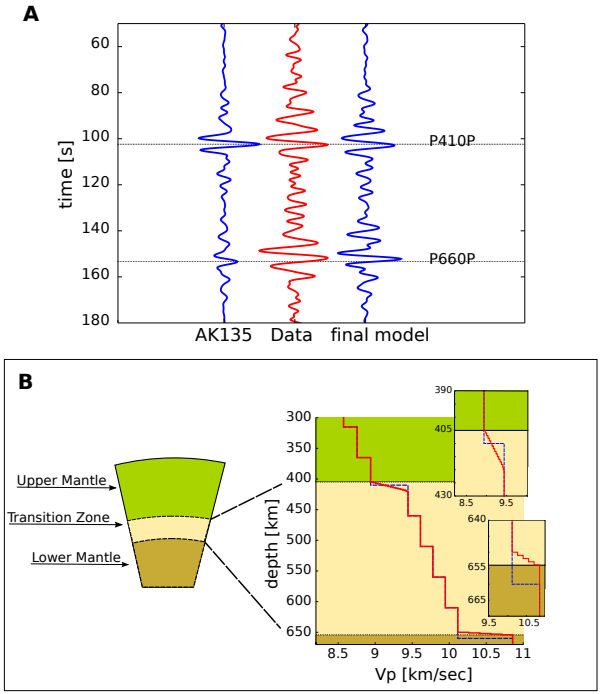

Campillo (Cargese, 2013)

Construct images from converted and multiply-reflected teleseismic phases

Burdick et al. (GJI, submitted)

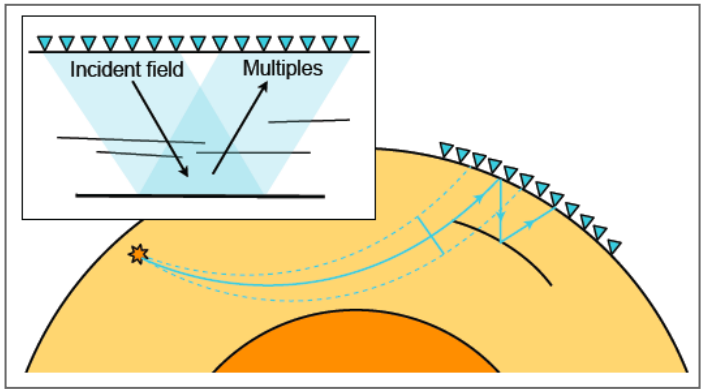

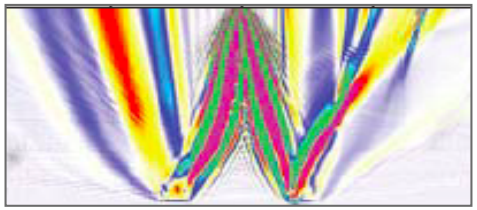

Wave-equation reflection tomography → full finite frequency (De Hoop et al., (GJI, 2006)

Actual model (used to create synthetic data)

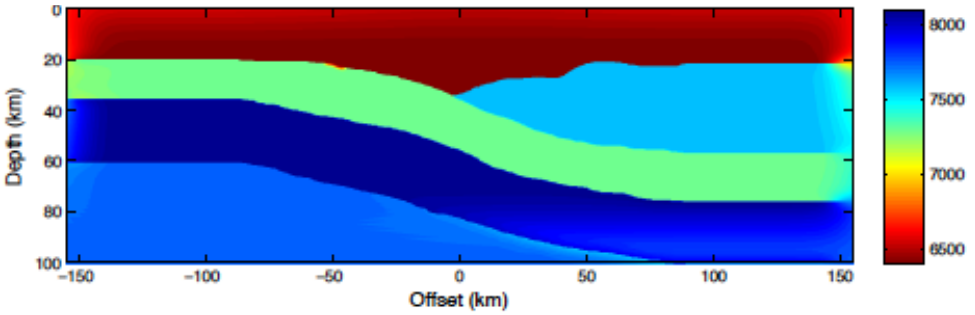

Reflectivity (singular part of model)

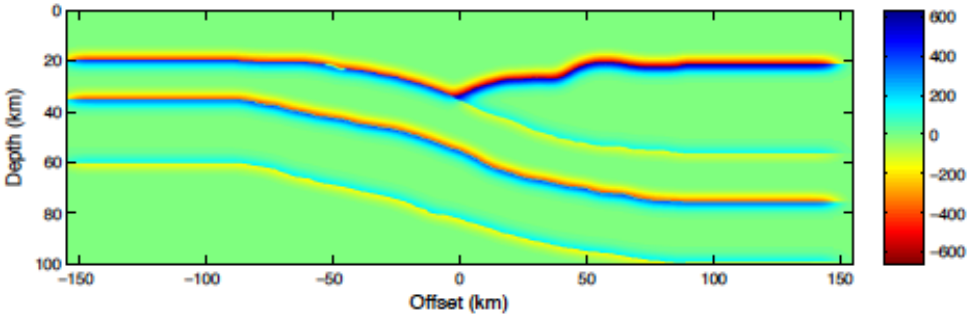

Wavespeed perturbation (smooth part of model)

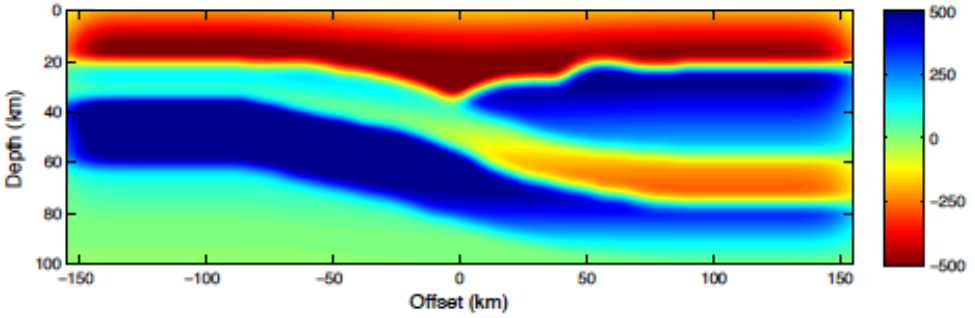

Separation of the direct and multiple fields: interferometry/cross-correlation

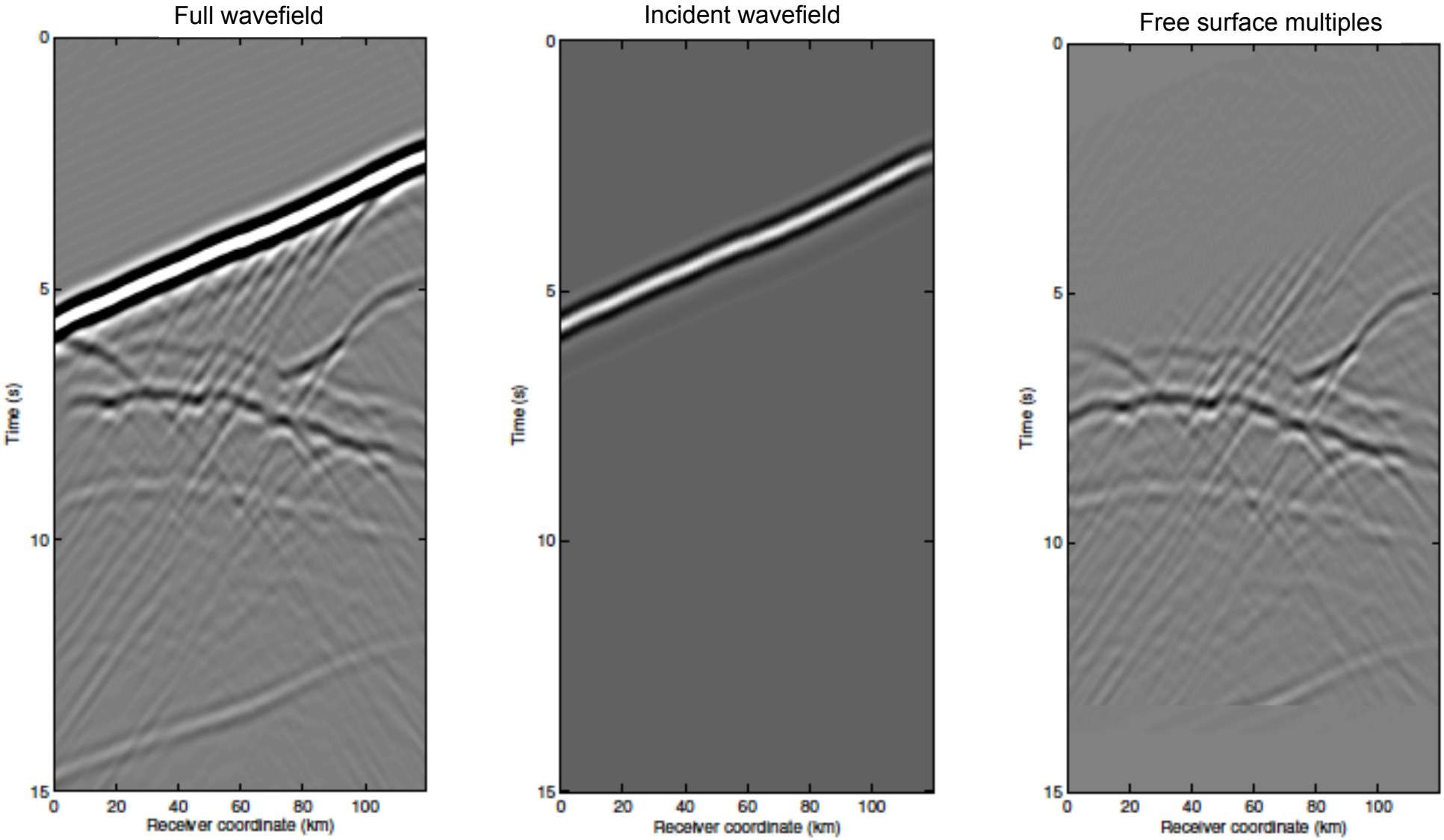

Burdick et al. (GJI, submitted)

Wave equation reflection tomography

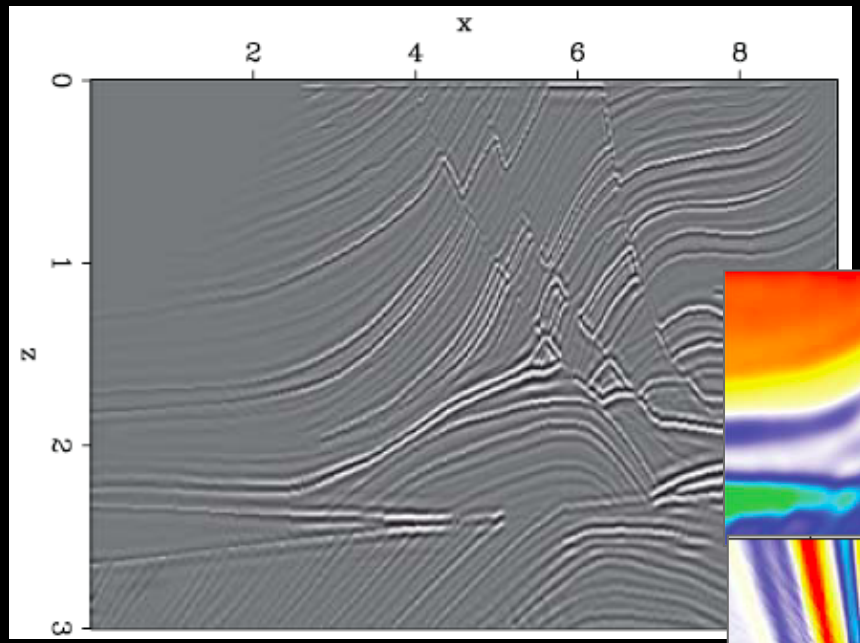

Stacked image

De Hoop et al. (GJI, 2006)

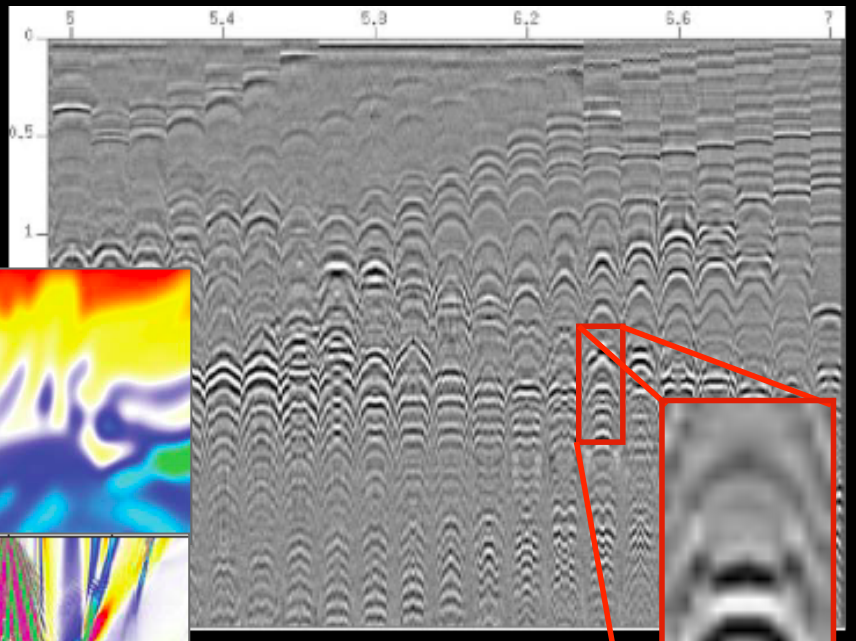

Angle gathers

Reflection angle

- Use structural image to constrain smooth 3D velocity model
- Determine model error via data redundancy - e.g. angle gathers should be flat → angle domain annihilators (based on normal moveout)

Challenges of teleseismic data

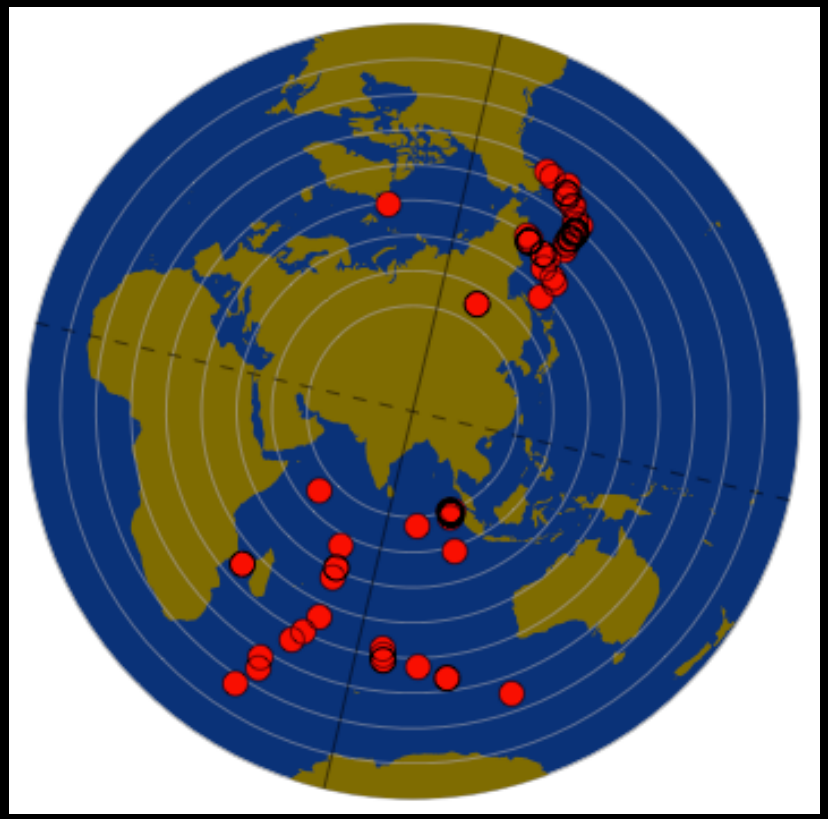

Events magnitude > 5.0
< 30° from great circle arc

1) Limited global seismicity & irregular array configurations → limited angular and azimuthal data → Angle domain annihilation not effective

Burdick et al. (GJI, submitted)

Challenges of teleseismic data

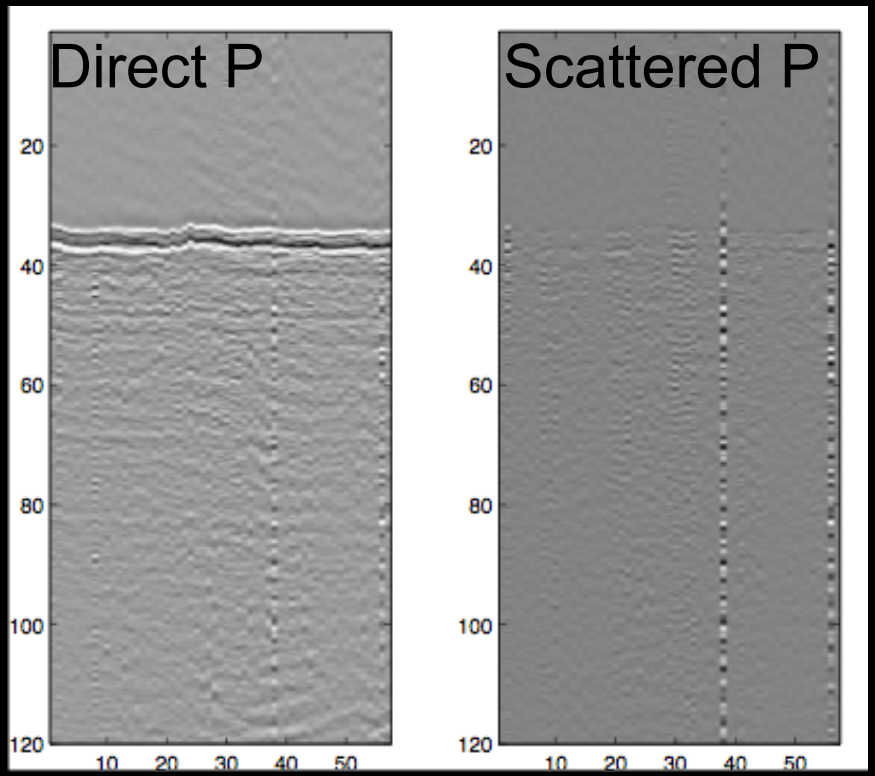

Direct and scattered fields separated by MCCC, singular value decomposition

1) Limited global seismicity & irregular array configurations → limited angular and azimuthal data

2) Unknown source functions, varying frequency content, long source-time signatures → imperfect deconvolution

Burdick et al. (GJI, submitted)

Single source images formed using inverse scattering for teleseismic sources arriving from different directions

Single source image for 23.7 deg incidence

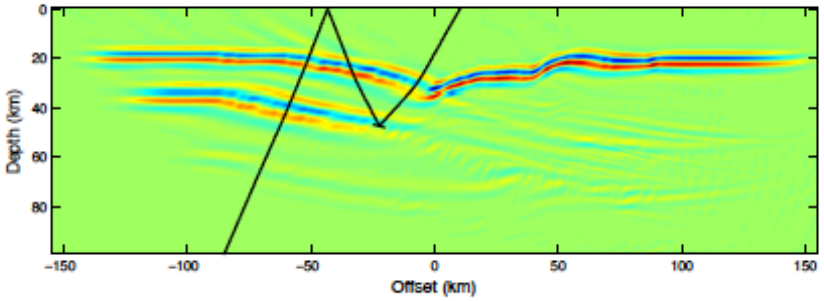

(a)

Single source image for 1.3 deg incidence

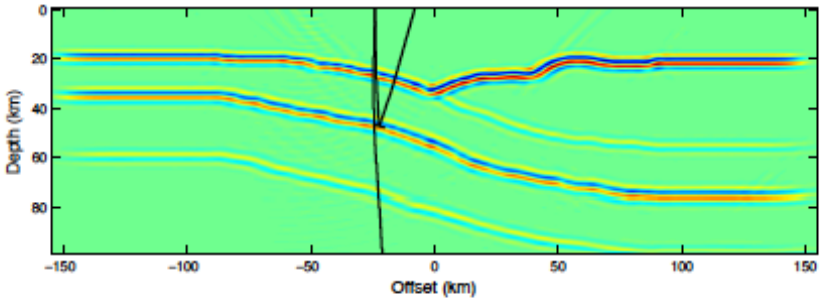

(b)

Single source image for -22.7 deg incidence

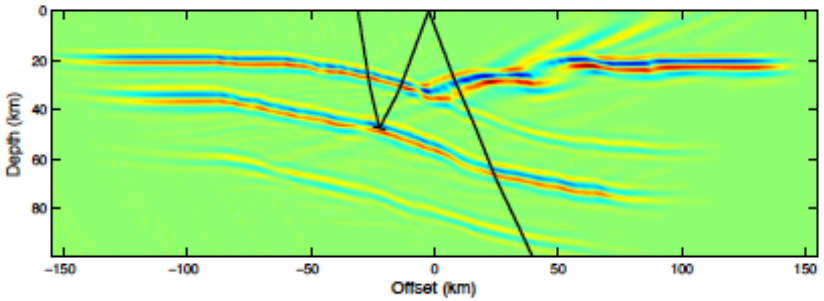

Power norm error function

- Misfit criterion based on **correlation of images** formed from different sources → maximum correlation gives best optimal velocity model
- More robust than error function based on depth move-out (angle domain annihilation)

Burdick et al. (GJI, submitted)

Checkerboard inversion test

True perturbation to model (km/s)

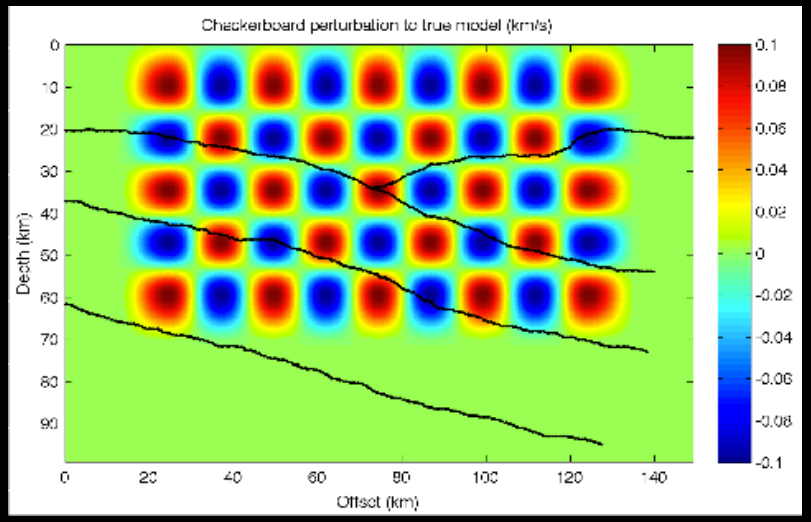

- Simple checkerboard basis projected onto 2D subduction model
- Perturbation recovered via least squares inversion

Inversion w/ all events (km/s)

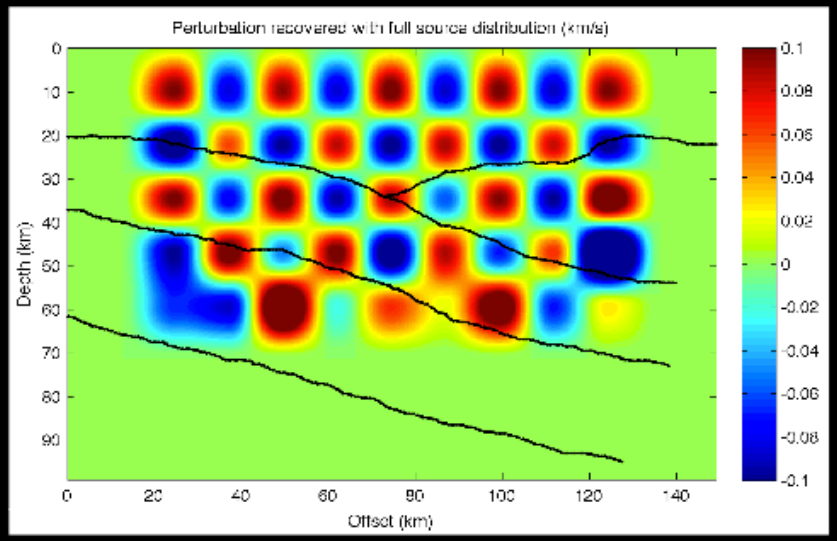

Inversion w/ realistic subset (15-30°)

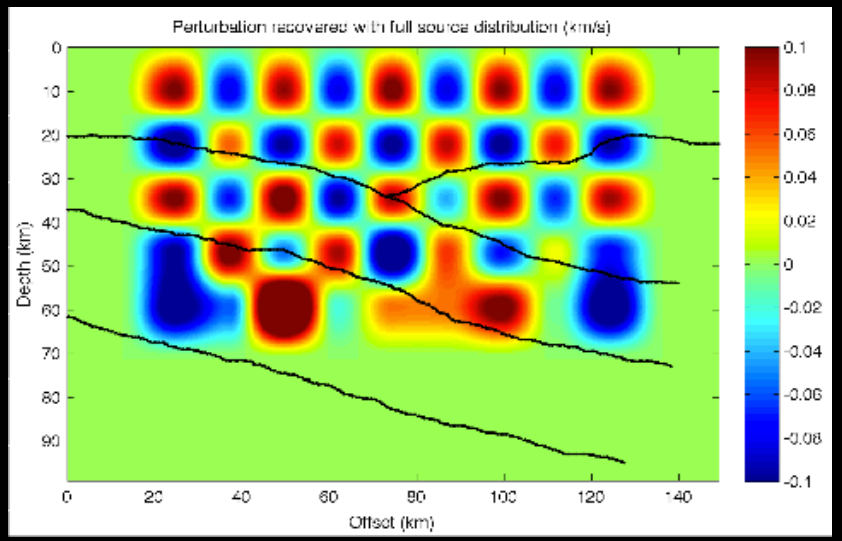

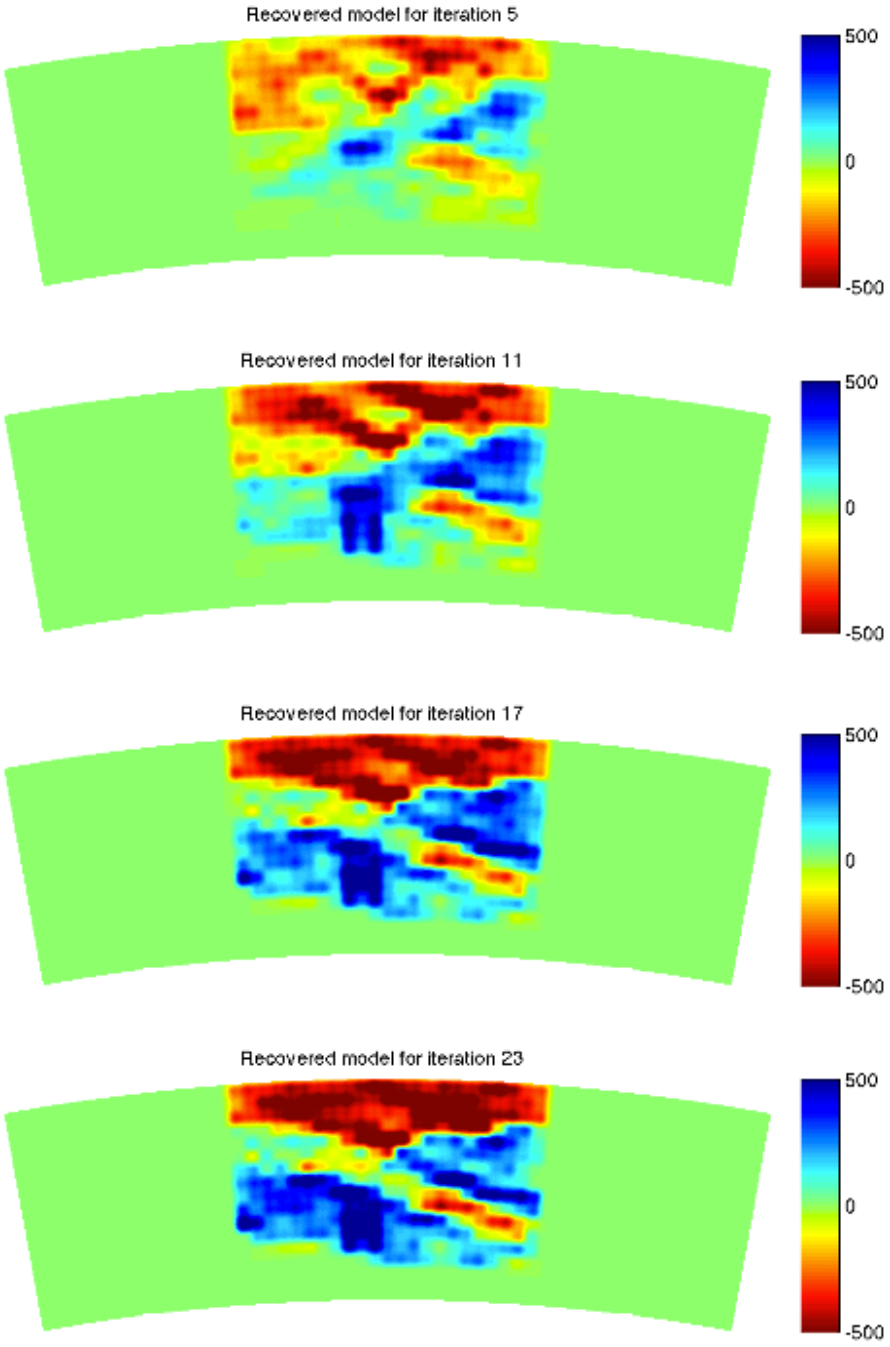

Burdick et al. (GJI, submitted)

Preliminary results

Inversion with fine basis, spherical coordinates

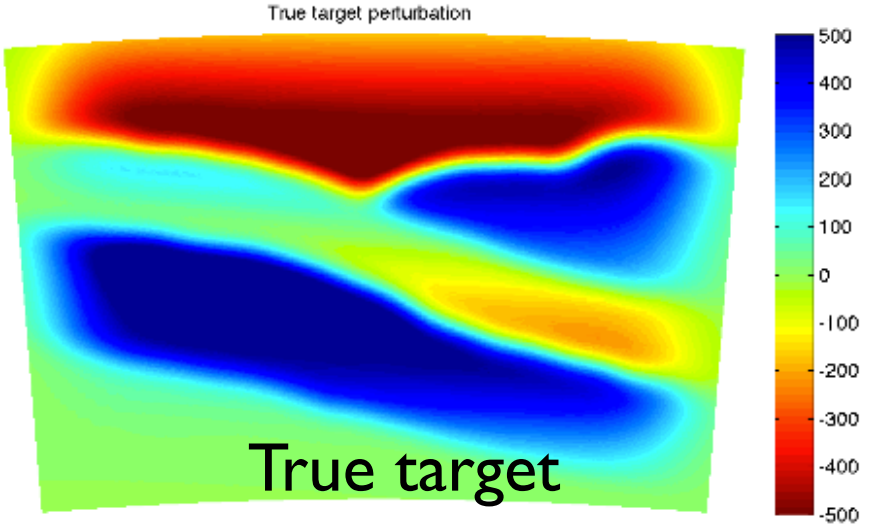

Cargese 2015 (or 2017)?

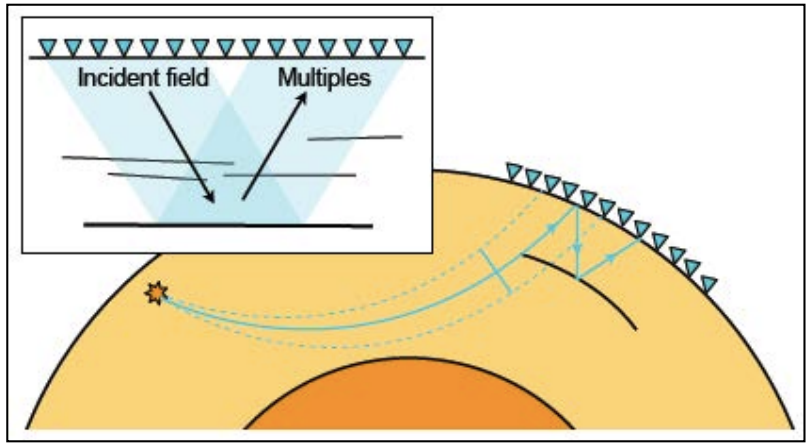

Burdick et al (GJI, submitted)

+

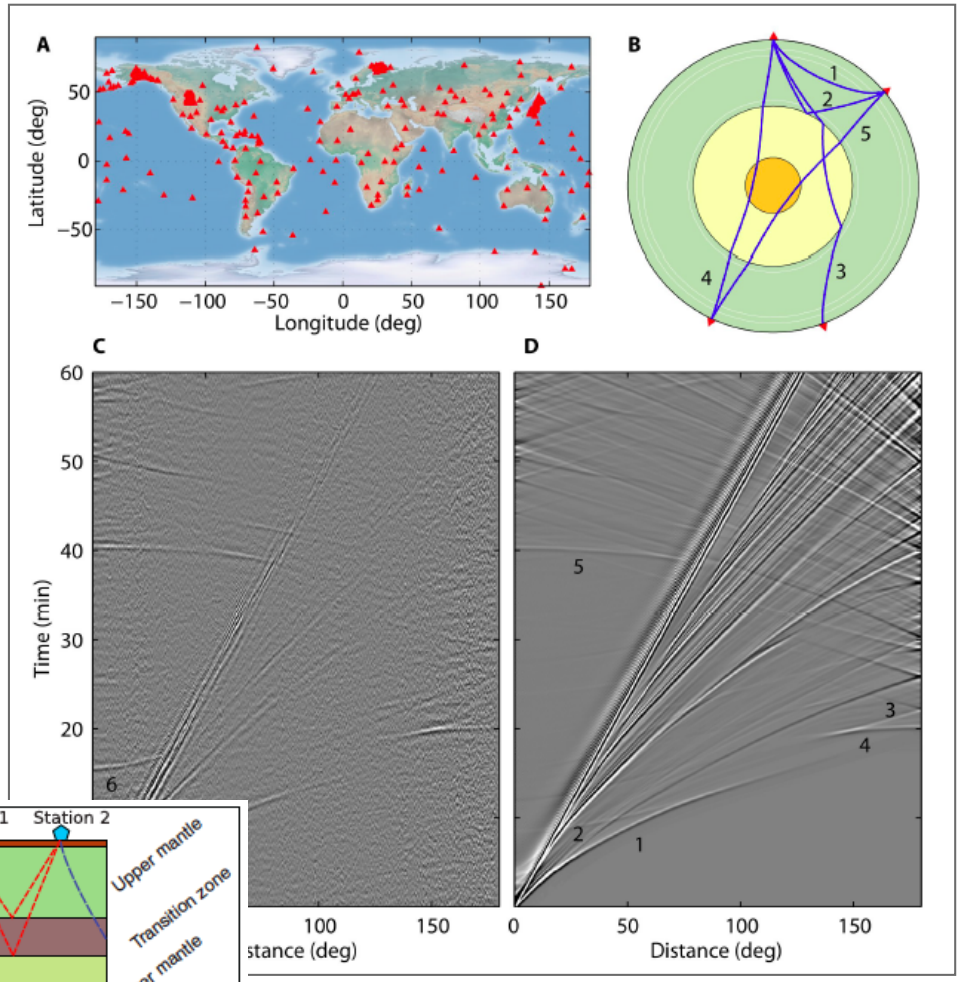

Poli et al (Science, 2012)

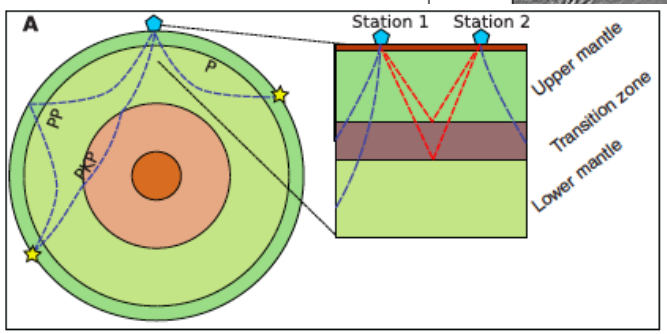

Boué et al (GJI, submitted)


Thank you

Image point moveout?
In what direction?

Image continuation direction

Reflector normal

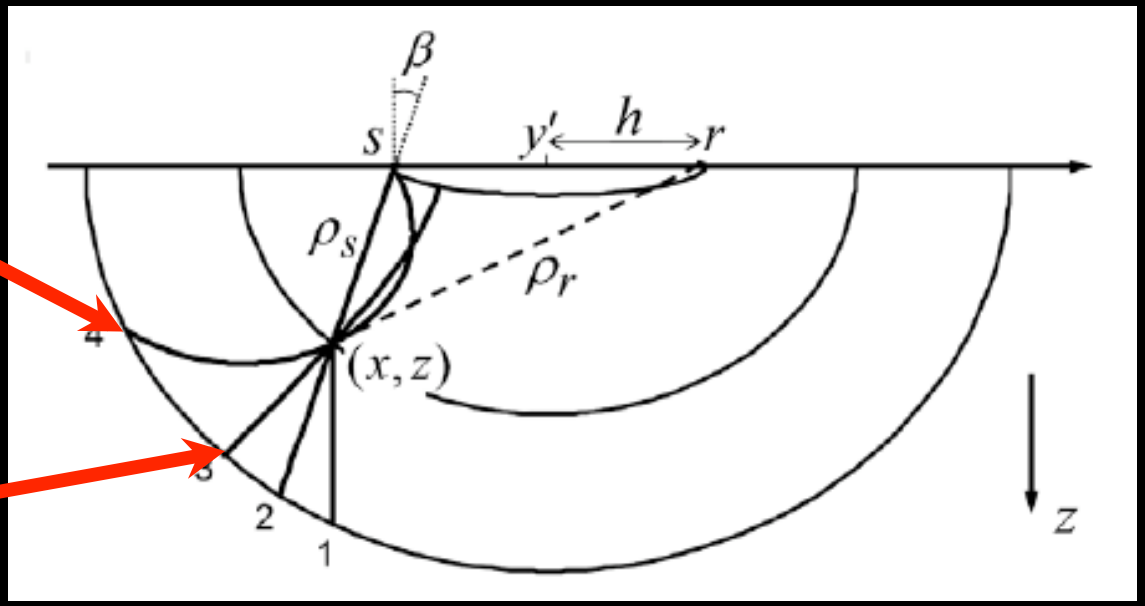

Duchkov et al. 2008

- Image continuation under velocity change is non-linear and not generally normal to reflector
- Solution to continuation ray system needed
- Instead: pure finite frequency measure

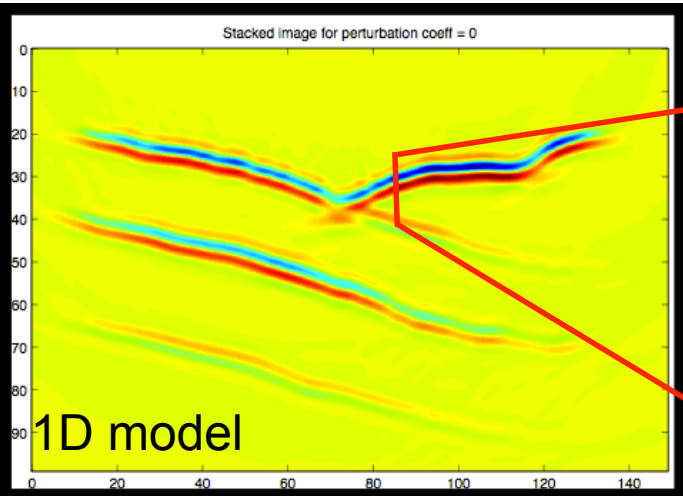

Too fast

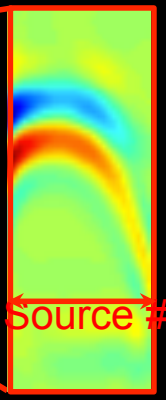

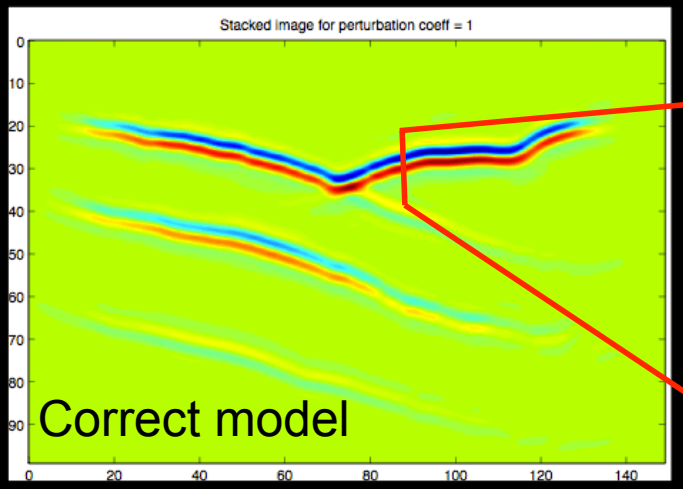

Just right

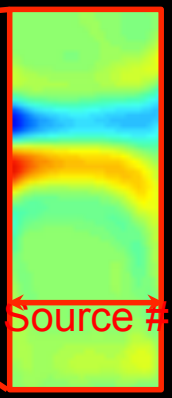

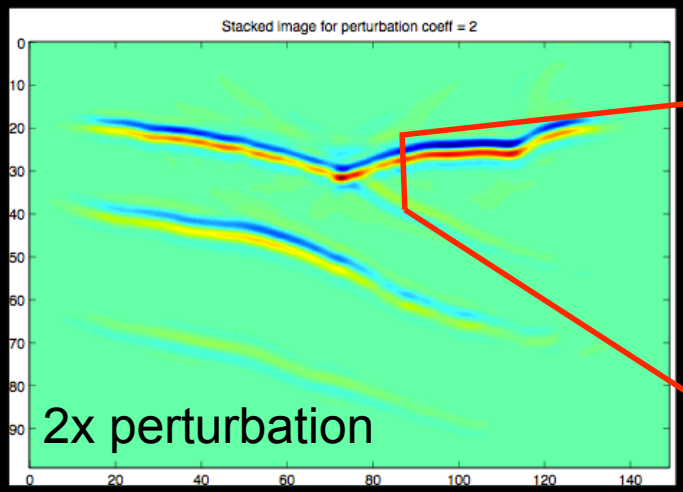

Too slow

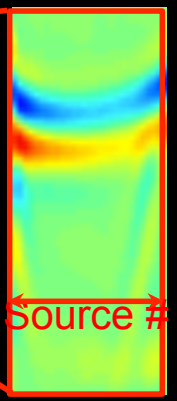

Residual moveout in source-index image gathers

Incorrect model creates measurable moveout in single-source images

Best way to quantify error? → misfit criterion

Burdick et al. (GJI, submitted)

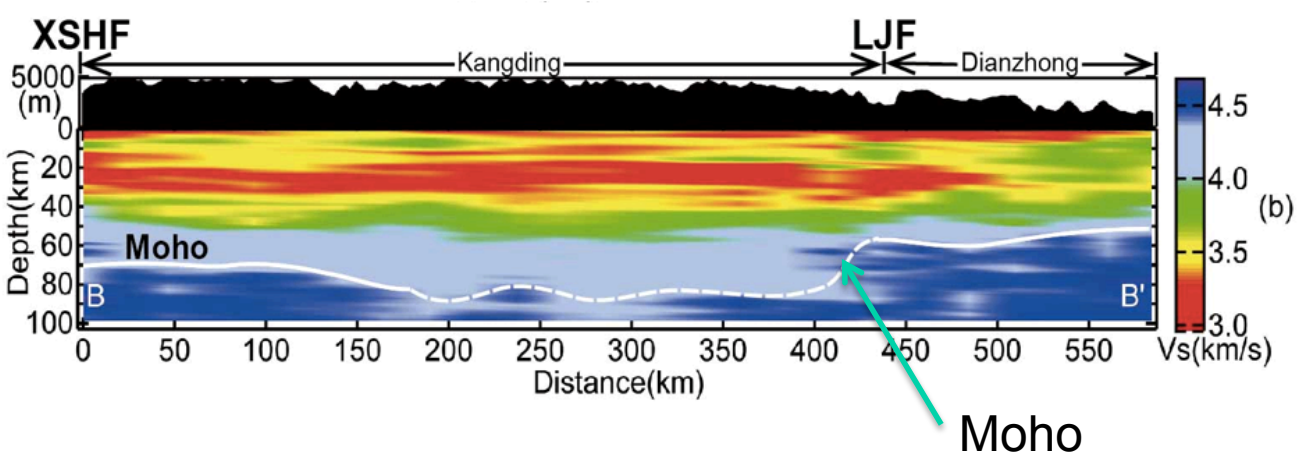

Moho

(crust-mantle interface; after Mohorovičić, 1857-1936)

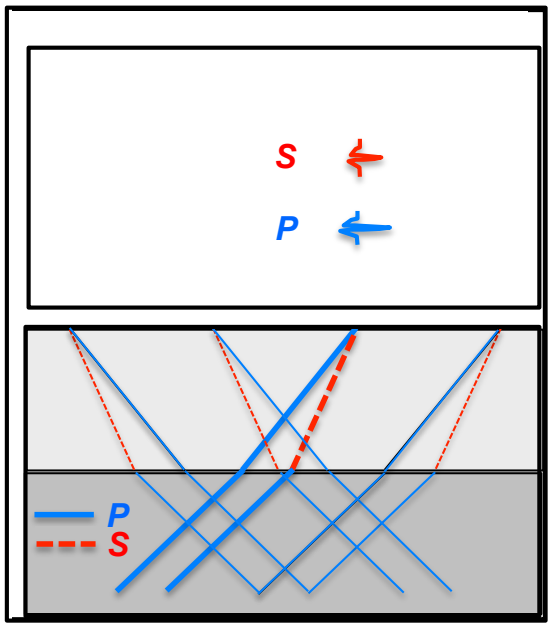

Imaging With Converted Waves (*P-to-S* or *S-to-P*)

Strong Moho topography

Problem: Traditional Receiver Function analysis assumes horizontal interfaces

PhD Research: Xuefeng Shang
(supported by Shell and CMG Program of NSF)
Shang et al. (GRL, 2012)